EXPERIMENTAL CONSTITUTIVE RELATIONS FOR HIGH TEMPERATURE DEFORMATION OF THE Pb-Sn EUTECTIC ALLOY

A Thesis Submitted
In Partial Fulfilment of the Requirements
for the Degree of

DOCTOR OF PHILOSOPHY

By

BHAGWATI PRASAD KASHYAP

to the

DEPARTMENT OF METALLURGICAL ENGINEERING

INDIAN INSTITUTE OF TECHNOLOGY KANPUR

DECEMBER, 1979

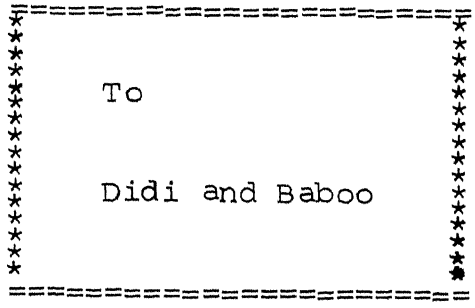
To
Didi and Baboo

CERTIFICATE

This is to certify that the present investigation 'EXPERIMENTAL CONSTITUTIVE RELATIONS FOR HIGH TEMPERATURE DEFORMATION OF THE Pb-Sn EUTECTIC ALLOY', has been carried out by Mr. Bhagwati Prasad Kashyap under my supervision and that it has not been submitted elsewhere for a degree.

G. S. Murty

(G. S. Murty)
Professor
Department of Metallurgical Engineering
Indian Institute of Technology
Kanpur, INDIA.

ACKNOWLEDGEMENTS

The author wishes to express his sincere and profound gratitude to Professor G.S. Murty for introducing him to the area of superplasticity and extending enthusiastic aid to bring this investigation in its present shape. His continuous encouragement and innumerable stimulating discussions throughout this study provided a pleasant academic environment that the author is fond of remembering.

The author is deeply indebted to Professor T.R. Ramachandran for valuable suggestions and providing some of the laboratory facilities required in this work. He is also grateful to Dr. V. Bansal for making his laboratory facilities accessible.

Sincere thanks are due to Drs. A.M. Gokhale and M.L. Vaidya for their advice during the period of this work, and to Vinod Nema for offering help in various computations involved in this work.

The author thankfully records the cooperation of Messrs. V. Kumar, M.M. Mungole, M.H. Rahman and staff of Physical- and Engineering Metallurgy laboratories for technical help and suggestions, and R.N. Srivastava for typing this dissertation.

The success of this work is due also, in no small part, to the inspiring support, expectations and patience shown by parents, brother Vijay, Mamaji Prof. Lokeshwar N. Verma and uncle Shri K.R. Madhariya, which made the author strive for higher studies.

B.P. Kashyap

TABLE OF CONTENTS

LIST OF TABLES

LIST OF FIGURES

FIGURE Page

FIGURE Page

FIGURE Page

SYNOPSIS

EXPERIMENTAL CONSTITUTIVE RELATIONS FOR HIGH TEMPERATURE DEFORMATION OF THE Pb-Sn EUTECTIC ALLOY

A Thesis Submitted
In Partial Fulfilment of the Requirements
For the Degree of
DOCTOR OF PHILOSOPHY
by

BHAGWATI PRASAD KASHYAP
to the
Department of Metallurgical Engineering
Indian Institute of Technology Kanpur
December 1979

High temperature deformation behaviour of the Pb-Sn eutectic alloy has been studied in this investigation over wider ranges of grain size and temperature than hitherto reported in the literature. Specimens with equiaxed grains in the grain size range of 9.7 to 32.0 μm were produced by means of deformation processing of the cast alloy along with different thermal treatments. The temperature range investigated was 0.65 to 0.97 T_m where T_m is melting point of the eutectic alloy in K. Mechanical testing was carried out in tension or compression by means of differential strain rate, constant cross head speed and stress relaxation tests. Internal stresses were measured by the stress-dip test. Microstructural observations were made both in longitudinal and transverse sections of specimens in order to correlate their flow behaviour with microstructures.

It is observed that heavy reduction of the cast alloy by extrusion or rolling results in mostly non-equiaxed microstructures. Specimens in the as worked state exhibit some degree of anisotropy in strength, strain hardening or softening upto some strain and microstructural instability during the subsequent mechanical testing. Because of this non-steady state nature of deformation, the mechanical behaviour of as worked alloy cannot be characterized in terms of a unique stress (σ) - strain rate ($\dot{\varepsilon}$) relation that is typical of high temperature steady state deformation behaviour. Even specimens with equiaxed grains in the as worked state did exhibit non-unique $\sigma - \dot{\varepsilon}$ relation. It is only after some prestrain in the subsequent tensile or compressive testing of the as worked alloy that steady state deformation is observed with unique $\sigma - \dot{\varepsilon}$ relation which is independent of the cross head speed and path through which a given strain rate is achieved. Thus, specimens having equiaxed grains of varying grain size obtained through prestraining of as worked specimens and suitable annealing treatments were used to study their steady state behaviour. In order to explore the deformation behaviour in the low strain rate range, stress relaxation test was also utilized. But anelastic effects are dominant in stress relaxation tests at high temperatures for smaller grain sizes. Due to this reason stress relaxation test is found to be feasible only in the case of relatively larger grain sizes.

Two regions are observed in the $\sigma - \dot{\varepsilon}$ plots of steady state deformation of specimens with equiaxed grains at various temperatures. The flow behaviour is rate sensitive at lower strain rates (region II) while rate insensitive flow is observed at higher strain rates (region III). In the superplastic region II, the strain rate sensitivity index m is 0.6 $\pm$ 0.1 for all grain sizes and temperatures studied, whereas the grain size exponent is 3.34 $\pm$ 0.23 which is independent of temperature. A noteworthy feature is that, in region II, two distinct activation energy (Q) values are observed depending on test temperature range. Below 0.89 T_m, the Q value is 44.7 $\pm$ 1.1 kJ/mole, while above this temperature, it is 81.1 $\pm$ 3.9 kJ/mole. The experimental constitutive equations of region II are not in agreement with any of the models of superplasticity proposed so far in the literature.

In region II, the magnitude of internal stress is found to be a significant fraction of the applied stress (σ) and its value is as high as 0.8 σ depending on strain rate, grain size and test temperature. The strain rate sensitivity index, grain size exponent and activation energy based on effective stress are $\simeq$ 0.82, $\simeq$ 2.8 and $\simeq$33.5 kJ/mole (below 0.89 T_m) respectively. The effective stress-strain rate data are in good agreement with the model of Ashby and Worrall for region II.

In region III, the observed m, Q and p,values are 0.09 ± 0.01, 100.0 ± 5.3 kJ/mole and 1.00 ± 0.72 respectively. These observations in region III are consistent with the prediction of Gifkins recovery creep model involving grain boundary sliding.

Deformation behaviour of specimens with banded structures as well as grains elongated in one or two directions were also investigated. Strength anisotropy, non-unique $\sigma - \dot{\varepsilon}$ relation and rapid microstructural instability are the observed features. As a consequence of superplastic deformation, the grains tend to become equiaxed.

CHAPTER I

INTRODUCTION

There are increasing demands to understand the limitations in the service life of many engineering components which exist in stressed state at elevated temperature. Some of the examples are nuclear fuel element cladding and gas turbine blades, in which the material behaviour is an integral part of overall performance of the structural component. Much of the existing fabric of our knowledge about the deformation of crystalline materials at elevated temperature derives from pure metals along several distinct lines which are being brought to form a complete theory [1-6]. The distinguishable feature of low and high temperature deformations is that any applied stress at a low enough temperature results in a unique strain however long we leave the stress on, which is no longer true when the test is done at high temperatures, especially above $0.5\ T_m$ where T_m is melting point in K. Any given stress held for some time will give increased strain with increased time at an elevated temperature. This time dependent deformation, called creep, is represented by a plot of strain as a function of time and is known as creep curve corresponding to the stress under consideration. Generally, the creep curves of annealed crystalline materials exhibit three stages.

These stages are: primary (or transient) creep in which the creep rate continuously decreases with time; steady-state (or secondary) creep having minimum and constant creep rate; and lastly, the tertiary creep in which the creep rate increases with time upto the point of fracture of the material. Besides applied stress, the temperature, as an independent variable, influences very much the nature of creep curve. The extent of these three stages thus depends on the stress and temperature.

1.1 STEADY STATE CREEP

Since the tertiary creep leads rapidly to large strains and structural failure, whereas transient creep is often rather small relative to the strains produced after long times from steady state behaviour, the major interest usually centres on the steady state region of creep for structural applications. Due to the fact that steady state creep rate increases markedly with both temperature and stress, it is of interest to know the exact relationship between these parameters along with the structural parameters, if any, that may influence the creep behaviour of materials. These relations between different parameters are known as constitutive equations, which are of immense use in engineering design against creep at elevated temperature in particular.

It is now well recognized that, except in the high stress range, the steady state creep rate ($\dot{\varepsilon}$) versus stress (σ) relation at any given temperature can be represented by a power law [e.g. (7)]

$$\dot{\varepsilon} = K \sigma^n \tag{1}$$

where K is a constant that depends on structure and temperature and n is the stress exponent. Further, creep being a thermally activated process, the steady state creep rate is expressed as a function of temperature (T) and stress by

$$\dot{\varepsilon} = K' \sigma^n \exp(-Q/kT) \tag{2}$$

where K' is a constant, Q is the activation energy for steady state creep, and k is Boltzmann constant. Further modifications in the creep relation have been suggested by incorporating the modulus of elasticity, temperature in the preexponential factor and diffusion coefficient in order to improve the correlation of secondary creep rates among the various metals and alloys [2, 8, 9]. Finally in the dimensionally correct form [2, 4, 10, 11], the most common empirical equation used in the creep literature for steady state creep region is

$$\dot{\varepsilon} = \frac{K'' D_o Eb}{kT} \left(\frac{\sigma}{E}\right)^n e^{-Q/kT} \tag{3}$$

Here E is the Young's modulus, $D_o e^{-Q/kT}$ is the diffusion coefficient, K'' and n are non-dimensional constants, and

b is burgers vector or atom size. Further improvements in the correlation of steady state creep data among the various metals and alloys may be achieved through the use of stacking fault energy as another useful parameter [12]. An alternate expression was suggested by Garofalo [13] to describe the steady state creep behaviour over the whole stress range. However, due to lack of physical basis for this type of expression, the power law relation is generally preferred in the lower stress range. More recently, a unified description of steady state creep has been proposed [14-16] which incorporates the effects of recovery and dislocation glide. In this approach, the glide process is driven by the effective stress, σ_e, which is the difference between the applied stress, σ, and the internal stress, σ_i. This approach leads to the constitutive equation in the form

$$\dot{\varepsilon} = \frac{K''' D_o Eb}{kT} \left(\frac{\sigma - \sigma_i}{E}\right)^{n'} e^{-Q'/kT} \qquad (4)$$

where n' and Q' represent the parameters based on effective stress ($\sigma_e = \sigma - \sigma_i$), such treatments have contributed towards a better insight into the nature of operative high temperature creep mechanisms. The consideration of effective stress or internal stress in place of applied stress is thermodynamically equivalent and the parameters of the constitutive equations based on applied, effective or internal stresses are interrelated [17] without any

additional assumptions on the mechanical equation of state. From the engineering convenience point of view also, eqn. (4) is attractive because of some advantages such as representation of steady state creep data by a single relation over the whole stress range especially for two phase materials [18-20].

1.2 GRAIN SIZE EFFECT IN STEADY STATE CREEP

The results of many investigations adequately support validity of eqn. (3) irrespective of the grain size, provided the grain size is above a critical level. For example, the steady state creep rates for single crystals of Al and Al-Mg alloys do not differ [21] by more than a factor of 2 from those of polycrystalline test specimens when tested over a wide range of stress. However, current evidence [22] suggests that below a critical grain size ($\sim$ 100 μm) the steady state creep rate increases with decreasing grain size at a given stress level. This dependency of creep behaviour on grain size is more significant below $\sim$ 10 μm. The steady state deformation of these fine grained materials encompasses an important regime of high temperature deformation known as superplasticity. In the region where the creep behaviour is dependent on grain size (d), the empirical relation governing the steady state creep behaviour is written in the non-dimensional form [11] as

$$\dot{\varepsilon} = \frac{A D_o Eb}{kT} \left(\frac{b}{d}\right)^p \left(\frac{\sigma}{E}\right)^n e^{-Q/kT} \qquad (5)$$

where p is the grain size exponent and A is a dimensionless constant. An important feature of the creep behaviour of fine grained materials is that log σ versus log $\dot{\varepsilon}$ plot exhibits a sigmoidal behaviour (Figure 1) with different set of parameters for each of the three regions. In region II, the strain rate sensitivity index 'm' (= 1/n) is significantly high leading to a viscous behaviour known as superplasticity. On the other hand, regions I and III exhibit relatively rate insensitive flow behaviour characteristic of the usual plastic deformation. Identification of the characteristics of different regions along with the operative mechanisms of flow is an objective that is being actively pursued by several workers, as is evident from the current literature. Several reviews [23-31] on the various aspects of deformation behaviour of fine grained materials exist in the literature. Some of the observations pertaining to different regions of the stress-strain rate plots as well as the mechanisms of flow that have been put forward to account for these features are controversial and further work needs to be done for a better understanding of the flow behaviour of these fine grained materials. Since the present investigation is concerned with relatively fine grained materials, some of these aspects pertaining to the

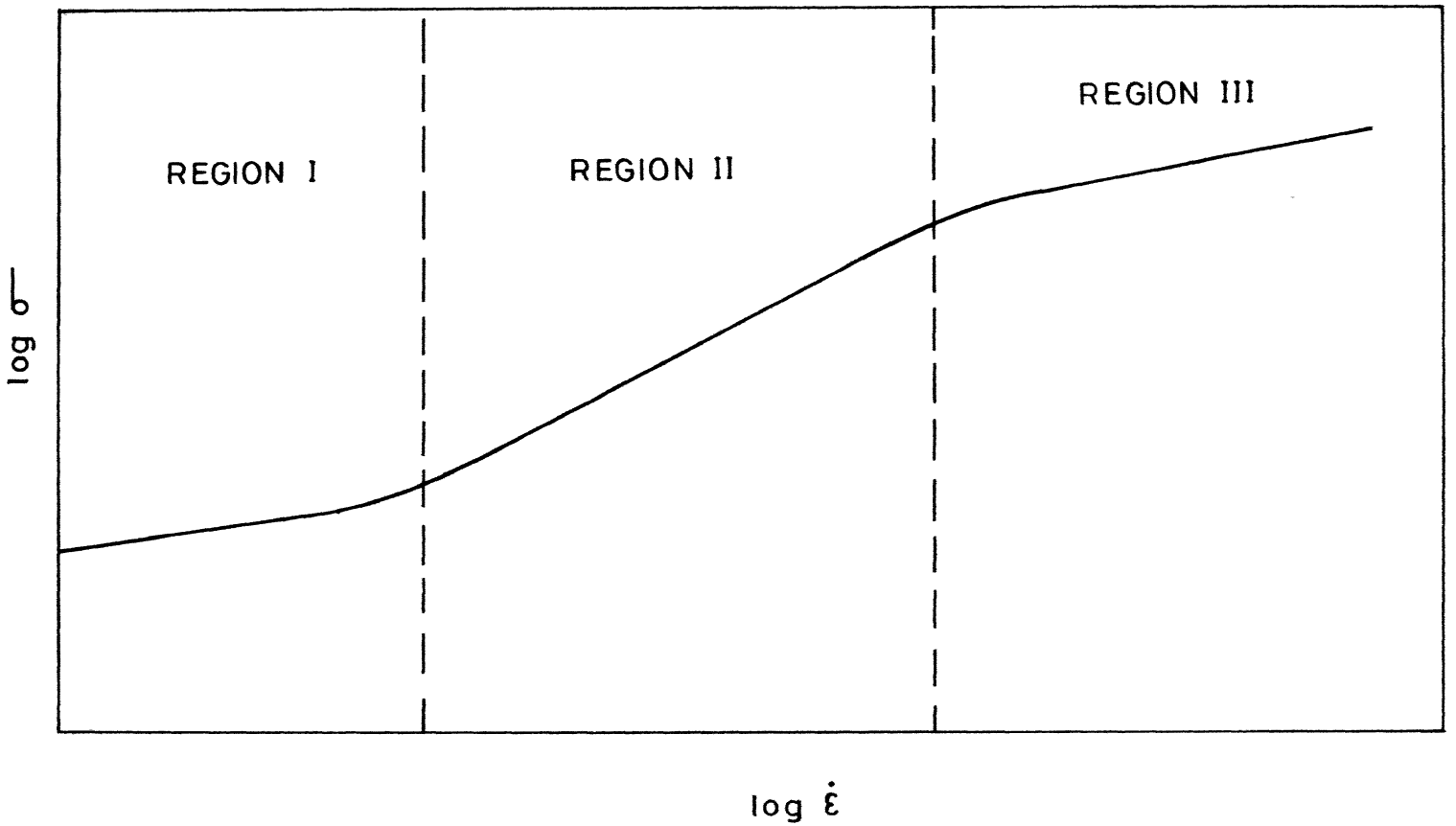

FIG. 1 A SCHEMATIC PLOT OF $\sigma - \dot{\varepsilon}$ BEHAVIOUR FOR STEADY STATE DEFORMATION OF FINE GRAINED MATERIALS AT ELEVATED TEMPERATURE

high temperature steady state deformation of only the fine grained materials are considered in the subsequent sections.

1.3 MECHANISMS OF STEADY STATE FLOW IN FINE GRAINED MATERIALS

In view of their relevance to the present study, various proposed mechanisms of steady state flow in fine grained materials are being presented here. Due to the fascinating phenomenon of superplasticity, there has been a greater interest in exploring the mechanisms of flow in region II in comparison to the other two regions of the deformation behaviour of fine grained materials. The mechanisms of superplastic flow are considered first and then the mechanisms of other regions, primarily from the viewpoint of constitutive equations. Recently, Gifkins and Langdon [32] have summarized the various mechanisms of superplasticity along with critical comments on the drawbacks of various models. One common aspect of all these theories of superplasticity is that grain boundary sliding plays a significant role in region II. Although mechanisms based on direct dislocation movement have also been proposed [33, 34] for superplasticity, the overall experimental observations do not seem to favor such mechanisms.

1.3.1 Diffusional Flow (N-H and Coble Creep Mechanisms)

This mechanism is based on stress directed flow of vacancies either through the grains or along the grain

boundaries. The grain boundaries perpendicular to the tensile axis act as sources of vacancies during tensile loading and the counter flow of atoms takes place into these boundaries from those parallel to the tensile axis leading to grain elongation in the direction of loading. In the Nabarro [35] - Herring [36] mechanism, the diffusion path is through the body of the grain, while in the Coble [37] mechanism it is along the grain boundaries.

It is now well recognized that pure diffusional flow is inadequate in giving rise to large plastic strain in polycrystalline materials other than the bamboo-type grain structures. Grain boundary sliding is an inevitable accompanying mode [38-42] of the diffusional flow and whichever of these two is slower under a given set of conditions, that one could be the rate controlling mechanism.

1.3.2 The Theories of Ball and Hutchison, and Mukherjee

These theories are based on grain boundary sliding with accommodation by dislocation motion. According to Ball and Hutchison [43], a group of grains slides as a unit along some common direction. A grain, which does not have its boundary along the common sliding direction and is across the sliding path of the group, acts as an obstacle to the sliding process. This leads to stress concentration resulting in emission of dislocations from triple points of the blocking grain and the dislocations move to the

opposite boundary until the back stress prevents further activation of the source and sliding stops. The leading dislocation in the pile up then climbs into and along the grain boundary. This results in further sliding at a rate governed by the kinetics of dislocation climb along grain boundaries to annihilation sites. Mukherjee [21, 44] also developed a similar theory but the dislocations are assumed to emanate from ledges in the sliding boundary and the specific requirement of the movement of groups of grains is not necessary.

1.3.3 The Theory of Ashby and Verrall

The Ashby and Verrall's theory [45] is based on grain boundary sliding with diffusional accommodation through the lattice as well as grain boundaries. The mechanism is derived from a grain switching event which leads to the retention of essentially equiaxed grain structure during superplastic deformation.

A group of four regular hexagonal grains in a two dimensional model is considered. These grains through a neighbor-switching event move from the initial state to a final one with an identical grain shape. In this process, the grains undergo accommodation strains and translate past each other by grain boundary sliding. This gives a true strain of 0.55 as a result of this switching event. A constitutive equation based on this mechanism is derived

and it is similar to the classical Nabarro-Herring-Coble equation but gives rise to a threshold stress for deformation and strain rates that are an order of magnitude faster. Because of the threshold stress, this mechanism predicts a sigmoidal relationship between stress and strain rate.

1.3.4 The Theory of Gifkins [46]

The roles of grain-boundary sliding and other creep mechanisms in fine grain superplasticity are coupled to develop a model based on the division of grains into their central "cores" and peripheral "mantles". Grain boundary sliding and its accommodation are limited to the mantle. This description is used to develop equations for creep rate in the different regimes.

1.3.5 The Theory of Gittus [47, 48]

This theory is developed to explain superplastic flow particularly in two-phase materials in view of the fact that most of the superplastic materials are two-phase alloys. It combines elements from the theories of both Ashby and Verrall [45] and Gifkins [46]. It is postulated that boundary dislocations, piled up in dislocation-interphase boundaries (IPBs) climb away into disordered regions of the IPB. Sliding then occurs at an IPB as dislocations glide toward the head of the pile up to replace those which have climbed into disordered regions of the boundary. An

energy barrier which would otherwise render sliding virtually impossible on dislocations - IPBs can be largely eliminated if the dislocations glide in pairs. This disorder (anti-phase domain boundary) which is created by the passage of the leading dislocation is then repaired by passage of its successor. A constitutive equation is derived on the basis of this mechanism. A threshold stress for flow is estimated with the assumption that it arises because of the interaction of glissile IPB superdislocations with grain boundary ledges. Furthermore, the activation energy for flow is predicted to be that for IPB diffusion.

1.3.6 The Theory of Padmanabhan [49]

This theory is derived for materials with ultrafine grains from the K $\hat{e}$'s model [50] in which plastic flow occurs by the shearing of groups of atoms in the boundary plane, so that there is interchange of atoms and vacancies leading to a liquid like Newtonian viscous flow. This mechanism is primarily based on the premise that 100% contribution to superplastic flow can arise from grain boundary sliding without the need of any accommodation process at the grain corners or grain boundary ledges. It is shown that the stress exponent n, in general, is a function of applied stress, grain size and temperature.

The parameters of the constitutive equations based on various mechanisms relevant to superplastic flow are summarized in Table 1.

TABLE 1

Parameters of the Constitutive Equations Based on Different Mechanisms for Region II

Mechanism	n	p	Q	A*
Nabarro-Herring diffusional flow	1	2	Q_l	13
Coble diffusional flow	1	3	Q_{gb}	48
Ball and Hutchison	2	2	Q_{gb}	100
Mukherjee	2	2	Q_{gb}	75-150
Ashby and Verrall	Limiting value of 1	2-3	$Q_{gb}-Q_l$	70
Gifkins	Limiting value of 1	2	Q_{gb}	64
Gittus	Limiting value of 2	2	Q_{IPB}	53.4
Padmanabhan	Limiting value of 1	2	Q_{gb}	-

* Values of A in eqn. (5) with shear modulus G in place of Young's modulus E.

1.3.7 Mechanisms in Regions I and III

(a) Region I

Although some controversy about mechanisms in region I exists, not much theoretical considerations have been invoked due to limited experimental evidence. Many investigators [24, 51, 52] suggested the presence of threshold stress, σ_o, to account for low strain rate sensitivity values in this region. It is assumed that $\dot{\varepsilon}$ is a function of $(\sigma - \sigma_o)$, the slope of the $\log \sigma - \log \dot{\varepsilon}$ curve ought to decrease asymptotically towards zero when σ tends toward σ_o. The mechanism of Ashby and Verrall [45] predicts the threshold stress for flow as a consequence of the increase in grain boundary area during the neighbour switching events of grains. Gittus [47, 48] has suggested that the grain boundary ledges can give rise to a threshold stress during grain boundary sliding. An alternative theory [46, 53] assumes the existence of a thermally activated mechanism in region I. It is suggested that this is GBS, rate controlled by barriers inherent in grain boundary structure and accommodation at triple edges occurs faster than GBS. Such a mechanism would give a variable value of n at low stresses and this, it has been suggested might bias values of activation energy and of the grain size dependence of strain rate determined using a high constant value of n. In this mechanism, the activation energy for flow in region I is

considered to be smaller than that of region II whereas Mohamed and Langdon [54] have observed that the activation energy in region I is equal to that of lattice diffusion in the Pb-Sn eutectic alloy.

(b) Region III

There is general agreement on the deformation in region III. In general, high temperature dislocation climb controlled creep [10] is believed to be the dominating process which can be described by equation (3). Typical values that represent such a mechanism are n = 4 to 5 and Q is the lattice diffusion activation energy. Such a mechanism predicts flow behaviour that is independent of grain size. But due to some grain size dependency of creep behaviour in fine grained materials, some empirical relation has been developed by Barrett, Lytton and Sherby [22] in order to account for this behaviour. A theoretical treatment has also been given by Gifkins [55] incorporating the grain size effect. In this model, the total creep rate is considered to be the cumulative effect of climb controlled creep, grain boundary sliding and its accommodation by the formation of triple point folds.

1.4 EXPERIMENTAL CONSTITUTIVE EQUATIONS IN RELATION TO THE MECHANISMS

It can be noted from the previous section that several mechanisms have been proposed for the high temperature

deformation of fine grained superplastic materials. All these mechanisms are primarily based on simplified conditions of the steady state power law type of creep deformation with the incorporation of the grain size effect. In assessing the applicability of these mechanisms to superplastic flow of various materials, it is all the more important to consider whether the experimental conditions conform to the idealized situations for which the mechanisms have been proposed. If not, it is of interest to know as to what extent the real conditions differ from the idealized ones. Some of these aspects are considered here in the context of assessing the operative mechanisms in the high temperature steady state deformation of fine grained materials.

1.4.1 Two Phase Nature of Microstructures

Superplastic materials are generally eutectic and eutectoid alloys having a microduplex structure, although single phase materials [56-58] have also been found to exhibit superplastic behaviour. Recently Gittus [48] has reviewed high temperature deformation of two phase structures and Brown [59] has critically summarized the agreements, controversies and need of formulating new principles governing the deformation of 2-phase alloys. Nearly all the experimental results, on these materials, show a number of common characteristics. On the other hand, it has been noticed that in the two phase systems exhibiting

superplasticity the structure and deformation behaviour of existing phases differ appreciably [60-62]. This can be realized from grain boundary sliding (GBS) data in the superplastic Pb-Sn eutectic [62] which shows largest sliding offsets at the Sn-Sn intercrystalline boundaries, small offsets at the Pb-Sn interphase boundaries, and negligible sliding at Pb-Pb intercrystalline boundaries. Unfortunately, except the model proposed by Gittus, the theories developed to explain the characteristics of superplasticity are not based on the two phase systems. Instead they are based on idealized single phase systems having an equiaxed structure.

1.4.2 Non-steady State Deformation and Microstructural Instability

The various proposed mechanisms deal with the steady state deformation where the flow stress is a unique function of steady state strain rate, temperature and grain size. This implies that the strain parameter does not have any effect on the stress-strain rate behaviour. In other words, the steady state nature of deformation and the applicability of the proposed mechanisms are valid to the extent that the structure remains stable, beyond which the microstructural instability and the accompanying strain effects can become significant enough to invalidate the steady state mechanisms. If the stress-strain rate data of fine grained materials are being obtained by the

differential strain rate test [63], the above aspects are to be examined carefully in order to assess whether the data thus obtained would represent steady state or not. Significant difference [64] in the values of the strain rate sensitivity index obtained from the same data of the differential strain rate test is an example of the nonvalidity of steady state approximation. In some of the reported studies, there have been significant microstructural instabilities along with the accompanying effects, as reviewed by Suery and Baudelet [65]. These microstructural changes are briefly considered below.

Many superplastic alloys consist of two phases where each phase exists as a separate grain. In some cases, there is clustering of the grains of each phase along the direction of mechanical working. In such cases, there is a tendency for the second phase grains to separate and to become rounder. The effect of this transition is that the stress level may continuously change with strain.

The fine grains subjected to deformation at elevated temperature are likely to suffer from grain coarsening. Experimental indication is that there are large variations in the size of the grains or phases with strain, strain rate and with temperature. For example, within one cycle of differential strain rate test, where the specimen elongation was no more than 30%, the fine equiaxed grains of Pb-Sn eutectic increased in size by a factor

of 2.35 at 170°C [66]. In another study [67] superplastic deformation of as rolled Zn-0.4% Al alloy has been reported to exhibit an increase in grain size by a factor of 8. This grain coarsening leads to an increase in stress level and decrease in m value. These microstructural changes can influence the $\sigma - \dot{\varepsilon}$ behaviour to some extent and in some cases the above two types of microstructural changes can lead to the appearance of steady state deformation due to the cancellation of mutual effects on flow stress [68]. Mukherjee [21] in a review of high temperature creep, remarks that in some cases microstructural instabilities lead to abnormally high creep rates. Occasionally investigators neglected to comment or even check on these possibilities when reporting their data. Edington et al. [30] site examples that m depends on strain in a complex way due to structural change of the material. Since parameters of the experimental constitutive equation are calculated from collection of $\sigma - \dot{\varepsilon}$ data, these values are likely to be affected because of this reason. It has even been argued [65, 69] that the sigmoidal shape of the log σ - log $\dot{\varepsilon}$ curves and the presence of region I are due to unstable microstructures rather than the true behaviour at constant microstructure.

1.4.3 Non-uniqueness in $\sigma - \dot{\varepsilon}$ Relationship

Constitutive equations with constituents involved therein are generally based on the assumption of unique $\sigma - \dot{\varepsilon}$ relationship for a given temperature and grain size. Recently, a few experimental results have appeared in the literature which point out non-uniqueness in the $\sigma - \dot{\varepsilon}$ relationship. If this were so, the previous simpler constitutive equations would be inadequate in such cases. A brief account of this aspect is presented below.

(a) Effect of test parameters

The uniqueness in $\sigma - \dot{\varepsilon}$ relationship implies that for any strain rate, there will be one unique value of stress, which will be independent of the path followed in reaching that strain rate. Padmanabhan et al. [70] have studied the effect of "Dynamic" mechanical history on stress-strain rate relations during superplastic flow in the Pb-Sn-Cd ternary eutectic alloy. In this work, a selected strain rate was reached by deforming a tensile sample from gauge length l_1 to l_2, l_2 to l_3 and l_3 to a higher level, at cross head speeds V_1, V_2 and V_3 respectively, such that the initial strain rate is the same in each case. It is found that the stress is not a single valued function of strain rate. Instead, the stress corresponding to a given strain-rate increased by a factor of more than two with increasing cross-head velocity although the grain growth was observed to be insignificant.

(b) Need of other microstructural parameters

In a study on superplastic Pb-Sn eutectic [71] no correlation between the mechanical behaviour and grain size was evident when specimens of similar grain size obtained by different mechanical and thermal treatments of the cast alloy were compared. Similar observations were also made by Paton and Hamilton [72] who have studied superplastic behaviour of Ti-6Al-4V alloys. From a comparison of $\sigma - \dot{\varepsilon}$ data of specimens of different grain sizes, it is found that the flow stress of larger grain size is below that of smaller grain size in some strain rate range. It is to note that in this work some specimens were having grains of equiaxed shape, while others had non-equiaxed grains. If the average grain size is used in such cases, the non-uniqueness in $\sigma - \dot{\varepsilon}$ relationship suggests that a single parameter such as grain size cannot adequately characterize the structure for the purpose of incorporating it in the constitutive equation. These observations suggest that other structural parameters such as volume fractions of two phases, grain aspect ratio, grain size distribution and crystallographic texture may also influence superplasticity and therefore these parameters may have to be considered in obtaining the appropriate constitutive equation in general.

1.5 OBJECTIVES OF THE PRESENT STUDY

It is thus evident that there are several limitations in the determination of experimental constitutive relations from the viewpoint of assessing the high temperature deformation mechanisms of fine grained materials. In order to obtain reliable experimental data for the purpose of evaluating the operative mechanisms, it is advantageous and desirable to consider relatively simpler experimental conditions first before dealing with more complicated situations. It is with this kind of general aim that the present work has been taken up. Although it is desirable to study a single phase material, Pb-Sn eutectic has been chosen because of the ease in maintaining finer grain size as in most of the studies of superplasticity. Special attention has been paid towards achieving the microstructural stability, the steady state deformation and the uniqueness of stress-strain rate relation at any given temperature. The parameters of the constitutive equation governing the steady state deformation have been determined experimentally over wider ranges of equiaxed grain size and temperature than hitherto reported in the literature. In addition to the differential strain rate test, stress relaxation test has been utilized to cover lower strain rate range upto a minimum of 10^{-7} sec^{-1}. Internal stress measurements are also made by the stress dip test in order to consider the

alternate constitutive relations in terms of the effective stress with the aim of achieving better insight into the operative mechanisms. Finally, deformation behaviour of specimens having banded and elongated grain structures that are deliberately produced by special processing, is also studied with a view to compare their behaviour with that of equiaxed structures.

CHAPTER II

EXPERIMENTAL PROCEDURE

2.1 ALLOY PREPARATION

In the present investigation lead-tin eutectic alloy of nominal composition 61.9 wt. % Sn and 38.1 wt. % Pb was prepared by making use of tin and lead, both of 99.99% purity.

At a time about 2.5 kg of charge with required amount of lead and tin was vacuum sealed in a 75 mm diameter pyrex tube. Melting was done by heating the charge in a tubular furnace to about 450°C and maintaining it there for ~1 hr. In the molten state the alloy was mixed thoroughly by turning the pyrex tube upside down. The melt at this stage was allowed to solidify in the pyrex tube.

There was pipe formation in the ingot thus obtained and therefore remelting with following modification, as a subsequent step, was adopted. The ingot was remelted in a pyrex glass container in air with intermittent stirring. The molten alloy was cast in a 75 mm diameter pyrex tube whose bottom end was closed tightly by means of a graphite block in order to provide a heat sink at the bottom of the mould. The pipe formation in the casting could thus be eliminated by directional solidification resulting from heat flow through this block. In a few cases, casting was

done in a smaller diameter pyrex tube. In some cases Pb-Sn eutectic melt obtained from the above procedure was cast in a 100 mm x 50 mm rectangular mild steel mould to obtain a flat ingot. Piping was eliminated by maintaining a hot top through heating.

The ingots thus obtained were homogenized at about 160°C for 72 hr in a silicone oil bath heated electrically by means of a mantle heater. The final composition of the alloy was checked by chemical analysis and found to be 61 wt. % Sn and 39 wt. % Pb.

2.2 MECHANICAL WORKING PROCESSES

The cast ingots were lightly machined to remove surface irregularities and pipe if any. These were then processed by one or more of the processes: extrusion, rolling, forging and swaging. Deformation processing was through the extrusion route in most of the cases.

(a) Extrusion

The cylindrical ingots of 75 mm diameter were extruded to 12.5 mm diameter (extrusion ratio = 36) either in one or two steps. In a few cases, rods were obtained with a lower extrusion ratio of the cast ingots. The extrusion was done at room temperature through specially fabricated dies made of high C - high Cr steel.

(b) Rolling

Flat ingots were rolled either at 100°C or at room temperature in several passes. The final thickness was 5 mm equivalent to a reduction in area of cross-section of $\sim$ 82%.

(c) Forging

An ingot of 50 mm diameter was forged at 100°C in different directions into a rod of 12.5 mm diameter.

(d) Swaging

Some of the rods obtained from the above processing methods were further reduced or given final finishing by swaging. In some cases swaging was done to a final diameter of 6.5 mm, yielding a total equivalent extrusion ratio of $\sim$133.

2.3 THERMO-MECHANICAL TREATMENTS TO GET DESIRED MICROSTRUCTURES

The processing methods were aimed to get controlled microstructures. This involved a combination of deformation processing methods given in section 2.2 with some heat treatment. The major processing was towards getting equi-axed microstructures with a large range of grain size. Microstructures typical of as worked state as well as specially designed microstructures were also incorporated.

2.3.1 Equiaxed Microstructures

As worked materials were machined to get samples of required size. These samples were deformed to $\sim$ 30% nominal tensile strain at 148°C at a constant cross head speed of 0.05 cm/mt using an Instron machine. Hereafter, this deformation will be called standard prior deformation and it is widely used in the present study due to its importance, which is discussed in Chapter III. Annealing of these samples was done at 160°C in an electrically heated silicone oil bath for varying periods upto a maximum of 240 days. The temperature was controlled within $\pm$1°C. In some cases standard prior deformation was given after the annealing treatment. To eliminate bending or warpage of tensile samples by their own weight during the long annealing treatment, suitable mild steel base plates were used for supporting the gauge and shoulder sections of specimens.

In a few cases, specimens in as worked state were directly annealed for a long time to get equiaxed grains of large size. On the other hand, some specimens having equiaxed grains in the as worked state itself were also obtained by alternate working in different directions. In this manner, equiaxed microstructures were also achieved without annealing or standard prior deformation of the worked alloy.

2.3.2 Non-equiaxed Microstructures

(a) Banded structures

After extrusion from 75 mm diameter to 47 mm diameter, the ingot was annealed at ~ 170°C for nearly 30 days in a silicone oil bath. This annealed ingot with large grains (~20 μm) was extruded further to 12.5 mm diameter rods. The rods thus obtained were swaged to 11.5 mm and 7.5 mm diameter rods. All the above working operations were done at room temperature. Specimens processed in this manner exhibited banded structures.

(b) Elongated grains

12.5 mm diameter rods obtained from extrusion of 75 mm diameter ingot were swaged further to a final diameter of 7.5 mm. This operation resulted in a microstructure with linear orientation [73] having grain elongation in the longitudinal direction.

Flat tensile samples were obtained with elongation of grains in two directions, termed as planar-linear orientation [73], in the following manner. The flat ingot was rolled from 50 mm to 25 mm thickness at room temperature and annealed at ~ 160°C for 30 days. This large grained block was further rolled to 5 mm thickness at room temperature. The resulting microstructure was consisting of grains elongated in two directions.

2.4 MECHANICAL TESTING

All the tests were done on a Floor Model Instron Universal Testing Machine. While most of the tests were performed in tension making use of round and flat samples, compression samples were used mainly to check strength anisotropy for different microstructures. True stress (σ), true strain (ε) and true strain rate ($\dot{\varepsilon}$) were calculated from the load-time record during deformation assuming uniform deformation along the gauge length. Special care was taken in maintaining precision of the load measurement in view of the small loads involved especially for flow at high test temperatures and low strain rates in samples of smaller grain size.

2.4.1(a) Tensile Test

Typical dimensions of flat and round tensile samples are given in Figure 2. In a few cases, round samples of gauge length in the range of 19 mm to 50 mm with diameter 4 mm or 8 mm were used. Tensile specimens were machined along the length of bars in the case of round specimens and along the rolling direction in the case of flat specimens. In the latter case, samples were also obtained in the directions at 45° and 90° to the rolling direction.

The grip assembly for round samples was similar to that used in a Hounsfield tensometer. In the case of

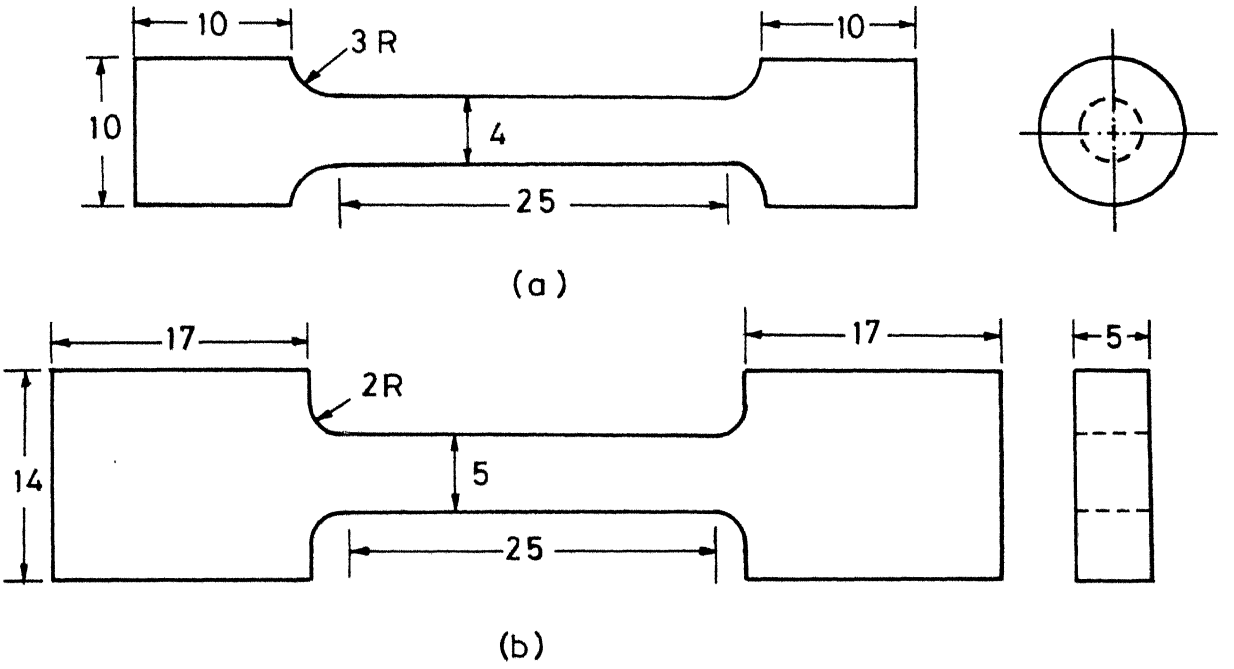

FIG. 2 TENSILE TEST SPECIMENS (a) ROUND (b) FLAT

flat specimens, care was taken in designing the grips in such a way that there is no possibility of slippage of specimen in the grips during loading. Tensile tests were carried out at temperatures from 25°C to 170°C. A silicone oil bath heated electrically in a mantle heater with a capability to control the test temperature with ± 1°C accuracy was used to attain the desired test temperature. A water bath with the required temperature adjustment was used for tests at 25°C.

(b) Compression test

Compression specimens in three orientations, with respect to the working direction, were machined from rods having desired microstructures. These orientations are 0°, 45° and 90° relative to the rod axis. Samples of 9 mm length and 6 mm diameter were used for compression testing. The friction between the end faces of the sample and the compression plates of the machine was minimized by using a lubricant. All the compression tests were done at room temperature.

2.4.1.1 Constant cross head speed test

In order to study the effect of large strain on the flow stress and microstructure it is desirable to conduct constant strain rate tests in the case of a strain rate sensitive material like the Pb-Sn eutectic. Due to lack of provision for maintaining constant strain rate,

constant cross head speed test was adopted for this purpose. After a sufficiently large elongation of the sample in these tests, the cross head speed was changed to the next higher level so that once again strain rate is closer to the initial one.

The true stress data obtained from these tests as a function of strain represent a situation of continuous decrease in strain rate. These data were corrected for constant strain rate making use of the strain rate sensitivity index (m) of the specimen obtained from a differential strain rate test with the assumption of constant 'm'.

2.4.1.2 Differential strain-rate test

Differential strain rate method [63] was adopted to obtain stress-strain rate data of different specimens at various temperatures. Starting with the lowest cross head speed of 0.005 cm/mt, the speed was successively increased to the next higher level to cover the total range of available speeds upto a maximum of 5 cm/mt. The load corresponding to each of the cross head speeds was thus recorded, from which, the true stress vs. true strain-rate data were calculated. In order to minimize the strain effects, the total strain accummulated in one cycle covering the whole range of cross head speeds is kept to a minimum level, where significant strain effects were noticed.

The strain rate sensitivity index 'm' was calculated either from the slope of log σ - log $\dot{\varepsilon}$ plot or in some cases from the relation

$$m = \frac{\log P_2/P_1}{\log V_2/V_1} \qquad (6)$$

where P_1 and P_2 are steady state loads corresponding to cross head speeds V_1 and V_2 respectively.

2.4.1.3 Stress relaxation test

Stress relaxation test was used to obtain $\sigma - \dot{\varepsilon}$ data at a lower strain rate range than that possible by the differential strain-rate test. Specimens were deformed at a selected cross head speed to steady state stress level corresponding to that strain rate. Having reached the steady state stress level, the cross head was then arrested and simultaneously the chart speed was suitably increased to record relaxation of load with time. The load-time recording in the relaxation test was continued until the rate of relaxation was immeasurably slow. The load was monitored upto a maximum period of 45 minutes. It was found necessary to first load the sample to a few percent strain at a constant cross head speed before the cross head is arrested for recording the load relaxation as a function of time in order to obtain reproducible stress relaxation data. Hence this practice was adopted in all cases of obtaining the stress relaxation data. The

stress-relaxation tests repeated several times under the same testing conditions were found to give the same $\sigma - \dot{\varepsilon}$ behaviour and thus the reliability of stress relaxation data was ensured.

$\sigma - \dot{\varepsilon}$ data at different points of stress relaxation curve were calculated from the load versus time curves of the relaxation tests. True stress at any point on the relaxation curve was calculated by dividing the load (P) at that point by the area of cross-section (A') of the sample just at the start of the relaxation test. The $\dot{\varepsilon}$ at these points was calculated from [74]

$$\dot{\varepsilon} = - M \dot{\sigma} \tag{7}$$

where $\dot{\sigma} \left(= \frac{1}{A} \frac{dP}{dt}\right)$ is stress rate and M is the elastic constant of the machine and specimen assembly. It is given by:

$$M = \frac{1}{E} + \frac{A'}{LS} \tag{8}$$

where E is the Young's modulus, L is the gauge length of the sample, and S is the machine stiffness which was evaluated by using a mild steel dummy sample for each combination of load cell and test assembly.

(a) Determination of machine stiffness (S)

A mild steel tensile sample of standard size was deformed at a selected cross head speed to a load well

within the elastic region of this specimen. The slope of the load-time record was measured. Knowing the area of cross section, A'_d, and gauge length, L_d, of the dummy mild steel sample, M_d was evaluated using

$$M_d = \frac{A'_d}{L_d S'} \qquad (9)$$

Here $S' = \frac{1}{v} \cdot \left(\frac{dP}{dt}\right)$ where v is the cross head speed. Substituting this M_d value for mild steel sample and the gauge length (L_d), area of cross-section (A'_d) and Young's modulus of mild steel in the equation (8), the stiffness of the machine, S, was calculated. This procedure of determining the quantity S was repeated for several cross head speeds and test temperatures to check for the constancy of stiffness of the machine. It was found to be independent of cross-head speed and test temperature in the ranges of interest to the present study. Since two load cells of 5000 kg and 50 kg capacity were employed in these experiments, the machine stiffness with each of these load cells was determined. The stiffness thus obtained for 5000 kg load cell is 3327 kg/cm and for 50 kg load cell is 1740 kg/cm.

(b) Estimation of Young's modulus values at different temperature

E values for the Pb-Sn eutectic alloy at different temperatures are not available in the literature. At 20°C the experimental E value for this alloy is

reported to be 21 x 10^3 MPa [75]. This value is different from E calculated by making use of the data of pure Pb and pure Sn and using the rule of mixtures (Vegard's law)[76]. Because of this difference between the experimental value and that calculated from pure Sn and Pb data at 20°C, the Young's moduli of the eutectic at other temperatures have not been calculated explicitly from those of pure elements. A better approximation to evaluate the Young's modulus for this alloy at different temperatures is through the use of the experimental value at 20°C as a base and then applying the temperature correction. The rate of change in E of the eutectic alloy with respect to temperature (dE/dT) is obtained from those [77] of pure Sn and Pb by making use of Vegard's law. By this method, the E value, in MPa, at any temperature was found to be

$$E_T = E_{293} - 77.82\ (T - 293) \qquad (10)$$

where E_T and E_{293} are the Young's moduli in MPa at the temperatures T and 293 K respectively.

2.4.2 Internal Stress Measurements by the Stress-Dip Test [78]

Tensile samples were deformed to steady state stress level corresponding to a selected cross head speed at each test temperature. Once the steady state was reached the cross head was stopped and instantaneous

unloading with simultaneous increase in chart speed to 50 cm/mt was done. After unloading to a certain load level, the load relaxation curve was recorded for a short time and the sign of the relaxation rate was noted. The specimen was once again loaded to the steady state stress level before unloading it to another level of stress to note the sign of relaxation rate. This process of unloading to different loads from the same steady state stress level was repeated till the sign of relaxation rate reversed. The load level at which the relaxation rate was nearly equal to zero for a short while was used for calculating the internal stress, whereas the load from which unloading was done was used to estimate applied stress. The difference between applied and internal stress was taken as effective stress. All these three stresses correspond to the steady state strain rate at which the specimen was deformed before unloading.

This procedure was repeated at various cross head speeds to get values of applied stress, internal stress and effective stress as a function of strain rate. The internal stress data were also obtained at various test temperatures.

2.5 METALLOGRAPHY

Metallographic samples were prepared by starting with flat surfaces obtained by light machining of the specimens. In some cases where the specimen sizes were too

small to handle, cold mounting of the specimens on perspex block, making use of chloroform which is a solvent for perspex, was adopted. This method was found to be the most convenient one for mounting this soft material without damaging the structure in the process of mounting.

The surface of the metallographic samples to be examined was scraped with a sharp edge of a glass slide to get a smooth shiny surface. This operation eliminated the normal step of using series of emery papers in conventional mechanical polishing. Further polishing was done on a polishing wheel with suspension of fine alumina powder.

The etchant used was a mixture of glycerol, acetic acid and nitric acid in the proportion of 4 : 1 : 1 respectively. The use of fresh etchant was found to give better microstructural details. Although Pb-rich (black) and tin-rich (white) phases could be seen with a relatively short etching time, longer etching time of about 60 secs was necessary to reveal the grain boundaries (white/white) in tin-rich phase.

The grain size measurement was done by using the linear-intercept method [79]. On micrographs showing nearly equiaxed microstructures (grain aspect ratio of 1 to 1.2) random lines were drawn and the number of intercepts with phase boundaries and grain boundaries was counted. The proportion of grain boundaries in the tin-rich phase

was much less as compared to the interphase boundaries. No distinction between interphase boundaries and grain boundaries was made in estimation of the grain size. Also the sizes of Pb-rich phase and Sn-rich phase were not significantly different. Hence the grain size measurement was not aimed at bringing separate measurements of these phases in each case. The intercept length in the case of equiaxed grains was converted to grain size [43] by multiplying with a factor of 1.74. When the grain shape was non-equiaxed, i.e. grain aspect ratio $\gtrsim 1.2$, lines on micrographs were drawn in two mutually perpendicular directions such that these lines are parallel to the major and minor axes of oriented grains. The larger intercept length in longitudinal section has been represented by $l_{\parallel}$ and the smaller one has been represented by $l_{\perp}$. The intercept length for equiaxed grains has been represented by l with suffixes L and T for longitudinal and transverse sections; the overall average intercept length is represented by l. The grain size is denoted by d in place of notation l for intercept length. In each case more than 300 intercepts were counted and the average size is reported with a 95% confidence limit. For equiaxed grains, shown by micrographs of both longitudinal and transverse sections, the intercepts counted in both sections were combined to evaluate the mean grain size, d.

CHAPTER III

RESULTS

Experimental results are divided into three broad aspects of high temperature deformation. These are: selection of suitable processing method including checking validity of unique stress versus strain rate relation for high temperature deformation, establishing constitutive equations for a wide range of grain size and temperature and finally the behaviour of specimens having banded structures and elongated grains.

3.1 PROCESSING HISTORY EFFECTS ON STRUCTURE AND PROPERTIES

Mechanical behaviour was studied in relation to the microstructure with the aim of assessing the role of processing in affecting the microstructure and thereby the mechanical properties.

3.1.1 Effect of Degree of Working

To study the effect of reduction in area by processing of cast ingots, initial diameters of 25, 50 and 75 mm were selected. These ingots were processed at room temperature by extrusion and swaging. The first two ingots were reduced to 10.5 mm diameter rods giving 82.4 and 95.6 percent reduction in area (RA) respectively, while the

75 mm diameter ingot was reduced to 10.5 mm and subsequently to 6.5 mm to get rods of 98 and 99.2% RA respectively.

Microstructures of longitudinal and transverse sections of these rods were observed. It was found that the degree of homogeneity and grain aspect ratio increase with increasing amount of working over 82.4% RA. In other words, within the range studied, increasing amount of working changes the microstructure towards elongated grains with smaller interphase spacings and greater degree of homogeneity, while microstructures in transverse section are equiaxed. The grain aspect ratio for specimens subjected to 98% RA and 99.2% RA were 1.8 and 3.2 respectively.

Tensile specimens from 98 and 99.2% RA were tested at a constant cross head speed of 0.05 cm/mt up to 30% elongation (nominal strain) at 148°C. Both of these specimens showed some tendency towards strain hardening. The flow stress of the former was 0.78 MPa as compared to 1.60 MPa for the latter at a nominal strain of 11% ($\dot{\varepsilon} = 2.5 \times 10^{-4}$ sec^{-1}).

The effect of degree of prior mechanical working on $\sigma - \dot{\varepsilon}$ data at 25°C is shown in Figure 3, from which it can be noted that at any strain rate the flow stress is more for greater amount of reduction of the ingot. However, this difference decreases as the strain rate increases.

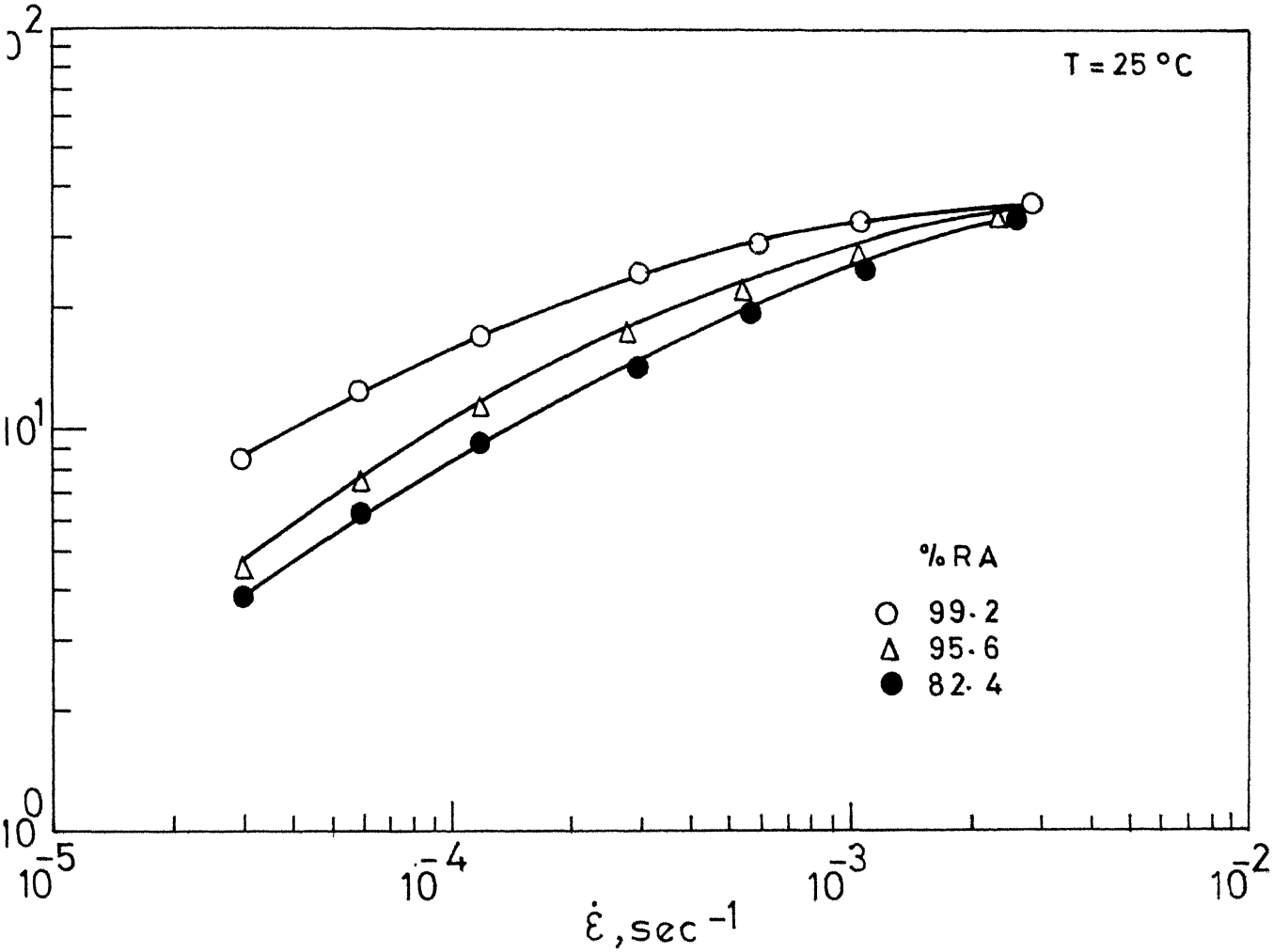

G. 3 INFLUENCE OF DEGREE OF PRIOR MECHANICAL WORKIN ON $\sigma - \dot{\varepsilon}$ BEHAVIOUR

For reductions below about 80% RA, the flow stress was found to decrease progressively with increasing reduction from that in as cast state. However, due to the nonuniform nature of microstructure, no detailed study of mechanical behaviour was undertaken in the lower range of reduction in area.

3.1.2 Material in the As Worked State

The effect of strain on the flow stress of as worked alloy was explored by means of the constant cross head speed test. The details of tests viz. initial strain rate, test temperature and strain are shown along with initial and final microstructural parameters in Table 2. Under these test conditions considerable decrease in strength was observed with increasing strain. This was so even after compensation for change in $\dot{\varepsilon}$ during deformation. The rate of softening was rapid in the beginning and slower in the later part. Thus the stress-strain curves showed two distinct regions of higher and lower slopes in sequence. The transition strain, defined as the strain at which the slope of $\sigma - \varepsilon$ curve changes, was observed to depend very much on initial strain rate and test temperature. At a given temperature, the transition strain was seen to increase with increase in initial strain rate. On the other hand, the transition strain decreased with increase

TABLE 2

Changes in Microstructural Parameters due to Tensile Deformation of Mechanically Worked Specimens

Initial Microstructural Parameters	Initial Strain Rate $\dot{\varepsilon}_i$ (sec^{-1})	Test Temperature (°C)	Strain ε (%)	Microstructural Parameters After Deformati			
				$l_{\parallel}$ (μm)	$l_{\perp}$ (μm)	l_T (μm)	$l_{\parallel}/l_{\perp}$
Initial State: 90% RA by rolling at 100°C							
$l_{\parallel}$ = 9.4 ± 0.8 μm	6×10^{-5}	25	48	8.3 ± 1.1	6.5 ± 1.1	7.0 ± 1.1	1.3
		60	38	7.4 ± 0.8	5.1 ± 0.2	4.7 ± 0.8	1.5
$l_{\perp}$ = 5.3 ± 0.6 μm		100	48	6.6 ± 1.2	4.5 ± 0.5	5.2 ± 0.7	1.5
l_T = 5.6 ± 0.4 μm	3×10^{-4}	25	75	7.9 ± 1.1	6.7 ± 0.9	7.1 ± 1.3	1.2
		60	70	9.0 ± 1.1	6.5 ± 0.7	8.1 ± 1.3	1.4
$l_{\parallel}/l_{\perp}$ = 1.8		100	82	7.2 ± 0.9	5.5 ± 1.3	5.4 ± 0.6	1.3
		148	65	8.0 ± 1.2	5.0 ± 0.7	6.7 ± 1.3	1.6
Initial State: 98% RA by extrusion at RT							
$l_{\parallel}$ = 7.9 ± 0.5 μm							
$l_{\perp}$ = 4.3 ± 0.1 μm	2.8×10^{-4}	148	26	6.8 ± 0.6	4.5 ± 0.4	4.9 ± 0.3	1.5
l_T = 3.9 ± 0.1 μm							
$l_{\parallel}/l_{\perp}$ = 1.8							

$l_{\parallel}$ = Intercept length measured parallel to working direction in longitudinal section.

$l_{\perp}$ = Intercept length measured perpendicular to working direction in longitudinal section.

l_T = Intercept length in the transverse section.

in test temperature. Figure 4 shows typical $\sigma - \varepsilon$ curves illustrating effects of test temperature as well as initial strain rate.

Tensile specimens from the extruded material (98% RA) were tested at 66°C with an initial strain rate of 8.4×10^{-5} sec^{-1} and at 148°C with an initial strain rate of 2.8×10^{-4} sec^{-1}. Strain softening at 66°C and strain hardening at 148°C were observed in these constant cross head speed tests. In the latter case, the flow stress increased by 50% at a strain of 10% and further increase in the stress was very small with a hardening rate of 0.7 MPa per unit strain. These observations were based on $\sigma - \varepsilon$ curves obtained by correcting for the change in strain rate during constant cross head speed tests.

It can also be seen from Table 2 that the microstructures significantly change with deformation depending on initial microstructural and test conditions. The grain aspect ratio decreases with deformation and typical micrographs illustrating this effect are shown in Figure 5.

Making use of specimens having initial microstructures shown in Figure 5, another set of tests was done at 25°C and 100°C to study the $\sigma - \dot{\varepsilon}$ behaviour and effect of strain through repeated strain rate cycling. At both the temperatures, strain softening was evident without any significant change in the strain rate sensitivity index (Figure 6).

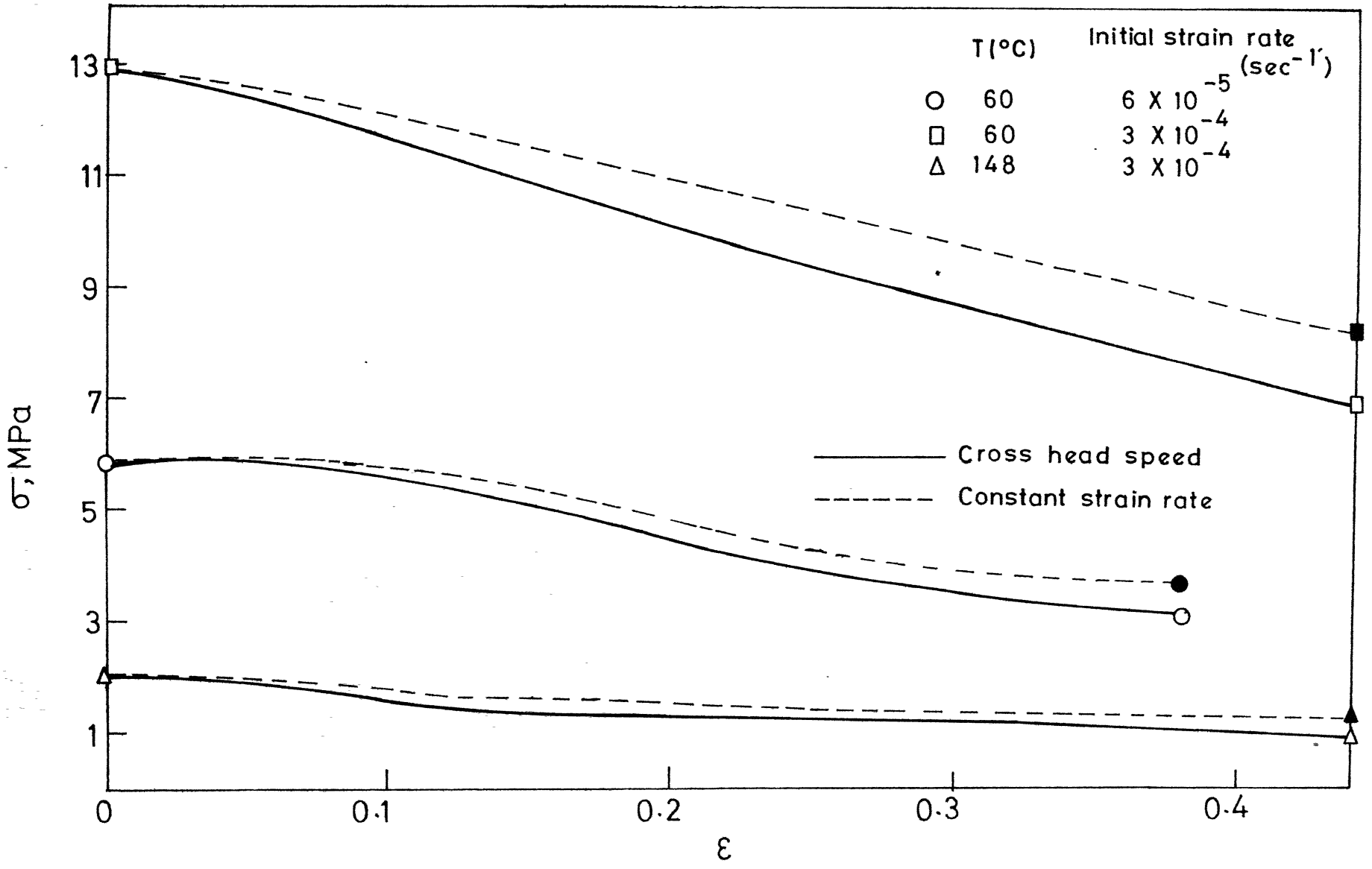

FIG. 4 σ-ε CURVES OBTAINED IN A CONSTANT CROSS HEAD SPEED TEST AT DIFFERENT TEMPERATURES AND INITIAL STRAIN RATES

(a) Longitudinal

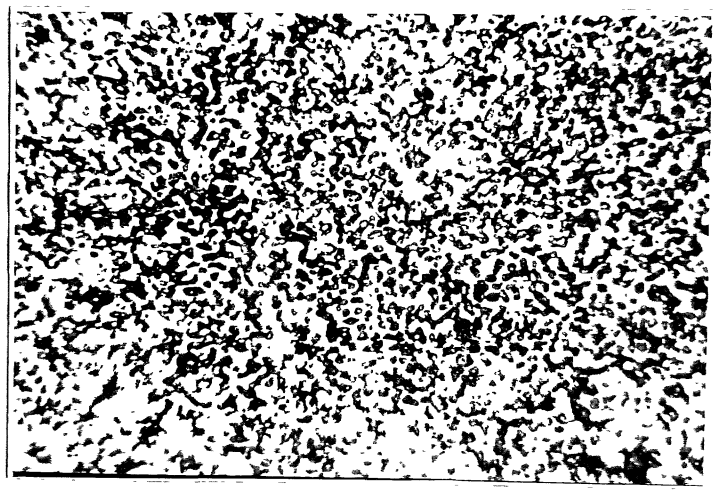

(b) Transverse

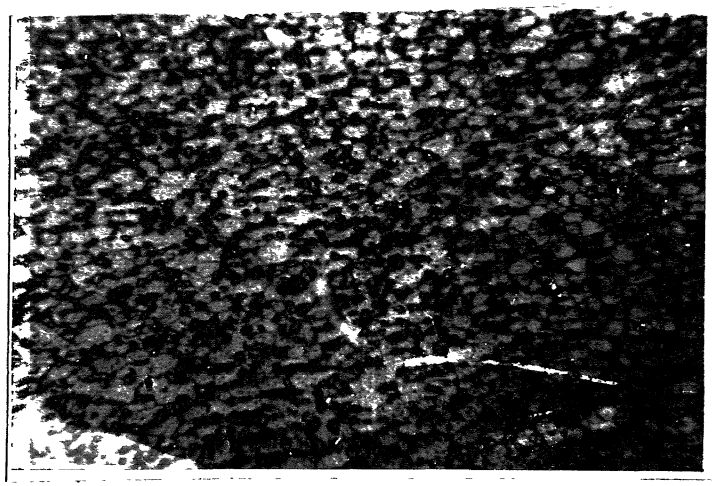

(c) Longitudinal

(d) Transverse

FIGURE 5. MICROSTRUCTURES IN AS ROLLED CONDITION (a AND b) AND AFTER CONSTANT CROSS HEAD SPEED DEFORMATION AT 60°C (c AND d, ε = 0.38, INITIAL $\dot{\varepsilon}$ = 6×10^{-5} sec^{-1}) (MAGNIFICATION: 300X).

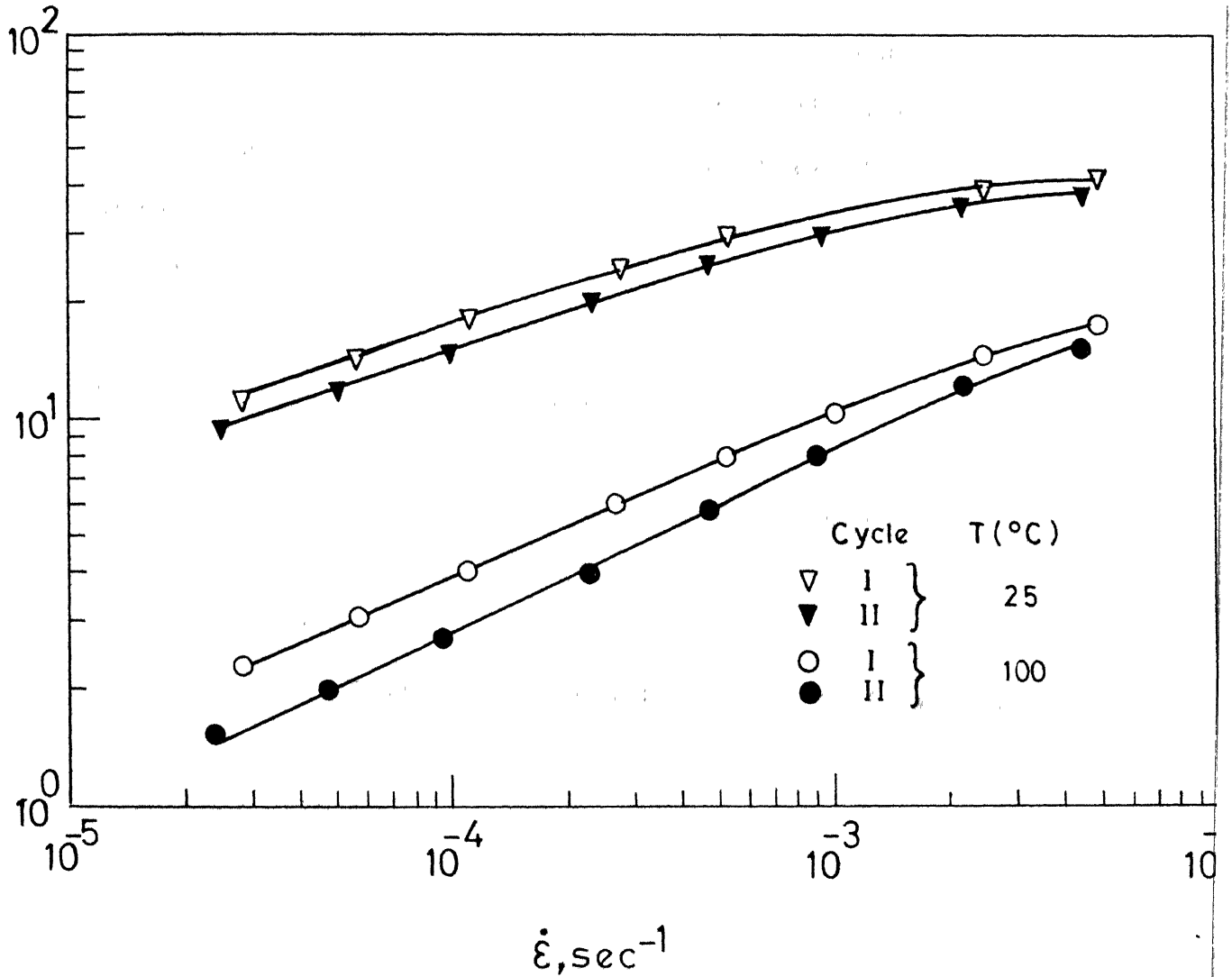

i. 6 EFFECT OF REPEATED STRAIN RATE CYCLING ON THE $\sigma - \dot{\varepsilon}$ BEHAVIOUR OF AS ROLLED SPECIMENS

Another specimen with initial microstructures shown in Figures 7a and b was tested to obtain $\sigma - \dot{\varepsilon}$ data at 170°C by repeated strain rate cycling. The $\sigma - \dot{\varepsilon}$ curves were found to be identical in all the four strain rate cycles through which the specimen was tested and the data of first and fourth cycles are shown in Figure 8. The microstructures of shoulder and gauge sections of this specimen were checked. By comparing the microstructures given in Figures 7c and d with the initial ones, it can be seen that the microstructure of the gauge section has changed significantly relative to the initial microstructure. On the other hand, there was no appreciable change in the microstructure of the shoulder section from that of the initial state. In the gauge section, the grain aspect ratio decreased from 1.8 to 1.2 with an increase in mean intercept length about 50% in the transverse section. The effect of annealing for a short time on microstructure and properties of the as worked alloy was also explored by annealing the as worked alloy for 2 hours at 150°C. As a result of this annealing treatment, the microstructures were not found to show any apparent change. However, the flow stress was found to be significantly higher after this annealing treatment. Typical data of this type are presented in Figure 9 for a specimen whose microstructure is shown in Figure 5.

(a) Longitudinal

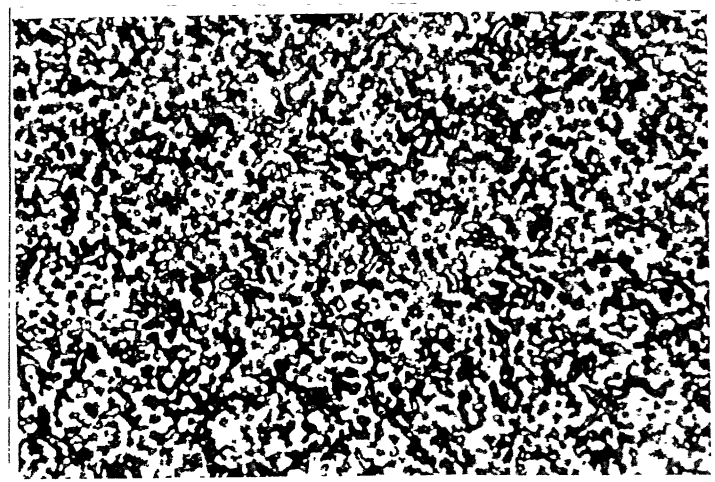

(b) Transverse

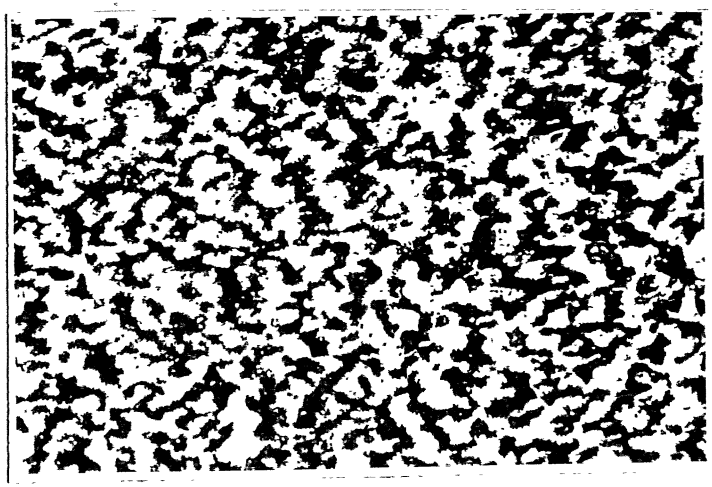

(c) Longitudinal

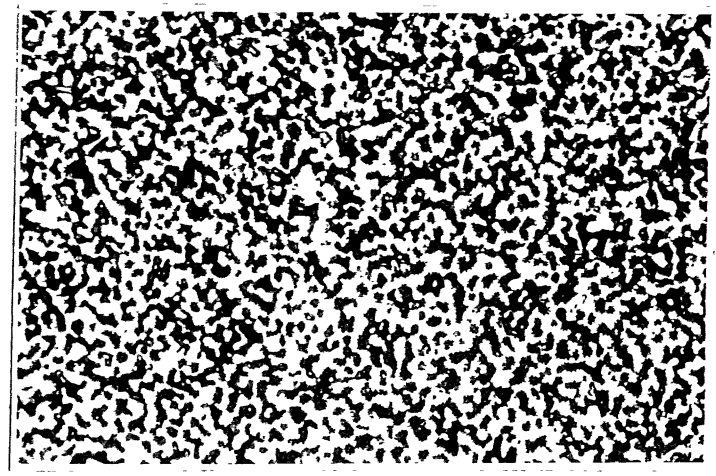

(d) Transverse

FIGURE 7. MICROSTRUCTURES IN AS EXTRUDED CONDITION (a AND b) AND AFTER REPEATED STRAIN RATE CYCLING AT 170°C (c AND d), ELONGATION ~ 40%) (MAGNIFICATION: 300X).

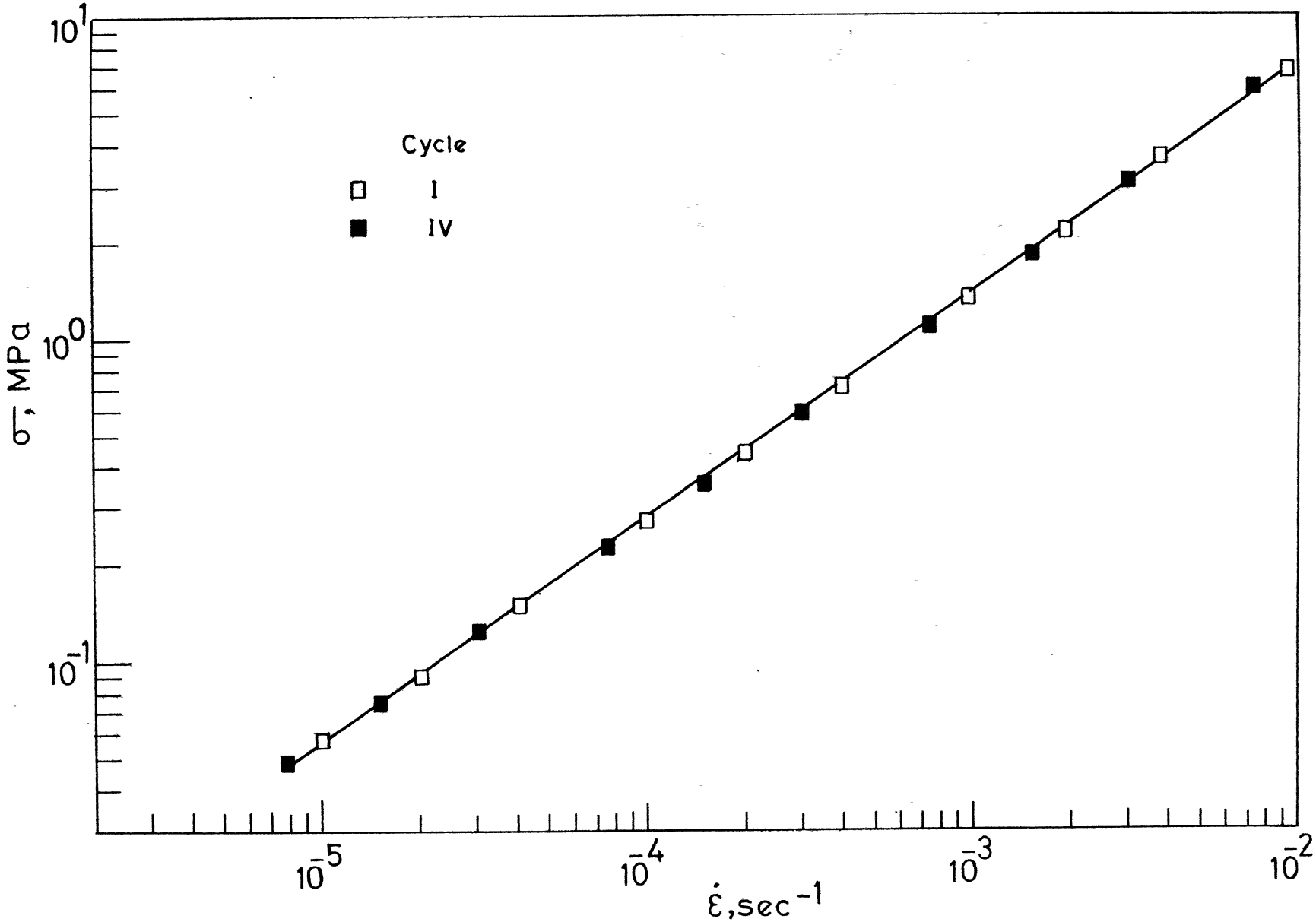

FIG. 8 EFFECT OF REPEATED STRAIN RATE CYCLING ON $\bar{\sigma}$ - $\dot{\varepsilon}$ BEHAVIOUR OF EXTRUDED MATERIAL AT 170°C

Since the as extruded or rolled alloy specimens consisted of slightly elongated grains, an attempt was made to produce equiaxed grains in the as worked condition itself. For this purpose, the cast ingot was forged at 100°C by repeatedly changing the direction of working. By working the cast alloy in this manner, equiaxed microstructure could be obtained. The specimens thus obtained were tested at 25°C for determining their $\sigma - \dot{\varepsilon}$ behaviour through repeated strain rate cycling tests. Some of these specimens were tested at 25, 66, 98 and 148°C after annealing them for 2 hours at 150°C. On comparing the data of first and second cycles, there was strain softening in both the as worked and short annealed states without any appreciable change in the slope of $\sigma - \dot{\varepsilon}$ plots. The $\sigma - \dot{\varepsilon}$ data of the first and second strain rate cycles are shown in Figure 10 for annealed samples tested at 25°C and 66°C. Also, comparison of $\sigma - \dot{\varepsilon}$ data of the annealed sample with that of as worked sample showed that the stress level of the former was higher which in the second cycle decreased to a level closer to that of the as worked specimen. Microstructural observations were made in the as worked state, after short annealing treatment and also after strain rate cycling in these cases. There was no significant microstructural change to account for the observed difference in strength at different stages. Further, the activation energy for

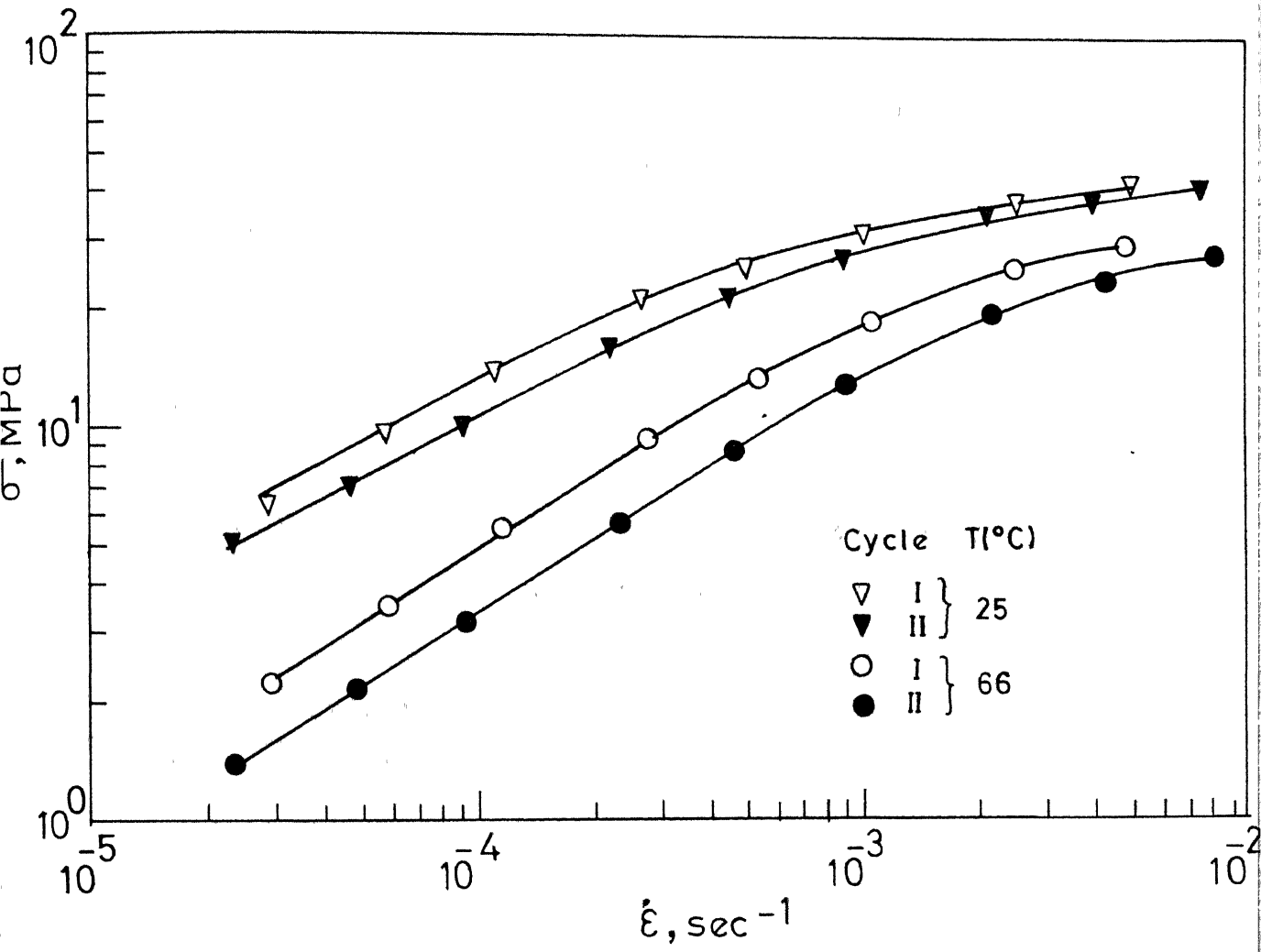

FIG. 10 EFFECT OF STRAIN RATE CYCLING ON $\bar{\sigma}$-$\dot{\bar{\varepsilon}}$ BEHAVIOUR SPECIMENS HAVING EQUIAXED GRAIN STRUCTURE (Anne for 2 hrs. at 150°C after working)

rate sensitive flow of these samples was calculated on the basis of data from first and second cycles. This value based on the first cycle data (55.1 kJ/mole) was found to be different from that of the second cycle (40.6 kJ/mole).

Another characteristic that was investigated for different specimens was strength anisotropy at room temperature by compression tests. Compression samples with microstructures typical of as worked state and after some tensile prestrain (Figure 7) were deformed at 0°, 45° and 90° orientations with respect to the extrusion axis. Compression tests in the as extruded state indicated considerable anisotropy in their strength whereas isotropic behaviour was characteristic of specimens subjected adequate tensile prestrain following mechanical working. Anisotropy was observed even after short annealing of the worked specimens for 2 hours at 170°C. Both in as extruded and annealed states, 45° orientation exhibited minimum strength and 0° orientation exhibited maximum strength, whereas the strength of specimens of 90° orientation was in between the above two values. These compression test data are shown in Figure 11 for extruded and prestrained specimens whose compression axis is at 0° and 90° orientations with respect to the extrusion axis. Microstructural observations indicated that anisotropy in mechanical behaviour is a consequence of non-equiaxed microstructures.

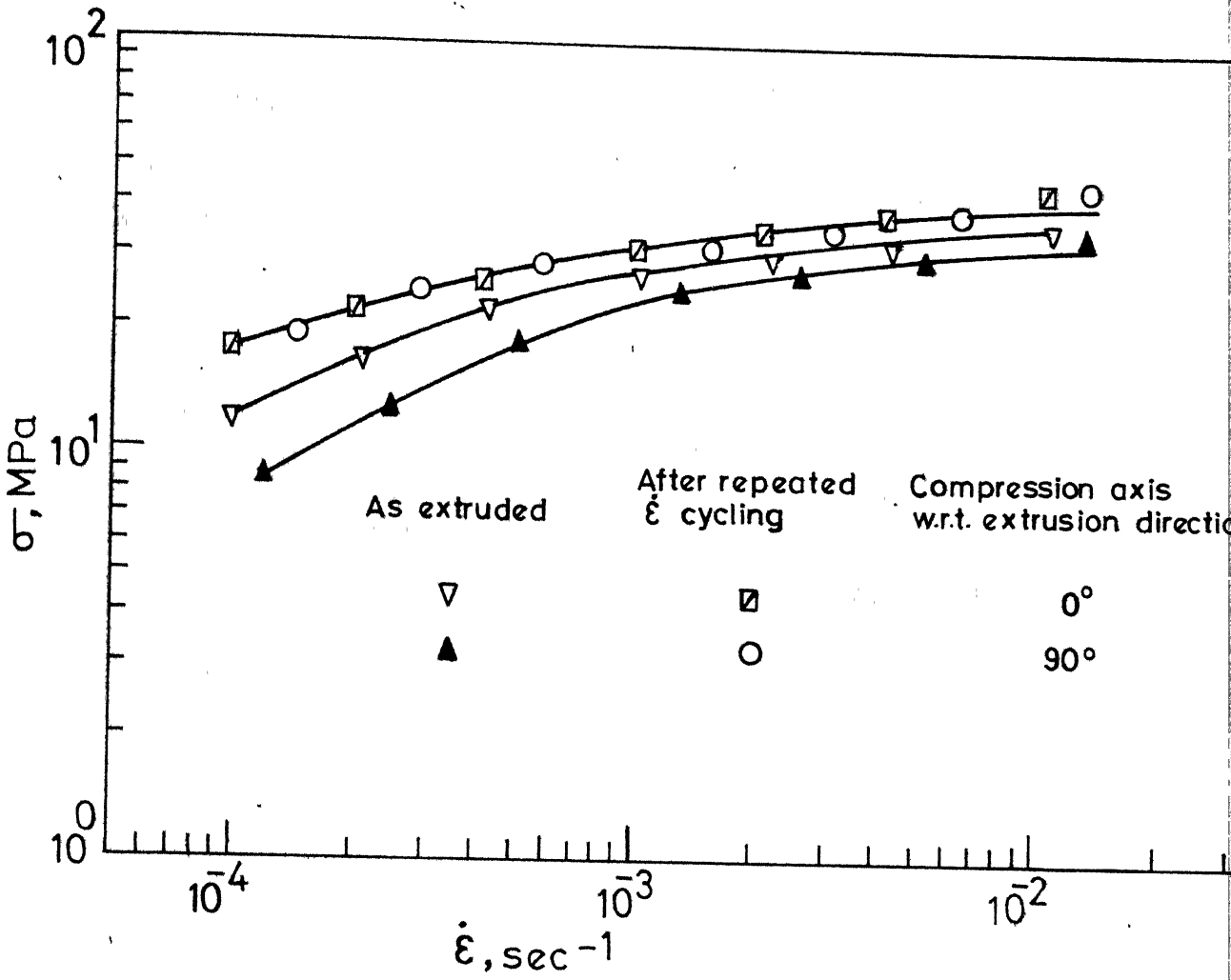

FIG. 11 ANISOTROPY IN $\sigma-\dot{\varepsilon}$ BEHAVIOUR OF AS EXTRUDED MATERIAL AND AFTER REPEATED STRAIN RATE CYCLING TESTS

It was found that irrespective of the processes adopted in getting the equiaxed grains, the anisotropy is eliminated completely if the grains are equiaxed. On the other hand, samples which retained non-equiaxed grains even after substantial annealing exhibited anisotropy in $\sigma - \dot{\varepsilon}$ behaviour.

To summarize, in the as worked state as well as after the annealing treatment of the worked material, the flow behaviour of the Pb-Sn eutectic indicated microstructural and/or mechanical instability. Hence, the structure-property correlations cannot easily be assessed under these conditions.

3.1.3 Effects of Prestraining of the As Worked Material and Tensile Test Variables

In the constant cross head speed and strain rate cycling tests, it was found that both the flow behaviour and microstructure tend to reach a stable state after some strain. This is evident from a relatively constant flow stress as a function of strain in the former test supported by microstructures and identical properties obtained by second and subsequent strain rate cycles in the latter type of test. Therefore, to correlate the structure with flow behaviour, the standard prior deformation consisting of $\sim$30% nominal strain with an initial strain rate of 3×10^{-4} sec^{-1} at 148°C, followed by annealing at 160°C for various times, as described in Chapter II, was adopted.

The mechanical behaviour of specimens with and without standard prior deformation was compared in the following manner. A specimen prepared from the as worked material was given standard prior deformation and then it was annealed at 150°C for 187 hours along with another one in the as worked state. Microstructures in the annealed state of both the specimens with and without tensile prestrain were examined and found to be identical with equiaxed (both in the transverse and longitudinal sections) grain size of 17.1 μm. $\sigma - \dot{\varepsilon}$ data of both these specimens were obtained at 118°C by means of repeated strain rate cycles along with intermittent 30% nominal strain at a constant cross head speed corresponding to a strain rate in region II. Figure 12 illustrates $\sigma - \dot{\varepsilon}$ behaviour of these samples. Only the data of first and fourth cycles are shown for the prestrained specimen, whereas first and second cycle data are shown for the other one. It may be noted from Figure 12 that a specimen without any prior deformation shows softening between the first and second cycles and the second cycle data coincides with those of the predeformed specimen which does not exhibit any strain softening. These observations suggest that tensile prestrain before or after annealing of the as worked material has the same effect. This is so, irrespective of the temperature at which the prestraining is done as long as the minimum strain at that temperature for stability (mechanical and microstructural) is exceeded.

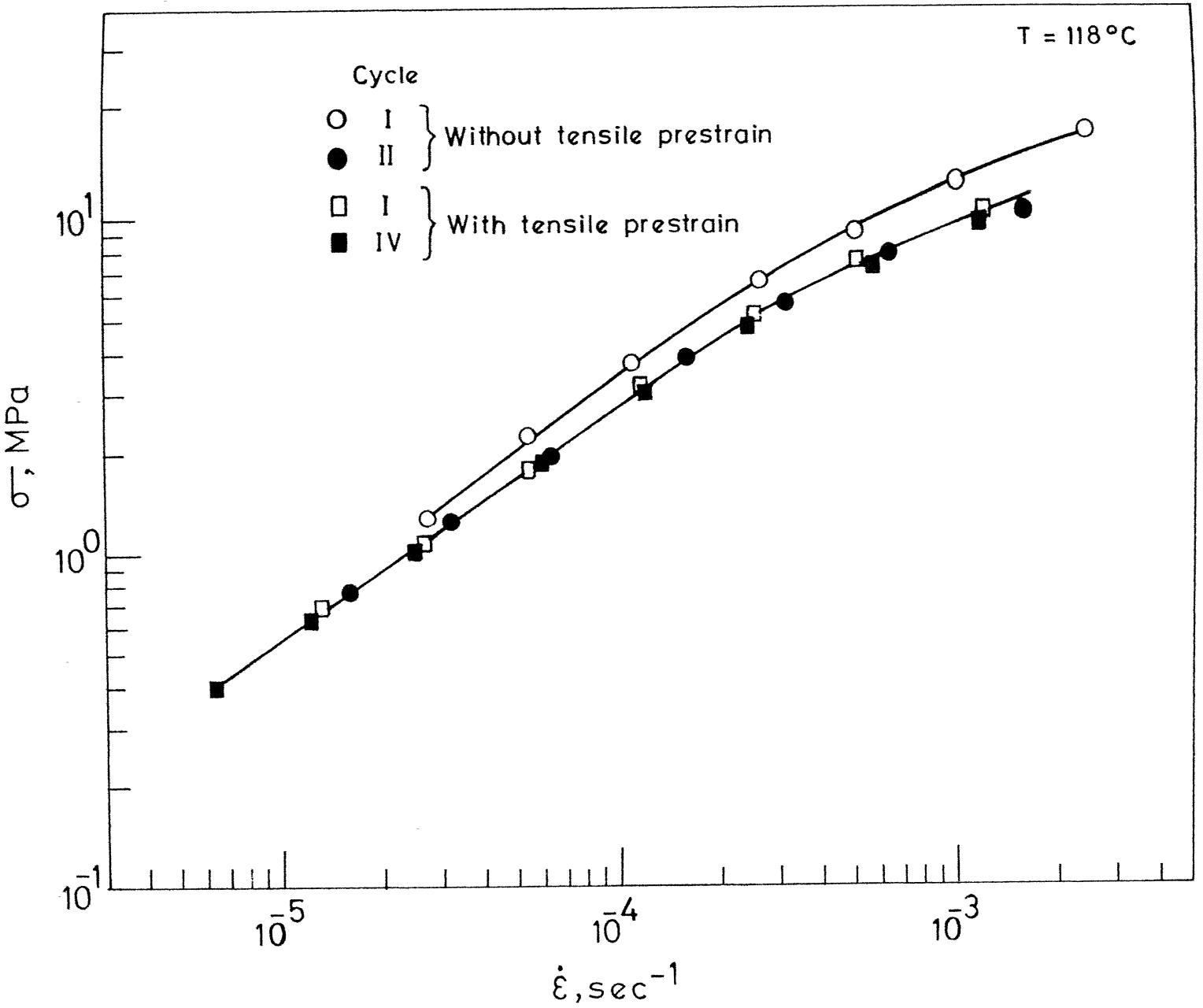

FIG. 12 EFFECT OF STRAIN RATE CYCLING ON σ–$\dot{\varepsilon}$ BEHAVIOUR OF EXTRU-

Parameters of the constitutive equation before and after standard prior deformations were also determined with a view to compare them. The tensile specimens with and without prior tensile deformation were annealed to get a range of equiaxed grains. Grain sizes of 13.1, 16.5 and 21.1 μm in each case were selected for this study. The test temperatures were 118, 148 and 170°C. Separate specimens were tested for obtaining the $\sigma - \dot{\varepsilon}$ data at each of the selected temperatures for all the grain sizes. The strain rate sensitivity index, m, from the slope of log σ - log $\dot{\varepsilon}$ plots did not show significant difference. In region II the grain size exponent was higher by 0.5 for the prestrained samples at all the test temperatures, whereas the activation energy was found to decrease by nearly 20% after standard prior deformation for all the grain sizes.

From the above observations, it may be noted that beyond some strain, the $\sigma - \dot{\varepsilon}$ behaviour for repeated strain rate cycling does not change and thus the specimens after some tensile prestrain have equiaxed grains which show unique $\sigma - \dot{\varepsilon}$ relation. This aspect was further checked with a specimen which was given standard prior deformation followed by annealing to get stable equiaxed grains. The test was done at 148°C and consisted of strain rate cycling. Between two strain rate cycles, the specimen was given 30% nominal strain in region II at the same temperature.

It was observed from the data of five such strain rate cycles that the $\sigma - \dot{\varepsilon}$ relation is identical irrespective of the strain accumulated. This behaviour is illustrated in Figure 13a by presenting the $\sigma - \dot{\varepsilon}$ data of first and fifth cycles where the intermediate deformation was more than 100% elongation.

Another set of experiments was done to check the effects, if any, of the initial gauge length of the specimen and cross head speed on $\sigma - \dot{\varepsilon}$ behaviour. Three tensile samples in as worked state with gauge lengths 2, 3.1, and 5.1 cm were tested at 118°C for three cycles of $\sigma - \dot{\varepsilon}$ data. In each cycle the $\sigma - \dot{\varepsilon}$ behaviour was not influenced by the gauge length difference. Further experiment was done with samples given standard prior deformation and annealing treatment. The gauge lengths after standard prior deformations of the samples were 2.4, 4 and 5 cms. Two sets of tests were done with these samples. In the first set, these samples were tested at 148°C for $\sigma - \dot{\varepsilon}$ data and then subsequently the temperature was lowered to 98°C at which the second cycle $\sigma - \dot{\varepsilon}$ data were obtained. In the second set, these samples after standard prior deformation were tested for $\sigma - \dot{\varepsilon}$ data at 66°C. These test results indicated that the gauge length of tensile specimens does not influence the $\sigma - \dot{\varepsilon}$ behaviour. Typical data of this nature from tests at 98°C are shown in Figure 13b. Since three different gauge

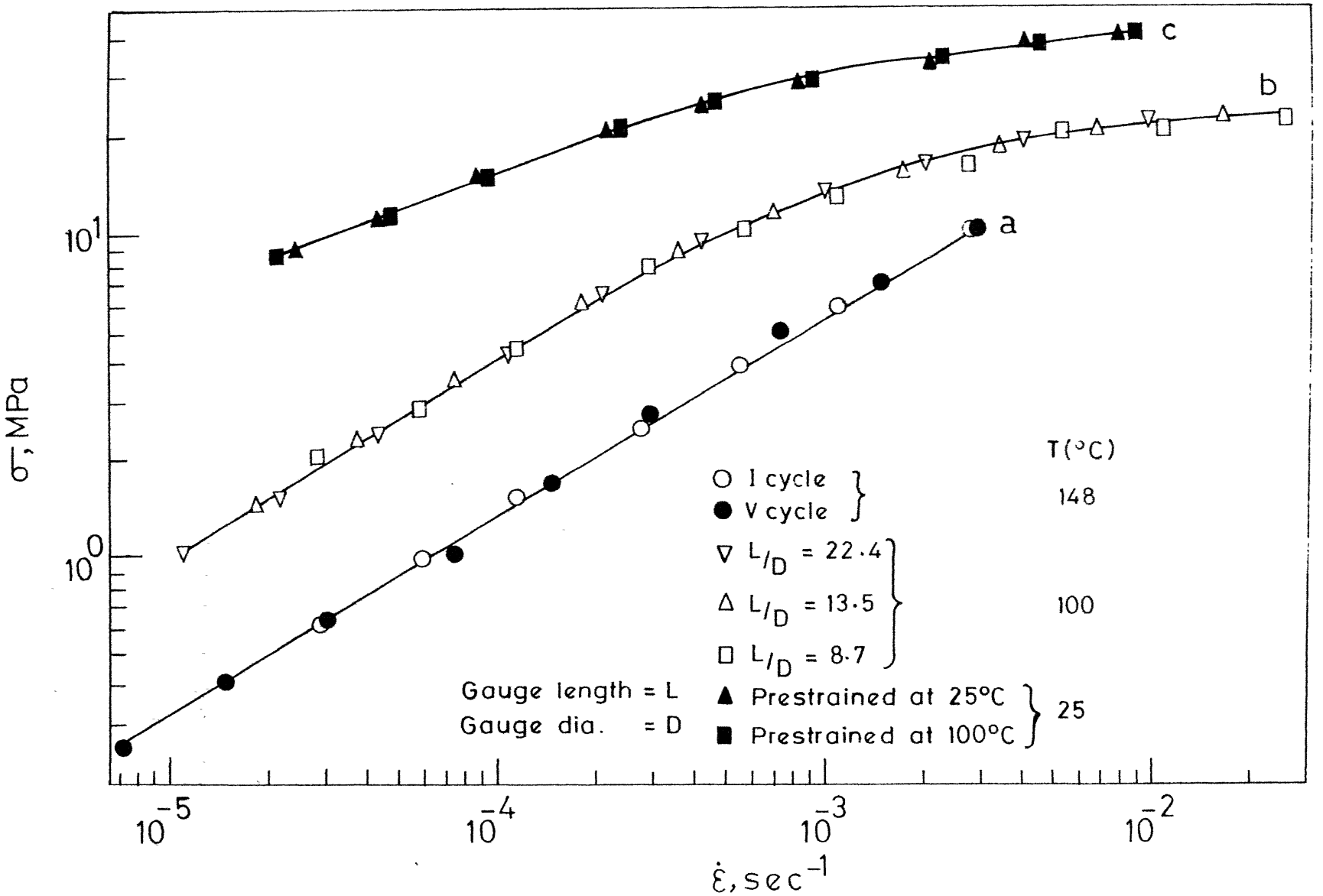

FIG. 13 EFFECT OF (a) LARGE STRAIN ON THE $\sigma - \dot{\varepsilon}$ BEHAVIOUR (b) GAUGE LENGTH OF TENSILE SPECIMENS AND (c) TENSILE PRE-STRAIN GIVEN AT DIFFERENT TEMPERATURES

lengths have been used to get a constant strain rate, the effective cross head speeds corresponding to this strain rate were also in the same proportion as that of the gauge lengths. Thus it is evident from the Figure 13b that any particular strain rate under consideration has yielded a constant stress value irrespective of the gauge length and cross head speed. Thus, the flow stress is a unique function of strain rate without any dependency on cross head speed.

Tests were also done to check the effect of difference in prestraining routes to stable state. In the first test, two tensile samples were taken. One specimen was prestrained at 25°C by the differential strain rate test through one cycle and the other one was prestrained at 98°C by two such cycles. Both of these specimens, after prestraining, were tested at 25°C over two cycles of strain rate change tests. It was observed that the $\sigma - \dot{\varepsilon}$ behaviour of both these specimens is identical (Figure 13c). In another test one tensile sample was prestrained at 118°C by three cycles of the strain rate change test in region II and then tested at 170, 148, 66 and 25°C. By comparing these data with those of separate tensile samples for each of these test temperatures after subjecting them to standard prior deformation, good agreement was noted between these data. Thus the above observations indicate that stress is a unique function of strain rate and does not depend on

the strain or path through which a given strain rate is approached, as long as the specimens are subjected to tensile prestrain to overcome the initial strain effects.

3.2 MECHANICAL BEHAVIOUR OF SPECIMENS HAVING EQUIAXED GRAINS

3.2.1 Microstructures and $\sigma - \dot{\varepsilon}$ Behaviour

Equiaxed microstructures with grain sizes in the range of 9.7 μm to 32.0 μm (Table 3) were obtained by subjecting specimens of as worked material to standard prior deformation and annealing.

Figures 14 and 15 show microstructures of two typical grain sizes 15.5 μm and 28.4 μm respectively. The $\sigma - \dot{\varepsilon}$ data for specimens of different grain sizes at various temperatures are shown in Figures 16 to 19.

The observed $\sigma - \dot{\varepsilon}$ behaviour of all specimens can be characterized as regions II and III of the high temperature steady state deformation of the fine grained materials. No region I was noticed in the investigated ranges of grain size, temperature and strain rate. The transition strain rate between regions II and III is observed to increase with increase in the test temperature for any grain size and also with decreasing grain size at any test temperature. The strain rate sensitivity index in each of the regions II and III is not significantly influenced by test temperature or grain size. In region II this value is 0.60 ± 0.10

TABLE 3

Grain Sizes (Equiaxed) of Specimens Used in Evaluating Parameters of Constitutive Equation

Intercept Length (μm)			Grain Size, $d = 1.74 \times \bar{l}$ (μm)
Longitudinal l_L	Transverse l_T	Average $\bar{l}$	
6.0 ± 0.6	5.3 ± 0.3	5.6 ± 0.3	9.7 ± 0.6
6.0 ± 0.4	6.8 ± 0.5	6.3 ± 0.4	11.0 ± 0.6
9.0 ± 0.4	8.8 ± 0.6	8.9 ± 0.3	15.5 ± 0.5
10.3 ± 0.5	9.8 ± 0.7	10.0 ± 0.5	17.4 ± 0.9
10.8 ± 0.6	12.2 ± 0.5	11.6 ± 0.4	20.1 ± 0.7
14.7 ± 1.1	12.4 ± 0.8	13.5 ± 0.8	23.4 ± 1.3
18.6 ± 1.2	14.7 ± 1.1	16.3 ± 0.9	28.4 ± 1.6
18.1 ± 1.3	20.8 ± 2.3	18.4 ± 1.1	32.0 ± 1.9

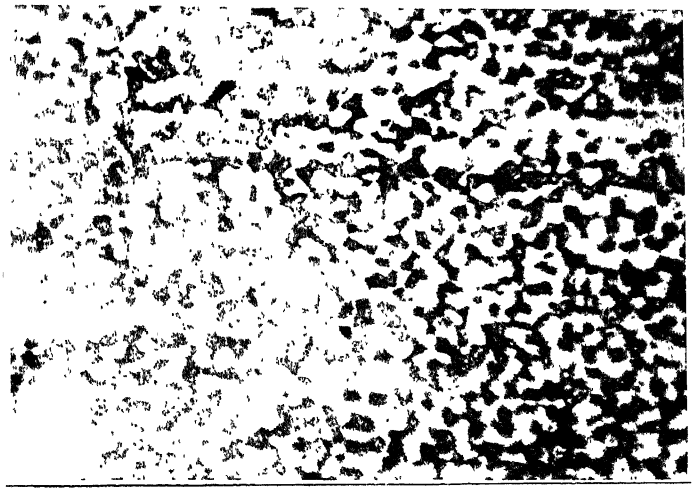

(a) Longitudinal

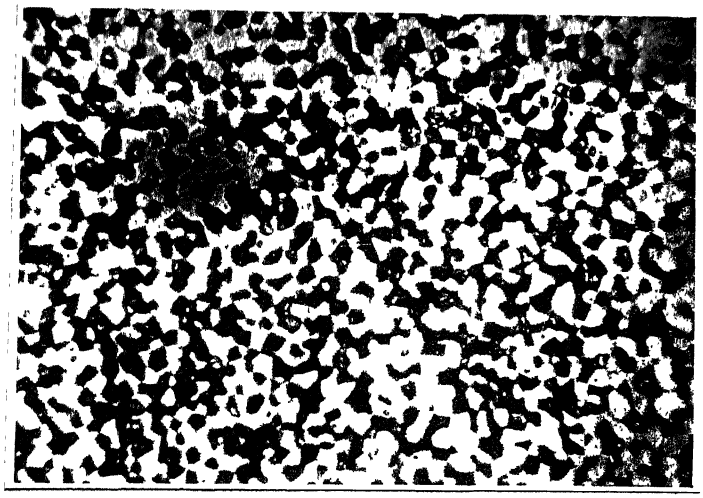

(b) Transverse

FIGURE 14. TYPICAL MICROSTRUCTURES AFTER STANDARD TENSILE PRESTRAIN FOLLOWED BY ANNEALING AT 160°C FOR 72 HRS. (GRAIN SIZE d = 15.5 μm) (MAGNIFICATION: 300X).

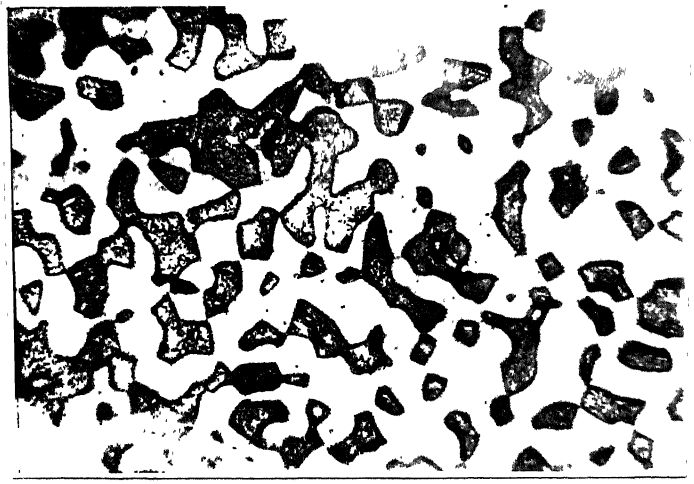

(a) Longitudinal

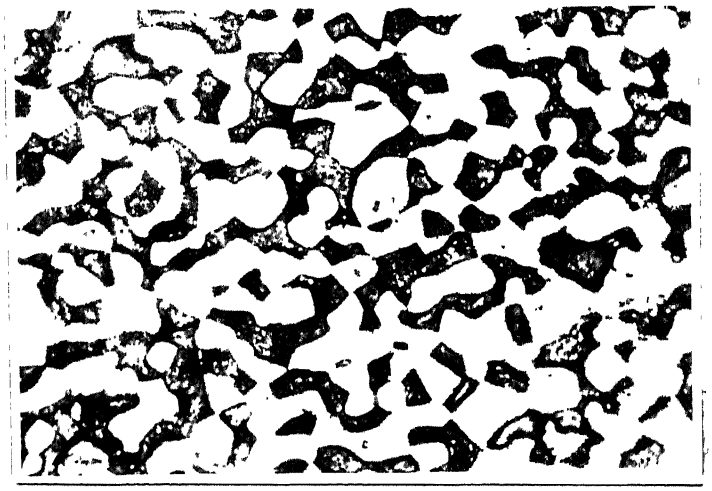

(b) Transverse

FIGURE 15. TYPICAL MICROSTRUCTURES AFTER TENSILE PRESTRAIN FOLLOWED BY ANNEALING AT 160°C FOR 2317 HRS. (GRAIN SIZE d = 28.4 μm) (MAGNIFICATION: 300X).

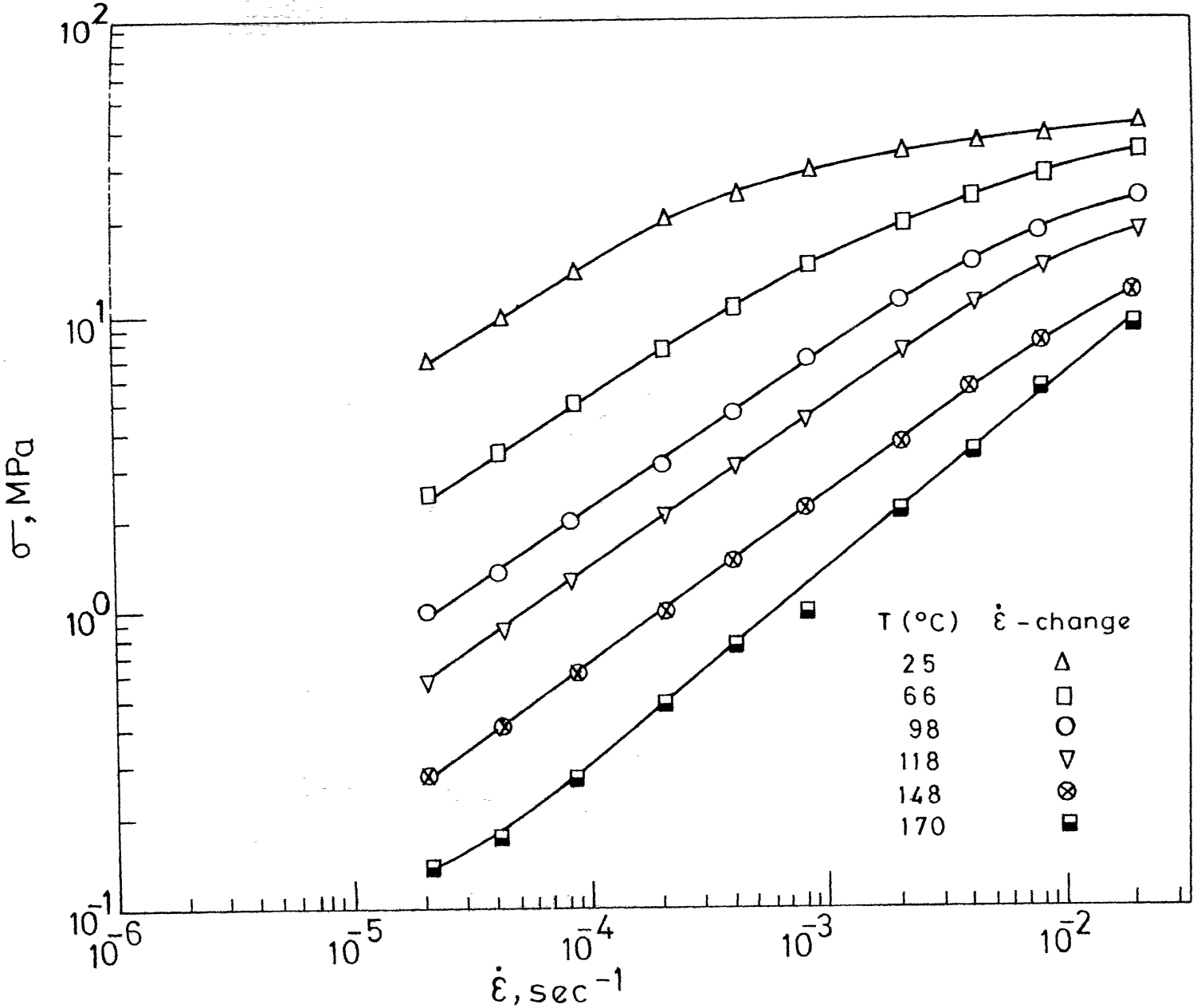

FIG. 16 $\bar{\sigma}$ - $\dot{\varepsilon}$ PLOTS FOR SPECIMENS OF EQUIAXED MICROSTRUCTURE (grain size d = 9.7 μm)

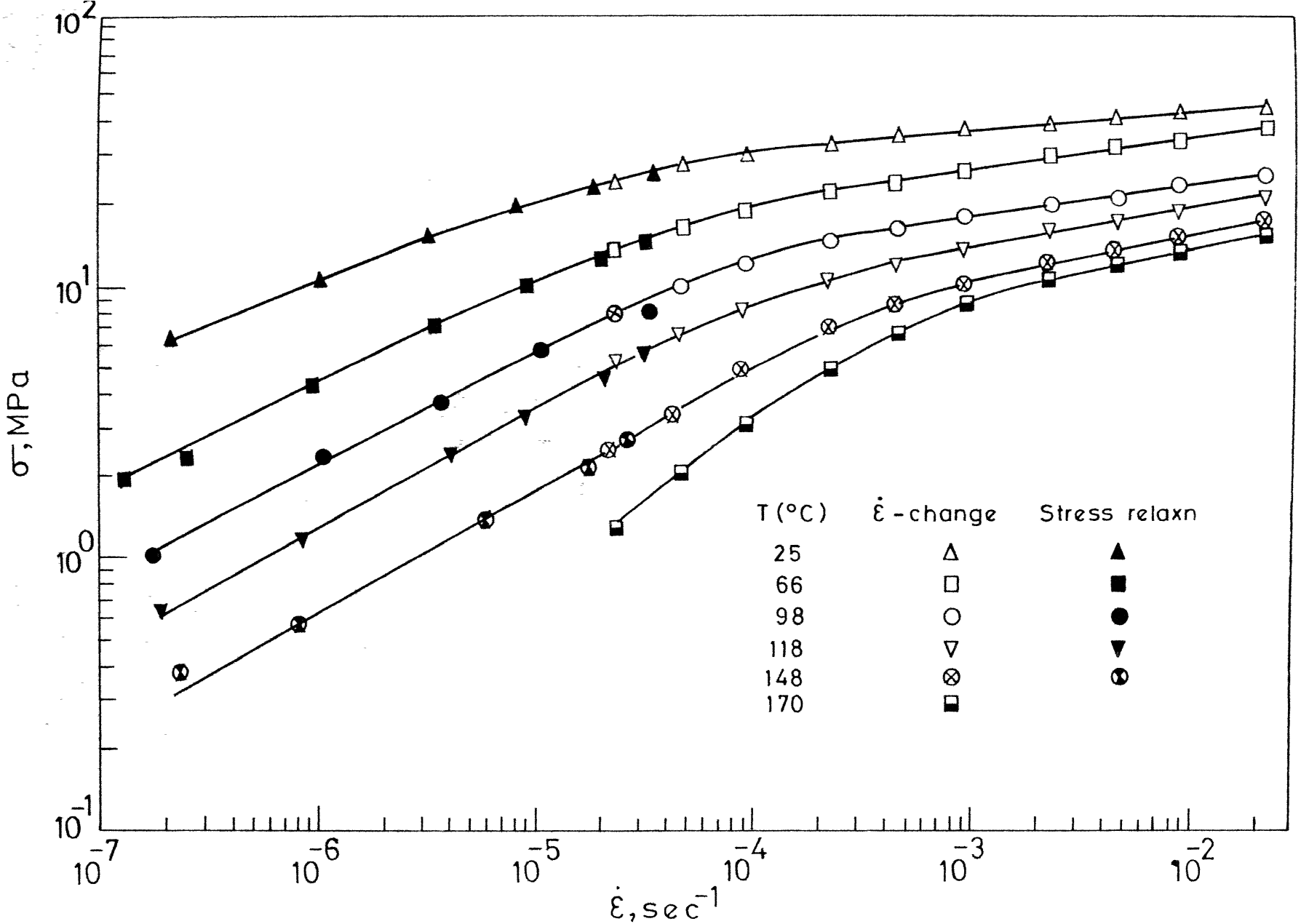

FIG. 18 $\bar{\sigma}$ - $\dot{\varepsilon}$ PLOTS FOR SPECIMENS OF EQUIAXED MICROSTRUCTURE (grain size d = 2.8 (μm)

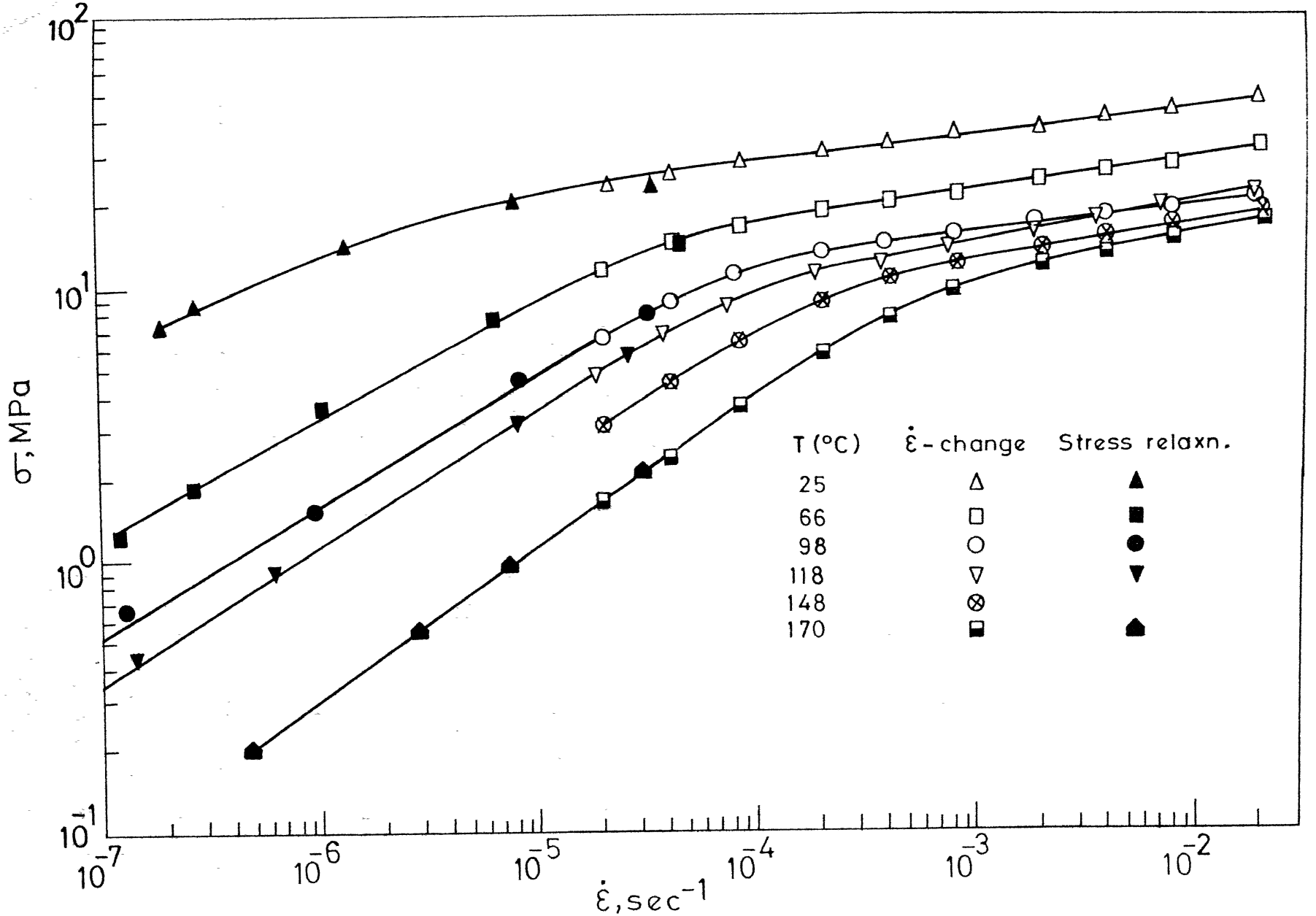

FIG. 19 σ - $\dot{\varepsilon}$ PLOTS FOR SPECIMENS OF EQUIAXED MICROSTRUCTURE

whereas in region III it is 0.09 $\pm$ 0.01. As typical cases, m versus $\dot{\varepsilon}$ plots at different temperatures are shown in Figures 20 and 21 for grain sizes of 9.7 and 32.0 μm respectively. The grain size effect on the $\sigma - \dot{\varepsilon}$ data is also illustrated in Figure 22 for a test temperature of 148°C.

3.2.2 $\sigma - \dot{\varepsilon}$ Data from Stress Relaxation Test

Although stress relaxation tests were performed for all grain sizes and test temperatures, $\sigma - \dot{\varepsilon}$ data could not be obtained by this method in all cases. This was because of the dominance of anelastic effects during the stress relaxation, especially at high temperatures in the lower grain size range. It was possible to obtain $\sigma - \dot{\varepsilon}$ data by this method at all temperatures only for grain sizes of 28.4 μm and 32.0 μm. For other grain sizes, the stress relaxation method was effective only in the lower temperature range.

The evidence for anelastic effect in the relaxation test was of the following nature. After noting the $\sigma - \dot{\varepsilon}$ behaviour of a specimen down to the lowest cross head speed of the Instron machine, stress relaxation tests were conducted starting at initial strain rates that are much higher than the lowest strain rate attained in the differential strain rate test. The data obtained by analyzing the relaxation curves were then compared in the overlapping strain rate range with those of differential strain rate test. The agreement between the two kinds of data would

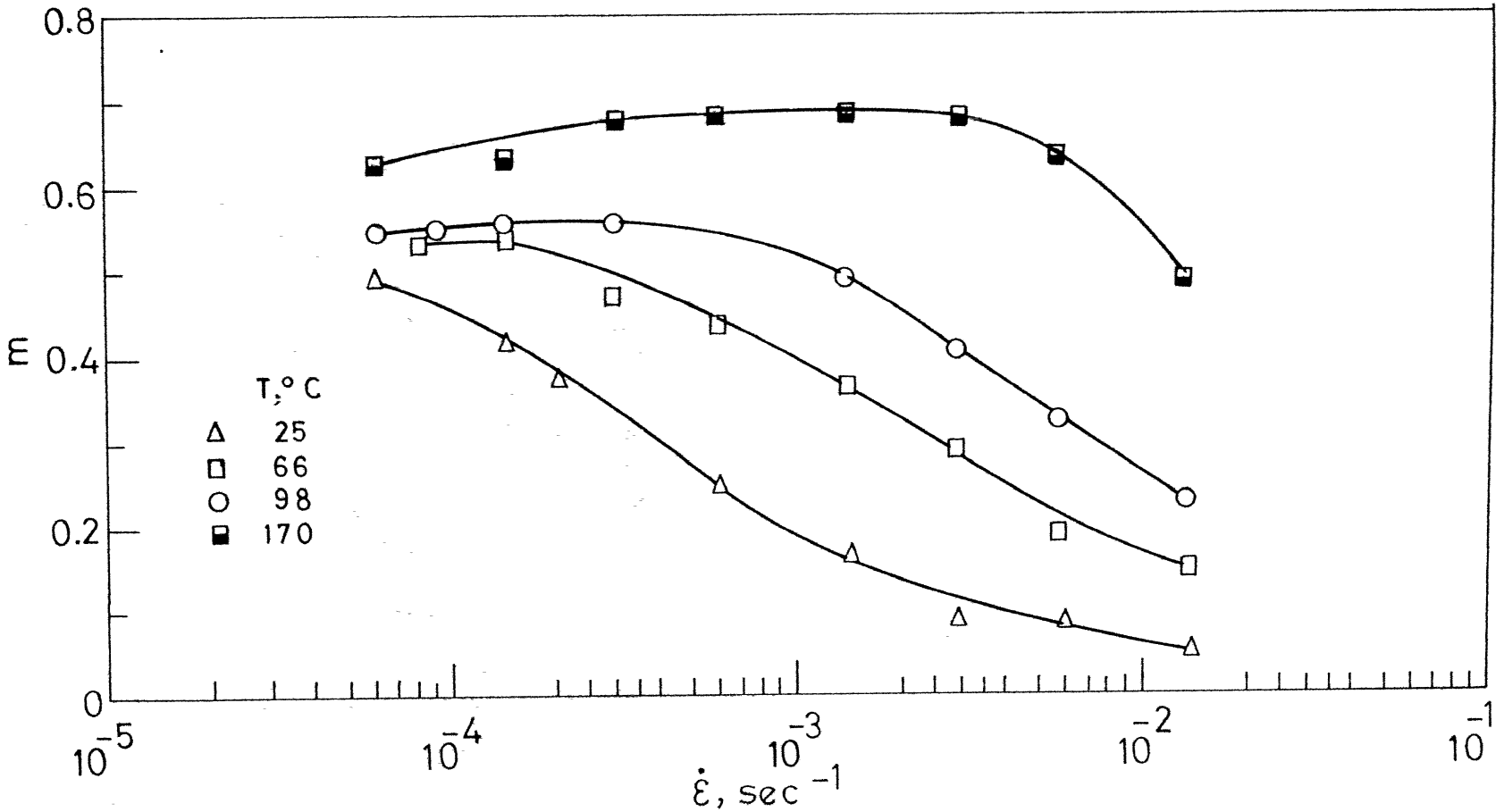

FIG. 20 VARIATION OF STRAIN RATE SENSITIVITY INDEX WITH STRAIN RATE AT DIFFERENT TEST TEMPERATURES (grain size = 9.7 μm)

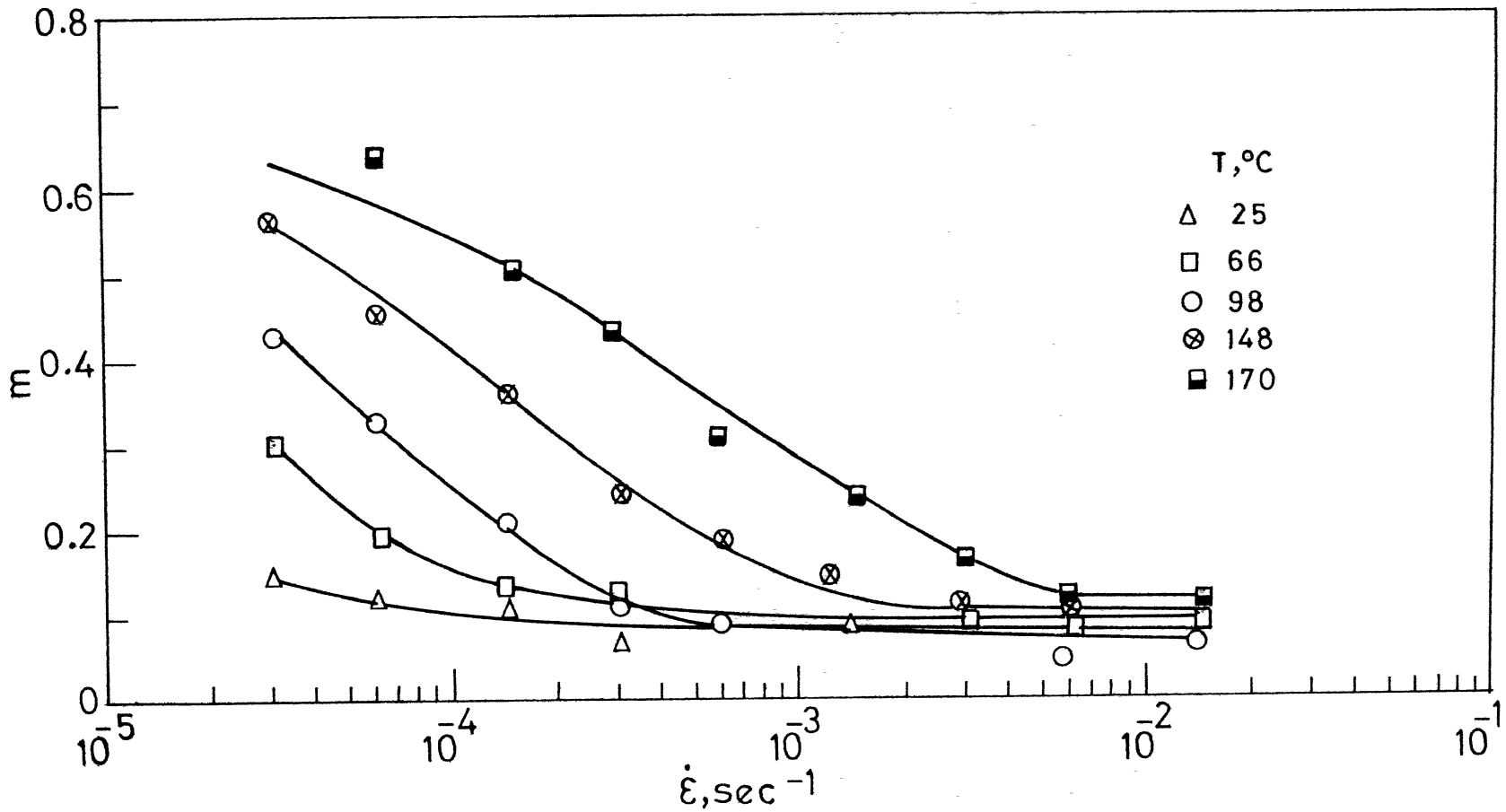

FIG. 21 VARIATION OF STRAIN RATE SENSITIVITY INDEX WITH STRAIN RATE AT DIFFERENT TEST TEMPERATURES. (grain size = 32 μm)

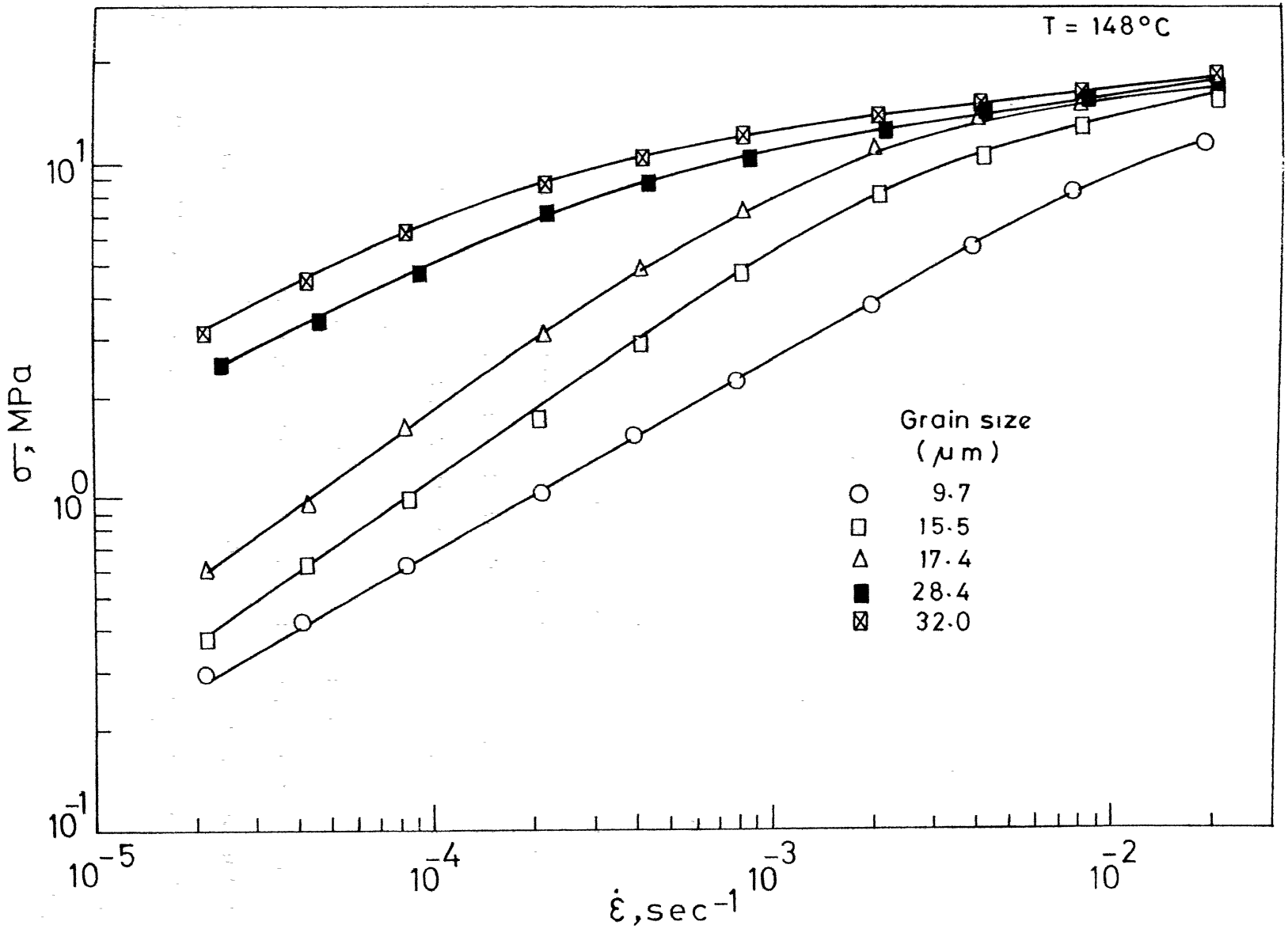

FIG. 22 PLOT OF $\bar{\sigma}$ – $\dot{\varepsilon}$ DATA AT 148°C FOR DIFFERENT GRAIN SIZES

indicate the absence of any anelastic effect. On the other hand, if the anelastic effect plays a significant role in the relaxation test, the evaluation of $\sigma - \dot{\varepsilon}$ data from the relaxation curves by considering only the elastic and plastic deformations would yield data that differ from the strain rate change test data. In that case, the discrepancy between the two kinds of data can be accounted for by considering the anelastic effect in the analysis of relaxation curves.

Typical examples of the above two kinds of effects in the relaxation test data are presented in Figures 23 and 24. From Figure 23, good match in the data obtained by the relaxation and strain rate change methods can be seen, whereas there is significant difference between the relaxation test and strain rate change test data of Figure 24. Moreover, there is a wide difference in the data of relaxation test depending on the initial stress level at which the relaxation test was started.

Schneibel and Hazzledine [80] have suggested a method of predicting the form of relaxation curve (S-H model) by considering the influence of anelasticity. In order to take into account the anelasticity effect, the anelasticity parameters of the material being considered must be known. In this model, the relaxation behaviour of an anelastic superplastic material is analyzed by means of a rheological model (Figure 25) consisting of a spring, dashpot and

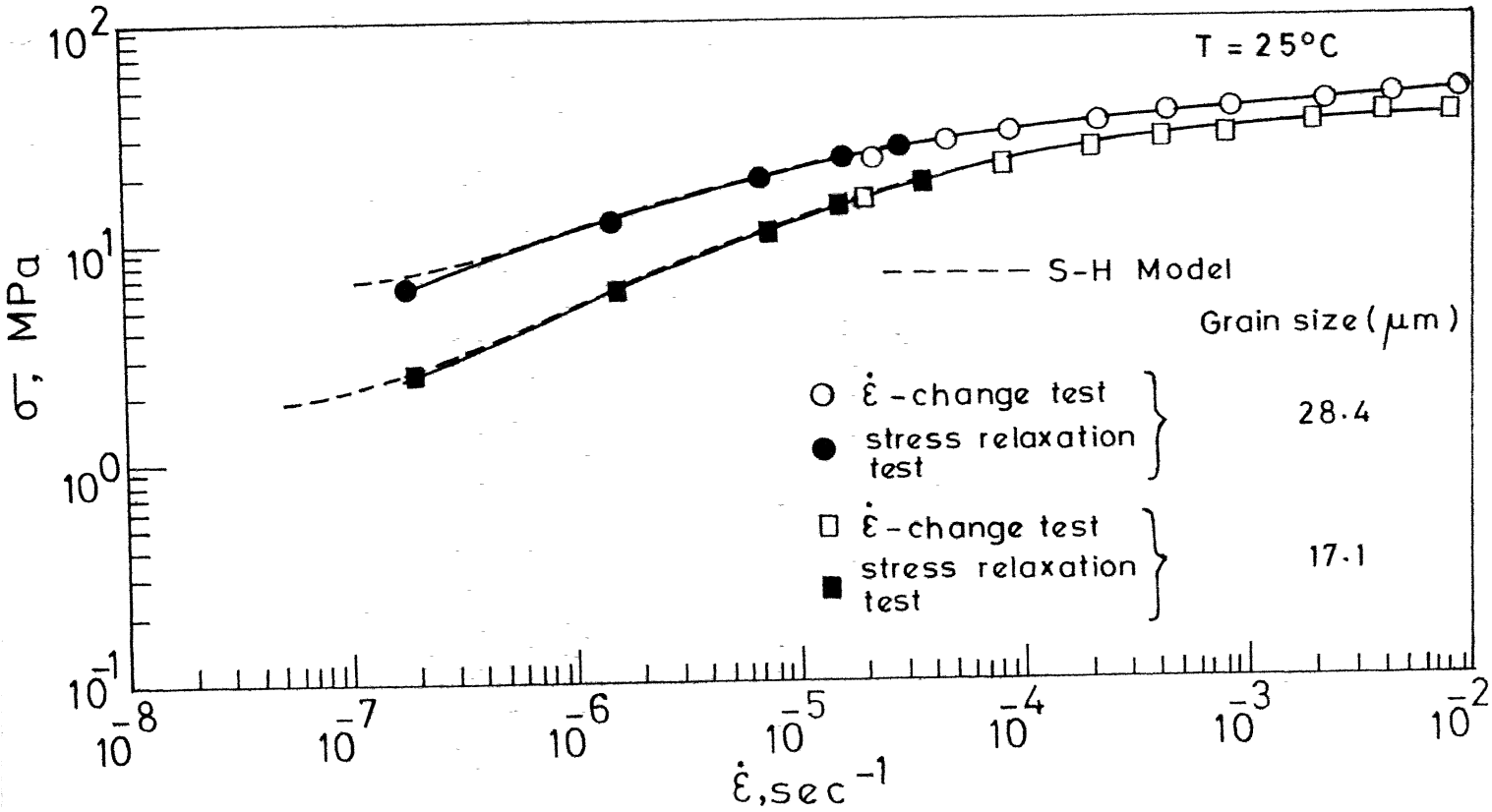

FIG. 23 σ - $\dot{\varepsilon}$ BEHAVIOUR DERIVED FROM A STRESS RELAXATION TEST WITH (S-H MODEL) AND WITHOUT CONSIDERING ANELASTICITY EFFECT

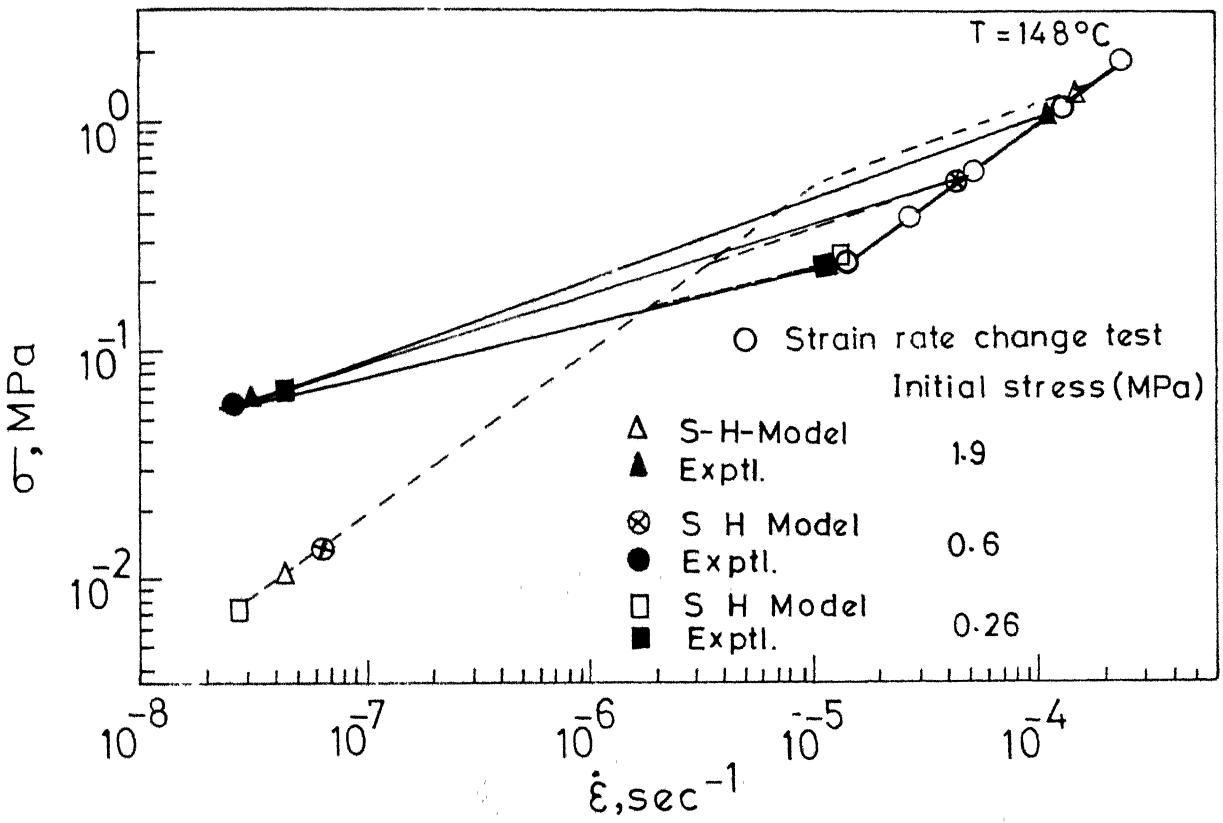

FIG. 24 INFLUENCE OF ANELASTICITY ON $\sigma - \dot{\varepsilon}$ BEHAVIOU OBTAINED FROM STRESS RELAXATION TESTS STARTI FROM DIFFERENT INITIAL STRAIN RATES.

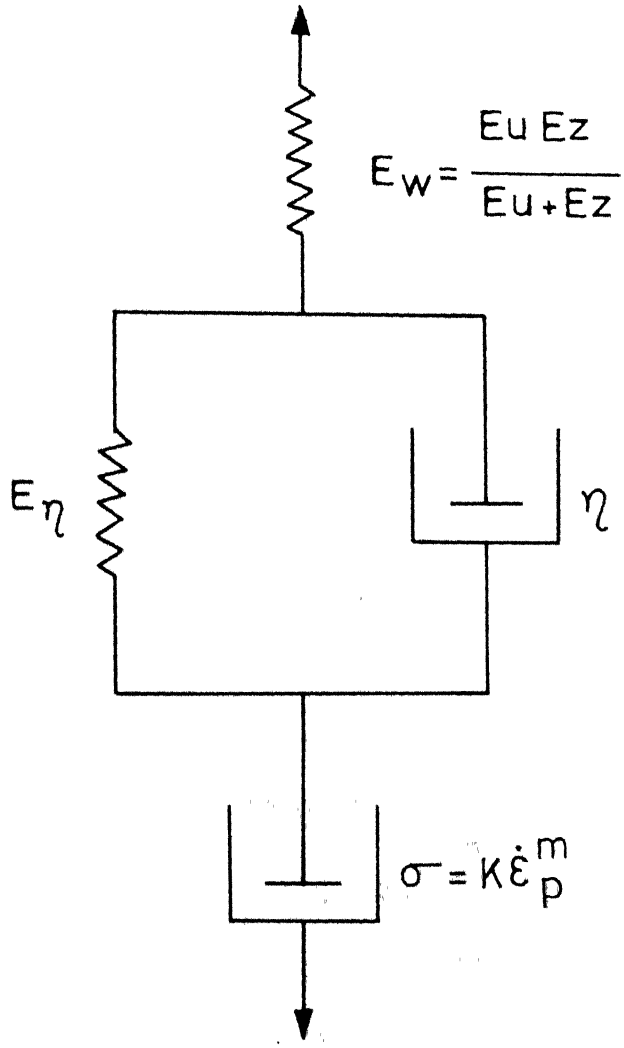

FIG. 25 RHEOLOGICAL MODEL REPRESENTING ANELASTIC SUPERPLASTIC MATERIAL (Schneibel and Hazzledine [80])

Kelvin body in series to simulate the elastic, non-linear viscous and anelastic behaviours of a material, respectively. The relaxation behaviour of such a body is governed by the differential equation in time

$$C_1 \ddot{\sigma} + C_2 \dot{\sigma} + C_3 \sigma^n = 0 \qquad (11)$$

Here, (i) $C_1 = \eta/(E_w + E_\eta)$ where η is the viscosity of linear dashpot in the Kelvin body. E_η is the modulus of the spring in the Kelvin body and $E_w = (E_u E_z)/(E_u + E_z)$ where E_u is the unrelaxed modulus of the material being considered and E_z is the effective modulus of the testing machine given by $\frac{LS}{A}$, where L, A and S are specimen length, cross-section area of the specimen and machine stiffness, respectively,

(ii) $C_2 = 1 + \frac{E_w + C_1}{K m} \left(\frac{\sigma}{K}\right)^{\left(\frac{1-m}{m}\right)}$ where m and K are material constants representing the non-linear viscous behaviour given by the relation $\sigma = K \dot{\varepsilon}^m$, and

(iii) $C_3 = \left(\frac{E_w E_\eta}{E_w + E_\eta}\right) \cdot \frac{1}{K^{1/m}}$ and $n = 1/m$.

Further, $\eta = \tau_a E_\eta$ where τ_a is the anelastic strain relaxation time.

By solving the equation (11) with the appropriate initial conditions, the relaxation behaviour of a material can be predicted.

The stress relaxation data of the present study have been analyzed on the basis of the above model to assess

the role of anelasticity. However, due to lack of appropriate information on anelastic parameters of the Pb-Sn eutectic, this analysis was primarily possible for tests at 25°C only. High temperature relaxation test data were also analyzed with certain approximations in some cases. The numerical values of the various parameters at 25°C used in the present analysis of data presented in Figure 23 are given in Table 4.

τ_a, for both the grain sizes (Table 4), was obtained by using the relation [81] that $\tau_a \alpha d$ and the reported value [80] of $\tau_a = 3 \times 10^4$ sec for the Pb-Sn eutectic alloy having a grain size of 3.5 μm.

The numerical integration of equation (11) was carried out by the Runge-Kutta-Gill method using a computer program to obtain σ versus t data of the relaxation test. These data were further converted to $\sigma - \dot{\varepsilon}$ data using equation (7) in order to compare them with the experimental data obtained from the relaxation test. It can be seen from Figure 23 that the experimental and predicted data agree very well with each other and also with that of strain rate change test in the overlapping strain rate range. Further, it may be noted that the stress level tends to level off at strain rates lower than $\sim 10^{-7}$ sec^{-1}, which indicates the influence of anelastic contraction in preventing stress relaxation at strain rates lower than

TABLE 4

Numerical Values of the Various Parameters Used in Stress Relaxation Analysis Through S-H Model

Parameters	Test Temperatures				
	25°C		148°C		
			Cross Head Speeds, vx, cm/mt.		
	d = 17.1 μm	d = 28.4 μm	0.005	0.02	0.1
E_u (MPa)	20.61×10^3	20.61×10^3	11.0×10^3	11.0×10^3	11.0×10^3
E_z (MPa)	7.20×10^3	6.5×10^3	2.82×10^3	2.9×10^3	3.1×10^3
E_η (MPa)	1.85×10^3	1.85×10^3	1.85×10^3	1.85×10^3	1.85×10^3
τ_a (ks)	8.40×10^4	2.00×10^3	1.00×10^{-2}	1.00×10^{-2}	1.00×10^{-2}
m	0.43	0.32	0.66	0.66	0.66
K (MPa s^m)	1652.00	915.00	417.80	417.80	417.80
M (MPa^{-1})	18.8×10^{-5}	20.20×10^{-5}	41.30×10^{-5}	41.30×10^{-5}	41.30×10^{-5}
σ_o (MPa) at t = 0	18.20	25.30	0.26	0.60	1.90

10^{-7} sec^{-1} in this material under these test conditions. Thus, in this case the utility of a simple relaxation test which neglects anelastic effect is limited to strain rates above $\sim 10^{-7}$ sec^{-1}.

The experimental relaxation test data obtained at 148°C have also been compared with those calculated by the S-H model. Experimental relaxation data were obtained by starting at various initial stress levels and the $\sigma - \dot{\varepsilon}$ data thus obtained by the usual analysis of relaxation test in which anelasticity effect is not considered were not only found to be different among themselves but also from those of the strain rate change test as illustrated in Figure 24. In considering the anelasticity effect by the S-H model, the anelastic parameters corresponding to the required temperature and grain size were first estimated from the room temperature parameters. In the estimation of τ_a, trial and error procedure was adopted in matching the predicted data with those observed experimentally. The various parameters used in the analysis are listed in Table 4. The $\sigma - \dot{\varepsilon}$ data were then generated by the S-H model starting at three different initial stress levels corresponding to the experiment and these data are shown in Figure 24. It may be seen that, by using a single value for the relaxation time, the initial parts of the $\sigma - \dot{\varepsilon}$ data obtained by the S-H model coincide with the experimental curves in all

cases. The differences between the predicted and observed relaxation curves at lower strain rates are likely to be because of a spectrum of relaxation times required to describe the high temperature anelastic behaviour rather than a single relaxation time that has been used. However, the trend in the dominance of anelastic effects in this case is quite clear. Thus, in these cases, simple relaxation test which does not consider the anelasticity effect is inappropriate in generating $\sigma - \dot{\varepsilon}$ data. Precise determination of $\sigma - \dot{\varepsilon}$ data by taking into account the anelasticity effect in the relaxation test could not be carried out due to lack of proper anelasticity data.

3.2.3 Determination of Parameters of the Constitutive Equations

In view of the steady state nature of deformation, the experimental data have been analyzed in terms of typical steady state creep equation with the incorporation of grain size effect (equation 5). From the $\sigma - \dot{\varepsilon}$ data of regions II and III the grain size exponent (p), activation energy (Q) and the dimensionless constant (A) have been evaluated for each of the regions making use of the regression analysis. These details are presented here. As already mentioned, the variation of the strain rate sensitivity index was within a narrow range for each of the regions and thus 'm' can be approximated as independent of grain size and

temperature. The corresponding stress exponent (n) values are 1.67 and 11.1 in regions II and III respectively.

(a) Grain size exponent

From equation (5), the grain size exponent 'p' can be written as

$$p = - \left[\frac{\partial \log(\dot{\varepsilon}/\sigma^n)}{\partial \log d}\right]_T \qquad (12)$$

Thus at a given temperature, p can be determined by considering strain rate at a fixed stress level or stress at a fixed strain rate for various grain sizes. Alternatively, p can be estimated from the plot of $\log(\dot{\varepsilon}/\sigma^n)$ versus log d at constant temperature.

The grain size exponent at various test temperatures was first estimated using constant strain rate and constant stress data in region II. A strain rate of 4×10^{-4} sec^{-1} and two stresses 1.6 MPa and 4.0 MPa were considered for this purpose. The values of p are found to be nearly the same irrespective of the test temperature. p at different temperatures was also estimated from a plot of $\log \dot{\varepsilon}/\sigma^n$ versus log d (Fig. 26). At 25°C the estimate of p in region II was based on data from two grain sizes only, due to lack of data in region II for other grain sizes. The values of grain size exponent in region II at different temperatures estimated from this analysis are listed in Table 5. Thus the most representative value of p in region II is 3.34 ± 0.23

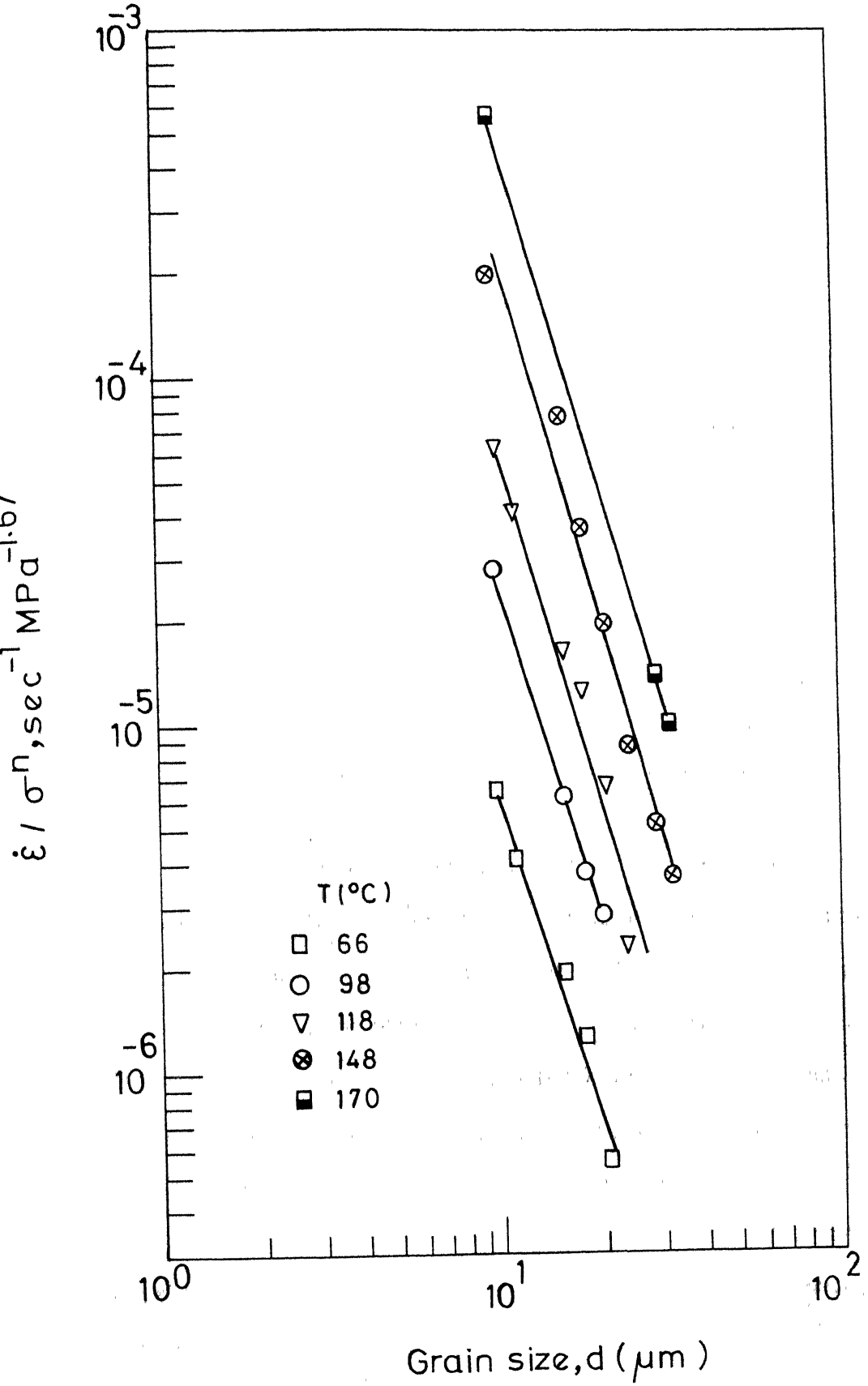

FIG.26 CROSS PLOT FOR GRAIN SIZE EXPONENT DETERMINATION IN REGION II AT DIFFERENT TEMPERATURE

TABLE 5

Experimental Grain Size Exponents at Different Temperatures in Region II

Test Temperature (°C)	Grain Size Exponent p
25	3.38
66	3.09 ± 0.34
98	3.24 ± 0.17
118	3.44 ± 0.35
148	3.59 ± 0.33
170	3.41 ± 0.05

An attempt was made to calculate the grain size exponent 'p' in region III by considering the stress level as a function of grain size at a fixed strain rate for each of the test temperatures. There was considerable scatter in the values of p thus obtained at various temperatures and no systematic trend in variation of p was noticed with respect to the temperature. It was then decided to process the data of all temperatures together in order to obtain a single representative value of the grain size exponent over the whole temperature range that was investigated. From equation (5), the grain size exponent can be written as

$$p = - \frac{d\left(\frac{Q}{RT} + \ln \frac{\dot{\varepsilon} T E^{n-1}}{\sigma^n}\right)}{d \ln d} \qquad (13)$$

Now, making use of the data of region III in the overall temperature and grain size ranges of this study along with the activation energy value for deformation in region III, which is presented in the next section, the value of p is calculated to be 1.00 ± 0.72.

(b) Activation energy (Q)

It may be seen, from the constitutive relation (5), that the activation energy can be evaluated by any of the following equations:

$$Q = - R \frac{d \ln\left(\frac{\dot{\varepsilon} T E^{n-1} d^p}{\sigma^n}\right)}{d(1/T)} \qquad (14)$$

$$= - R \left[\frac{\partial \ln(\dot{\varepsilon} T E^{n-1})}{\partial (1/T)}\right]_{d,\sigma} \qquad (15)$$

$$= nR \left[\frac{\partial \ln(\sigma T E^{n-1})}{\partial (1/T)}\right]_{d,\dot{\varepsilon}} \qquad (16)$$

Activation energy values for deformation in regions II and III have been determined by considering the data for each grain size at constant σ as well as $\dot{\varepsilon}$ and also the overall data for all grain sizes as per the above three equations. Details of Q determination in regions II and III are given below.

In region II activation energy values were determined by using the data corresponding to constant stresses of 1.6 MPa and 4.0 MPa and also by considering a constant strain rate of 4×10^{-4} sec^{-1} for each of the grain sizes. The Q values thus obtained were found to be the same as shown in Table 6 for various grain sizes. Some typical plots

TABLE 6

Experimental Activation Energy Values in Region II

Grain Size, d (μm)	Activation Energy, Q (kJ/mole)	
	$T \leq 135°C$	$T \geq 135°C$
9.7 ± 0.6	44.00 ± 1.66	88.24
11.0 ± 0.6	43.53 ± 2.75	-
13.1 ± 1.2	-	75.17
14.8 ± 0.6	-	82.6 ± 6.5
15.5 ± 0.5	44.92 ± 4.60	-
16.5 ± 1.6	-	86.14
17.4 ± 0.9	46.59 ± 8.92	-
20.1 ± 0.7	53.05 ± 0.54	-
21.1 ± 1.6	-	84.43
28.4 ± 1.6	-	77.22
32.0 ± 1.9	-	74.12

of the logarithmic temperature-compensated strain rate ($\dot{\varepsilon} TE^{n-1}$) versus the reciprocal of the absolute temperature at constant stress are shown in Figure 27 for a few grain sizes. On the basis of the overall data of all grain sizes, Arrhenius plot of $\ln(\frac{\dot{\varepsilon} TE^{n-1} d^p}{\sigma^n})$ versus 1/T was made to determine the activation energy values (Figure 28). For this plot, the quantity $(\frac{\dot{\varepsilon} TE^{n-1} d^p}{\sigma^n})$ was evaluated for each of the test temperatures making use of the data of all grain sizes. This quantity was observed to be almost the same irrespective of the grain size at each of the temperatures and an average of these values was considered for the Arrhenius plot.

A noteworthy feature of the Arrhenius plots was that there are two distinct slopes in these plots indicating two values of activation energy in two different regions of temperature. The slope above $\sim$ 135°C is higher than that below this temperature. This was further confirmed by testing specimens at 170, 160, 148, 135 and 118°C for $\sigma - \dot{\varepsilon}$ data and making Arrhenius plots from these data. The activation energy in the higher temperature range is nearly twice that in the lower range. The observed activation energy in the lower temperature range (below $\sim$ 135°C) is 44.7 $\pm$ 1.1 kJ/mole, whereas in the higher temperature range the value is 81.1 $\pm$ 3.9 kJ/mole.

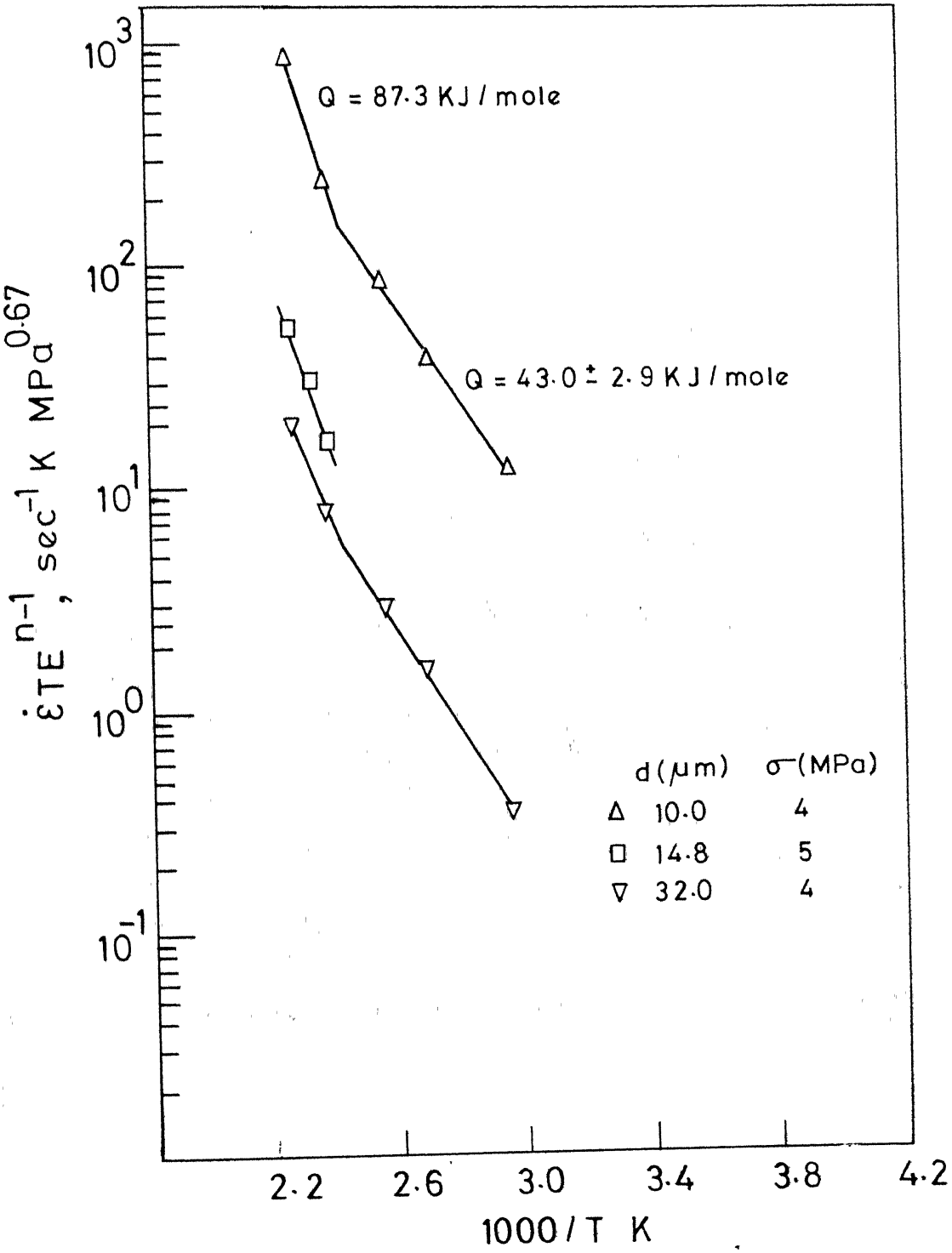

FIG. 27 PLOT OF TEMPERATURE COMPENSATED $\dot{\varepsilon}$ VS. RECIPROCAL TEMPERATURE IN REGION II

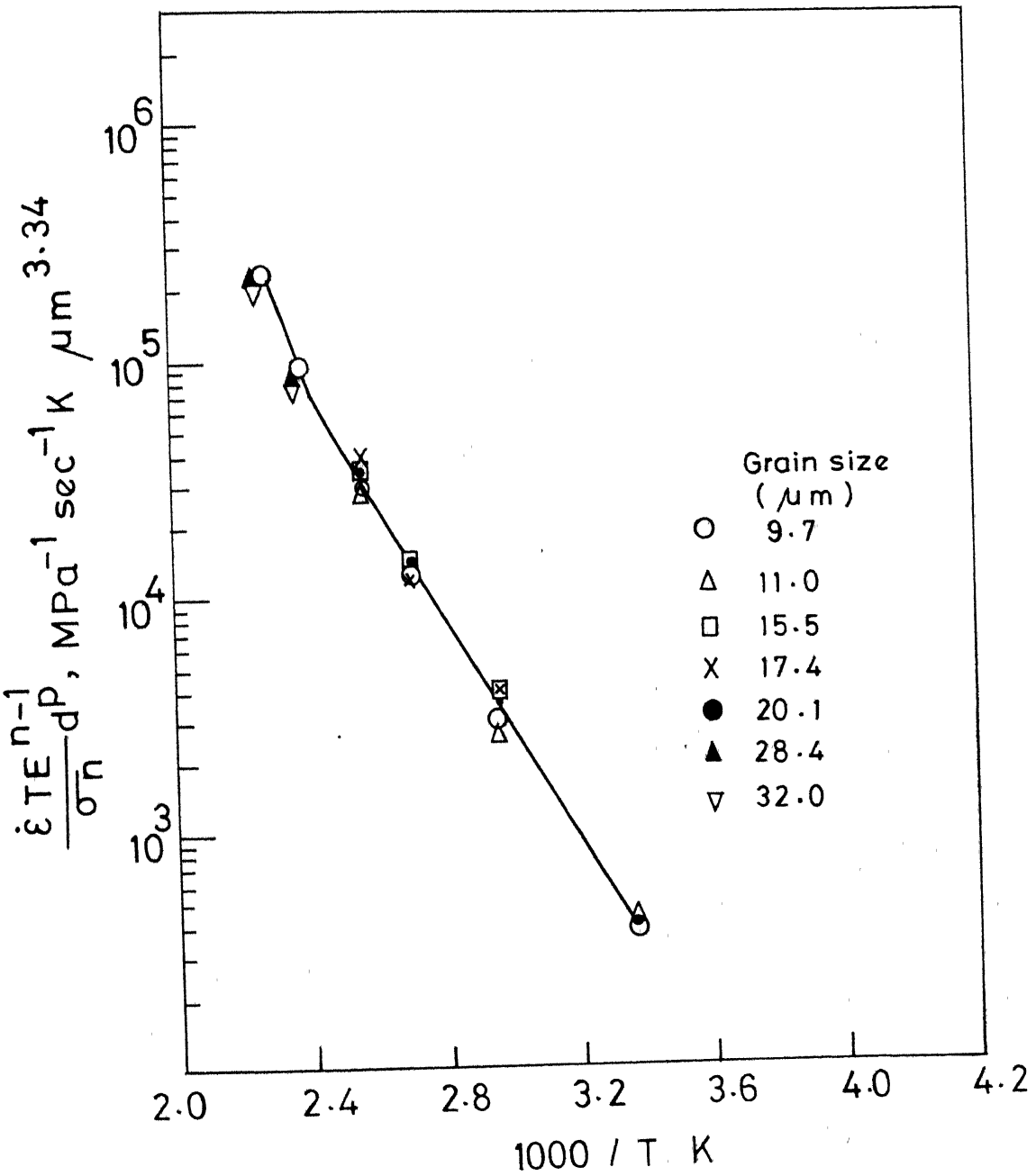

FIG. 28 ARRHENIUS PLOT FOR ACTIVATION ENERGY DETERMINATION IN REGION II

In region III the value of activation energy was calculated using

$$Q = R \left[\frac{\partial \ln \frac{\sigma^n}{\dot{\varepsilon}_{TE}{}^{n-1}}}{\partial (1/T)}\right]_d \qquad (17)$$

These plots for two different grain sizes are shown in Figure 29. The values of activation energy for different grain sizes are seen to be independent of the grain size (Table 7). The observed Q value is 100 ± 8.8 kJ/mole in this region.

TABLE 7

Activation Energy Values in Region III for Different Grain Sizes

Grain Size, d (μm)	Activation Energy, Q (kJ/mole)
15.5 ± 0.5	103.66 ± 16.59
17.4 ± 0.9	105.09 ± 1.97
20.1 ± 0.7	91.43 ± 6.91
28.4 ± 1.6	99.76 ± 9.89

(c) Dimensionless constant (A)

The constant AD_o of the constitutive equation was determined from equation (5) by using the appropriate values

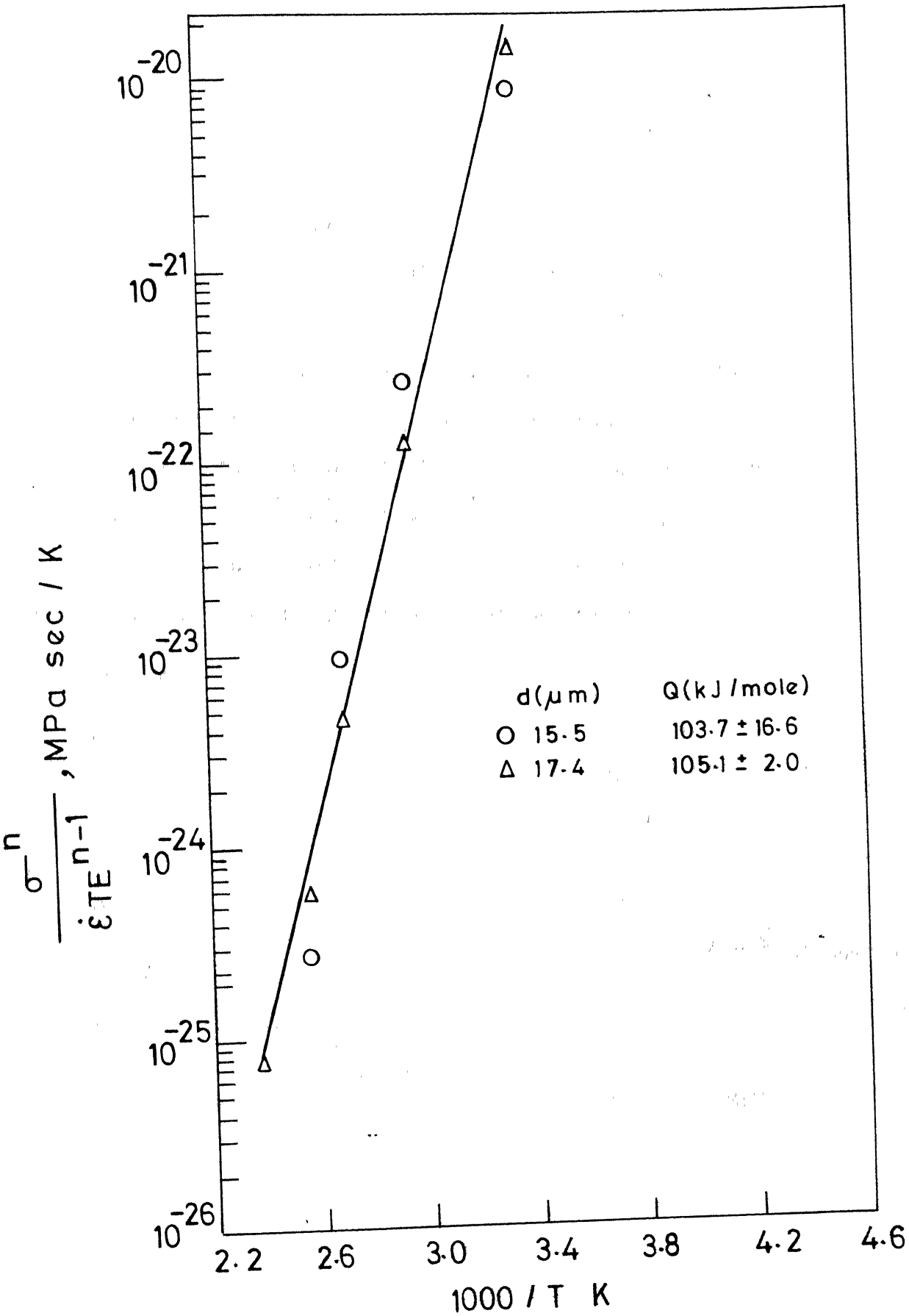

FIG. 29 ARRHENIUS PLOT FOR ACTIVATION ENERGY DETERMINATION IN REGION III

of the parameters n, p and Q corresponding to regions II and III. Taking b value as 3.2 Å, the values of AD_o thus obtained in region II are 1.8×10^{11} cm^2 sec^{-1} and 4.5×10^6 cm^2 sec^{-1} in the temperature ranges above and below ~ 135°C respectively. Using D_o = 4 cm^2 sec^{-1} and 6.44×10^{-2} cm^2 sec^{-1} for lattice and grain boundary self diffusion of Sn [82] respectively, the values of A are 4.6×10^{10} and 7.1×10^7 in the temperature ranges above and below ~ 135°C respectively. In region III the values of AD_o and A are 1.0×10^{32} cm^2 sec^{-1} and 2.5×10^{31} respectively.

Thus, the representative constitutive equations for regions II and III are summarized as follows:

(i) Region II

a) Below ~ 135°C

$$\dot{\varepsilon} = \frac{7.1 \times 10^7 \, D_{ogb(Sn)} \, Eb}{kT} \left(\frac{b}{d}\right)^{3.3} \left(\frac{\sigma}{E}\right)^{1.67} e^{-\frac{44.7 \text{ (kJ/mole)}}{RT}} \quad (18)$$

b) Above ~ 135°C

$$\dot{\varepsilon} = \frac{4.6 \times 10^{10} \, D_{ol(Sn)} \, Eb}{kT} \left(\frac{b}{d}\right)^{3.3} \left(\frac{\sigma}{E}\right)^{1.67} e^{-\frac{81.1 \text{ (kJ/mole)}}{RT}} \quad (19)$$

(ii) Region III

$$\dot{\varepsilon} = \frac{2.5 \times 10^{31} \, D_{ol(Sn)} \, Eb}{kT} \left(\frac{b}{d}\right)^{1} \left(\frac{\sigma}{E}\right)^{11.1} e^{-\frac{100 \text{ (kJ/mole)}}{RT}} \quad (20)$$

where, $D_{ogb(Sn)}$ and $D_{ol(Sn)}$ are pre-exponential factors in the grain boundary and lattice diffusion coefficients for Sn respectively.

3.2.4 Internal and Effective Stress Data

Internal stress measurement by the stress dip test was done in the temperature range of 25°C to 148°C for grain sizes of 11.0 to 23.4 μm. In a few cases, for comparison, internal stress was measured by the alternate unloading and relaxation, called incremental unloading method, from steady state load reached with a selected cross head speed. At 66°C and 118°C with the grain size of 11.0 μm, the internal stress measured by the latter technique was significantly lower than that measured by the stress dip technique. Hence, incremental unloading method was not adopted for internal stress measurements.

Just as in the case of applied stress, the internal stress was observed to be a function of strain rate, temperature and grain size. Some typical data of applied, internal and effective stress against strain rate are shown in Figures 30-33. Also shown in these figures is a comparison between the steady state strain rate corresponding to the stress level at the start of relaxation test as obtained from the differential strain rate test and that ($\dot{\varepsilon}_{ro}$) estimated from the slope of the load versus time curve of the relaxation test at t = 0.

(a) Region II

The data based on internal stress measurements are presented in Tables 8 and 9 for some typical cases.

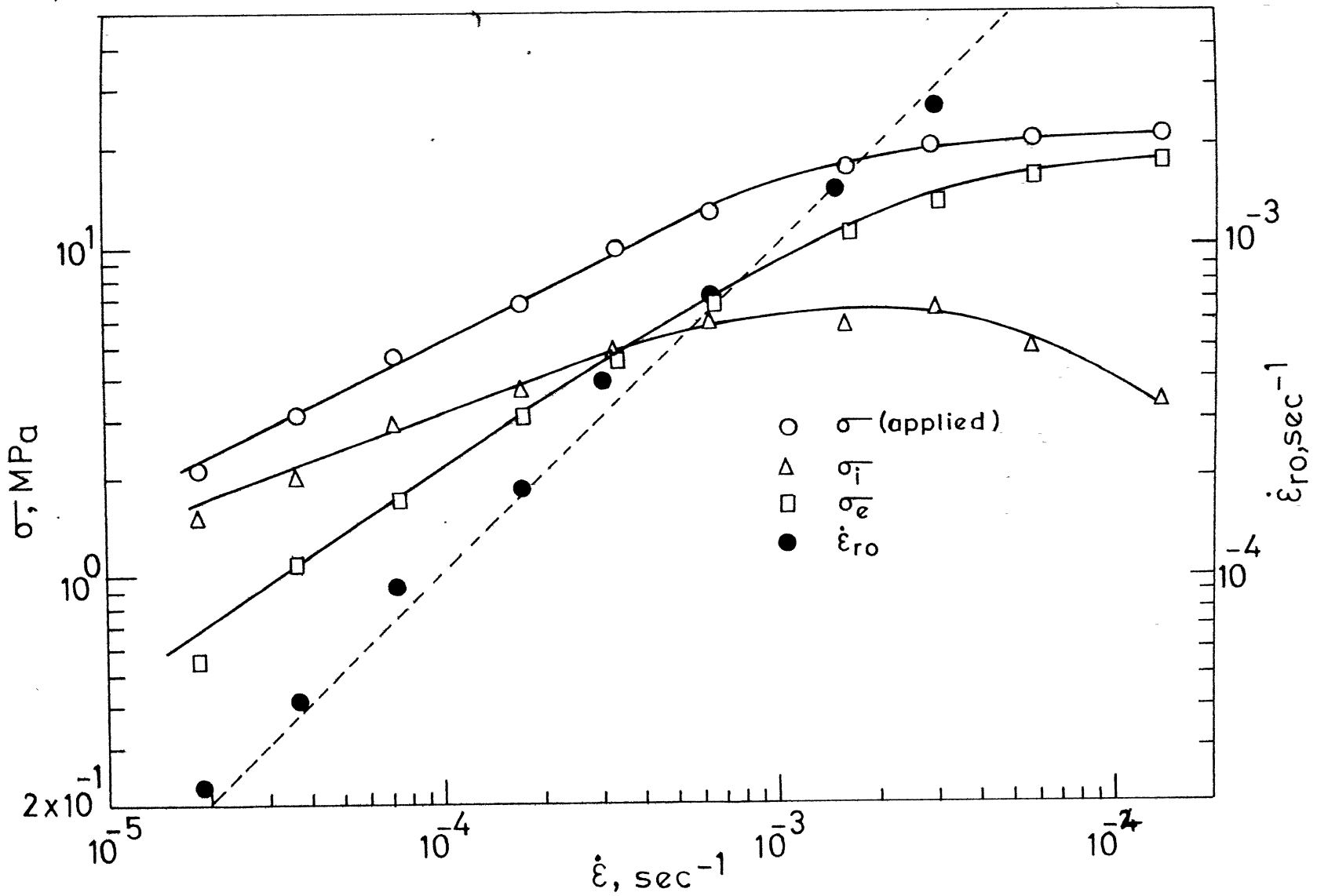

FIG. 30 APPLIED, INTERNAL AND EFFECTIVE STRESSES AS A FUNCTION OF STRAIN RATE (d = 11.0 μm, T = 66°C)

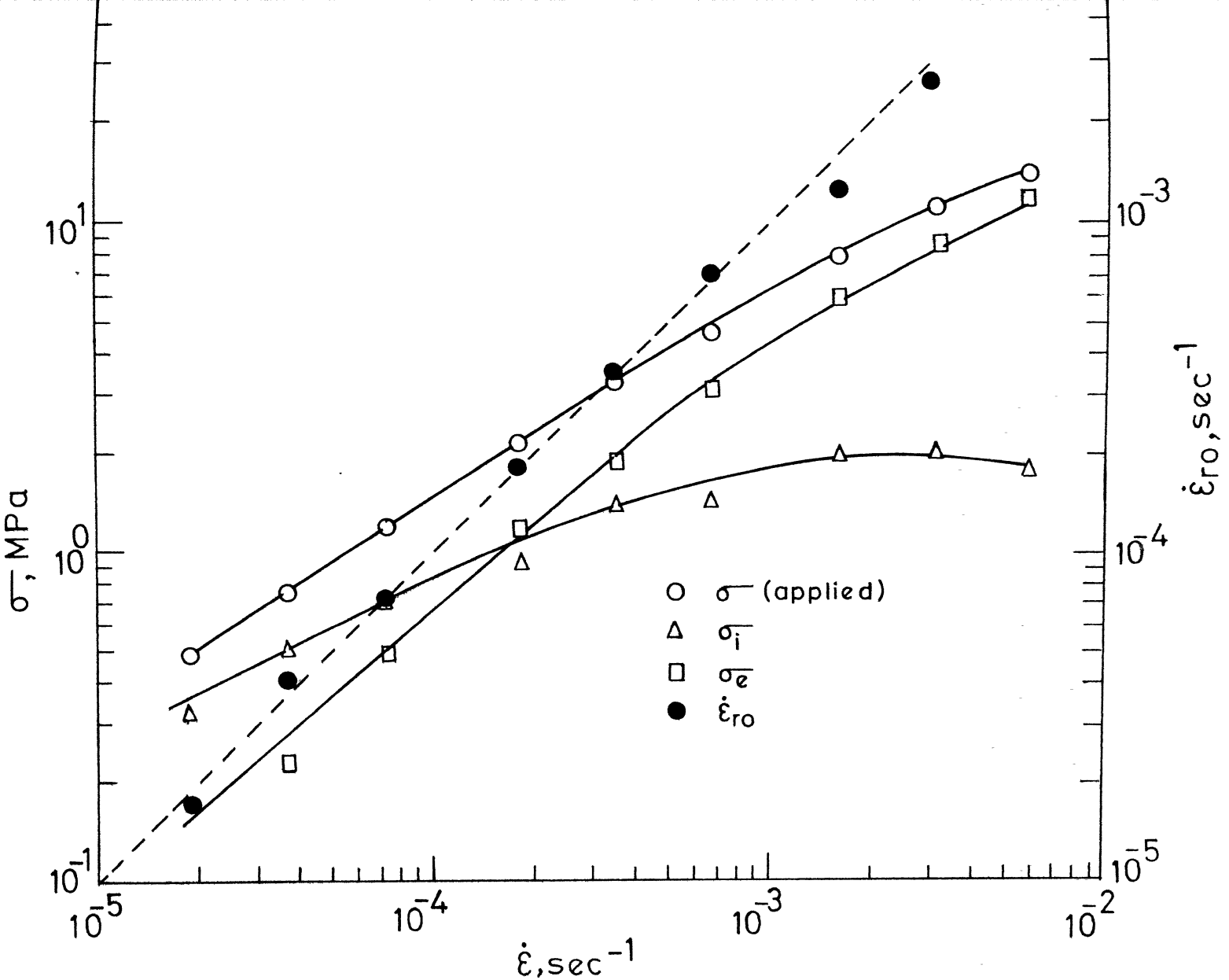

FIG. 31 APPLIED, INTERNAL AND EFFECTIVE STRESSES AS A FUNCTION OF STRAIN RATE ($d = 11.0\ \mu m$, $T = 118°C$)

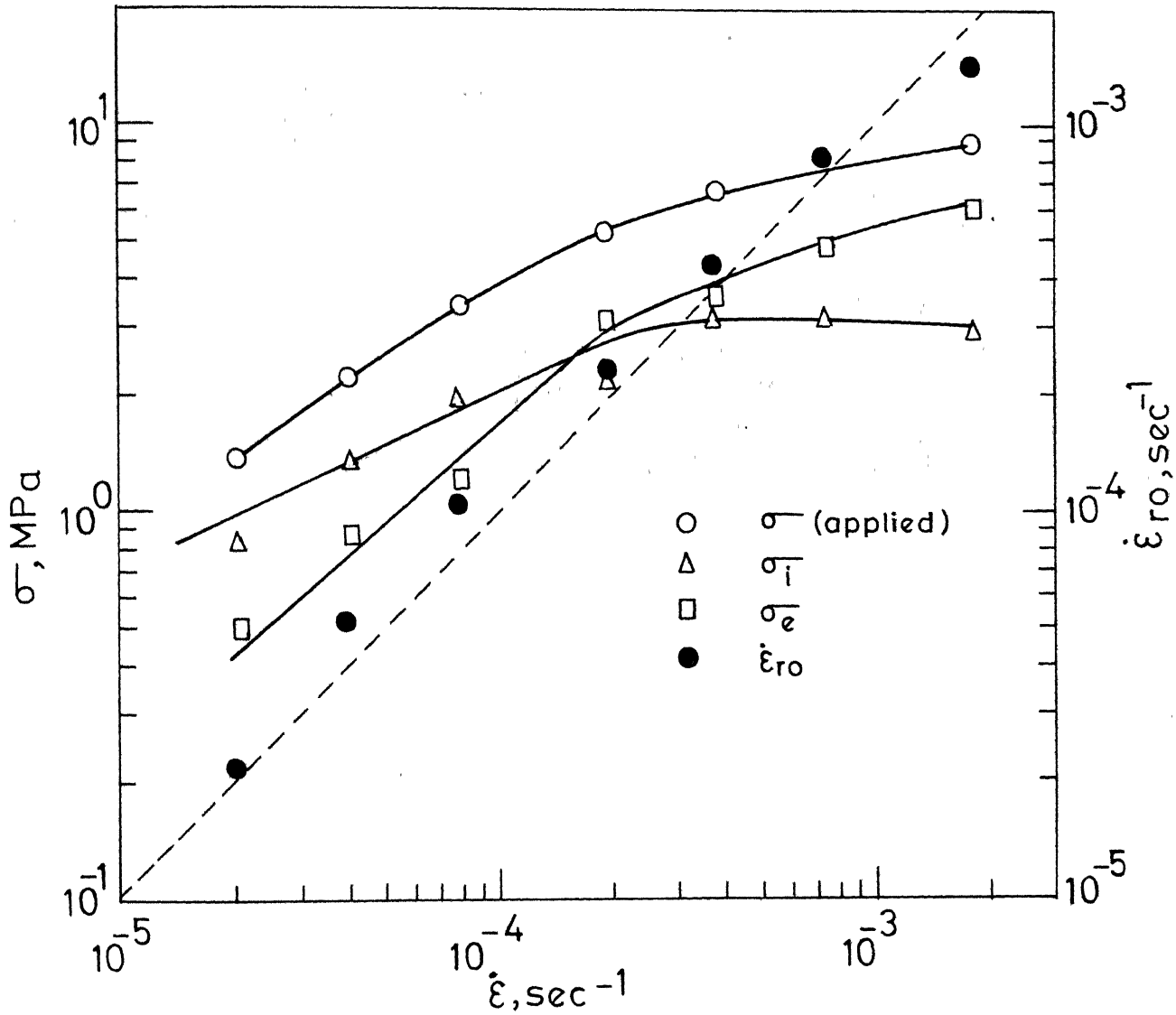

FIG. 32. APPLIED, INTERNAL AND EFFECTIVE STRESSES AS A FUNCTION OF STRAIN RATE (d = 23·4 μm, T = 148 °C)

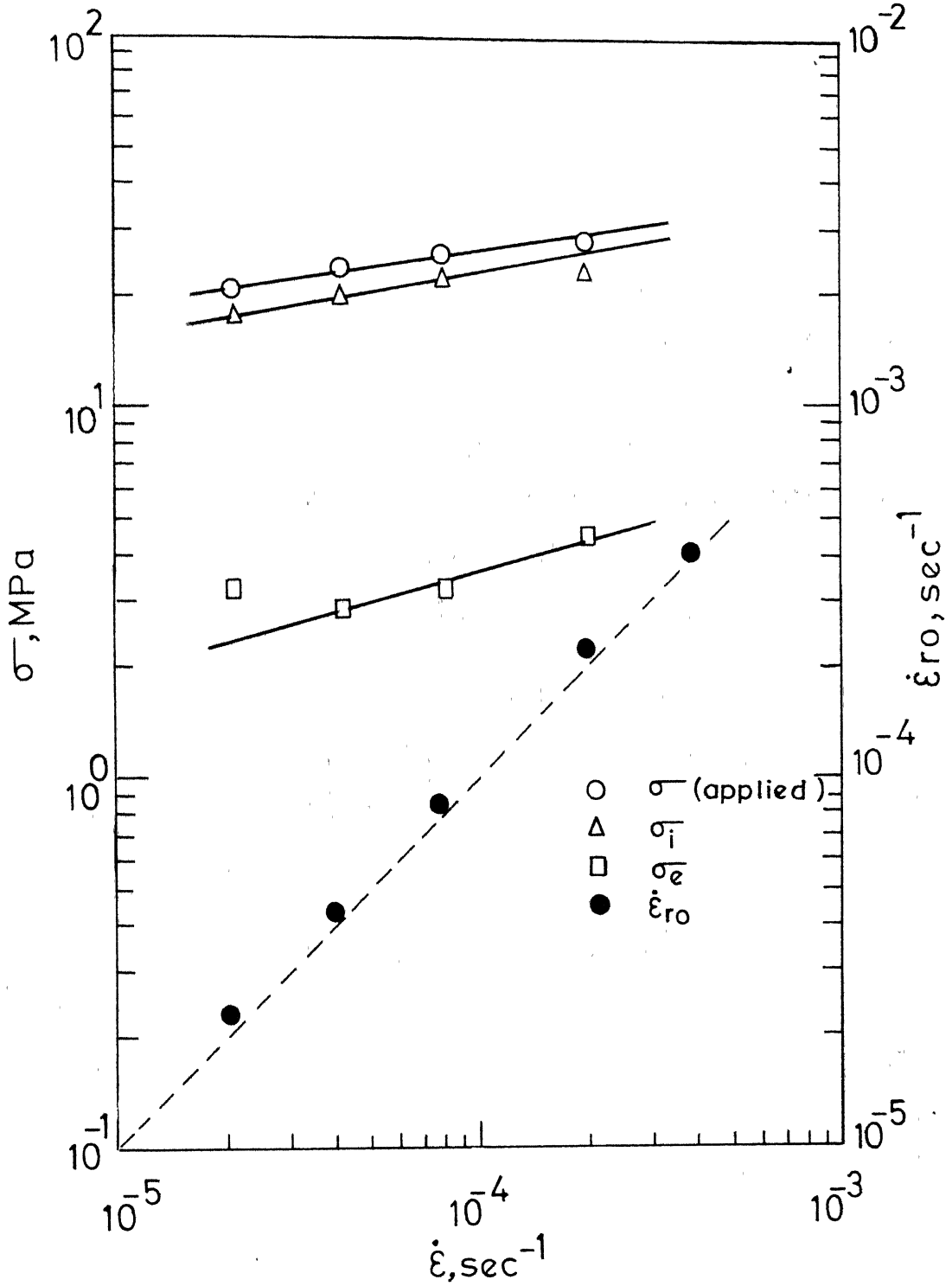

FIG. 33 APPLIED, INTERNAL AND EFFECTIVE STRESSES AS A FUNCTION OF STRAIN RATE (d= 23·4 μm, T = 66 °C)

TABLE 8

Applied (σ), Internal (σ_i) and Effective (σ_e) stresses and Corresponding m Values at $\dot{\varepsilon} = 2.4 \times 10^{-5}$ sec^{-1} in Region II

Stress	Stress (MPa)				Strain Rate Sensitivity Index, m			
	25°C	66°C	118°C	148°C	25°C	66°C	118°C	148°C
				d = 11.0 μm				
σ	10.80	2.50	0.56	0.32	0.43	0.50	0.65	0.70
σ_i	8.75	1.82	0.38	0.19	0.43	0.38	0.50	0.42
σ_e	2.05	0.68	0.18	0.13	0.56	0.71	0.88	0.91
				d = 17.1 μm				
σ	-	6.85	1.50	-	-	0.42	0.70	-
σ_i	-	5.00	0.99	-	-	0.40	0.59	-
σ_e	-	1.85	0.51	-	-	0.70	0.98	-
				d = 23.4 μm				
σ	-	-	4.20	1.55	-	-	0.49	0.67
σ_i	-	-	2.84	0.97	-	-	0.46	0.54
σ_e	-	-	1.36	0.58	-	-	0.64	0.87

TABLE 9

σ_i/σ and Strain Rate Sensitivity Index Values at 148°C in Region II

Grain Sizes μm	Stress Ratio, σ_i/σ			Strain Rate Sensitivity Index		
	$\dot{\varepsilon} = 3\times10^{-5}$ sec^{-1}	$\dot{\varepsilon} = 10^{-4}$ sec^{-1}	$= 3\times10^{-4}$ sec^{-1}	Applied m	Internal m_i	Effective m_e
13.1	0.72	0.60	0.50	0.62	0.39	0.80
16.5	0.72	0.65	0.58	0.63	0.52	0.76
23.4	0.61	0.55	-	0.67	0.59	0.87

It may be noted that the strain rate sensitivity index (m_e) based on effective stress is always higher than that corresponding to the applied stress. The internal stress (σ_i) is seen to be a considerable fraction of the applied stress (Table 9).

For a given grain size and test temperature, the ratio σ_i/σ is found to decrease with increasing strain rate. However, in the case of larger grain sizes the ratio was less sensitive to strain rate at lower temperature range.

Furthermore, at a given strain rate and test temperature, the applied, internal and effective stresses are observed to increase with increasing grain size but the ratio σ_i/σ is nearly independent of grain size (Figure 34).

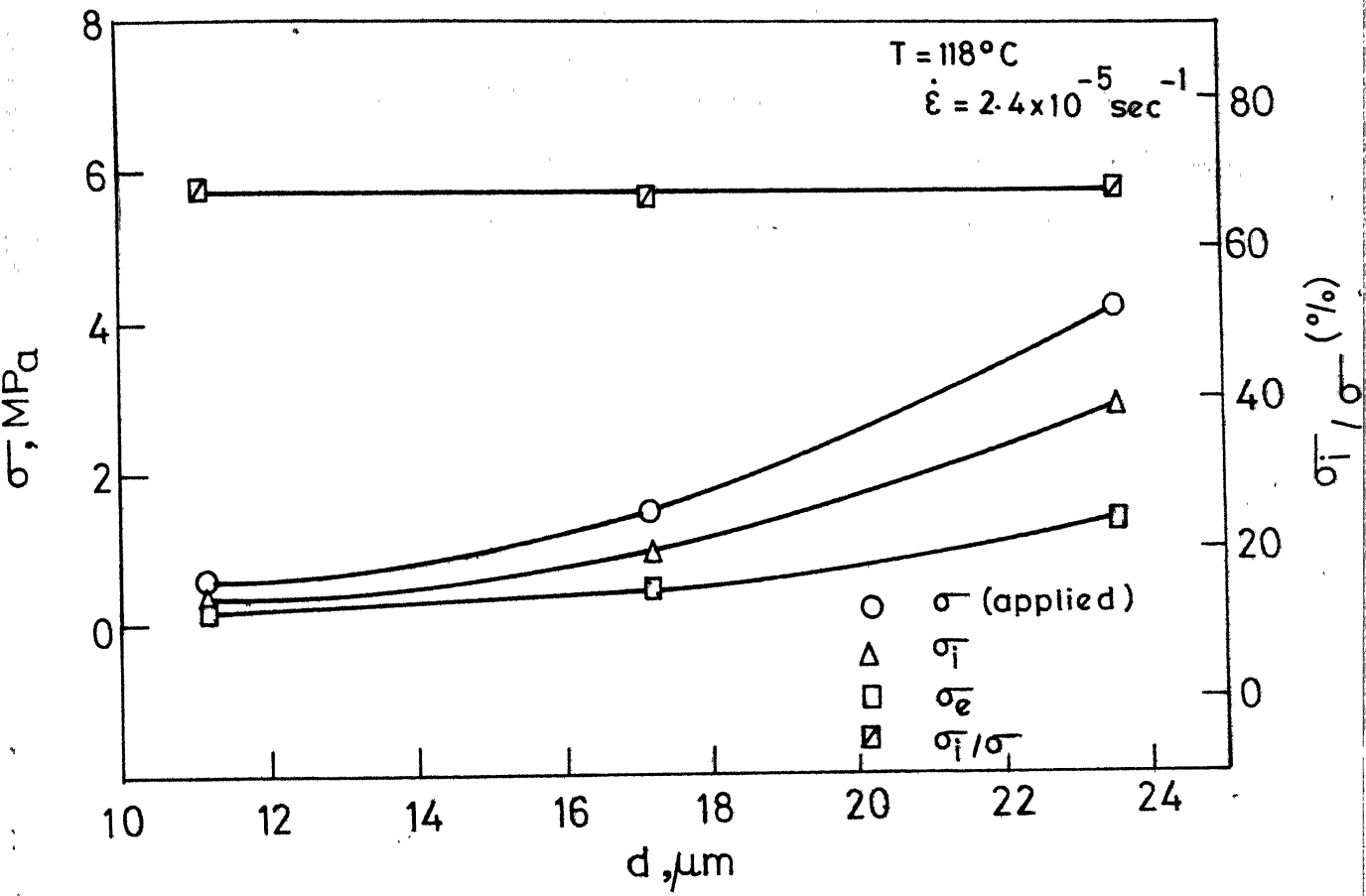

FIG. 34 INFLUENCE OF GRAIN SIZE ON APPLIED, INTERNAL AN EFFECTIVE STRESSES IN REGION II.

The temperature effects on these data are illustrated in Figure 35 by considering the data at a constant strain rate for a grain size of 11 μm. It is seen that the applied, internal and effective stresses decrease with increase in temperature. A slight decrease in the ratio σ_i/σ with increasing temperature is also noticed. By considering the data at a higher strain rate, σ_i/σ is observed to decrease more rapidly with temperature than the one shown in Figure 35.

In order to study whether there is any strain dependency of internal stress, internal stress measurements were repeated as a function of strain rate on the same specimen after considerable strain. As in the case of applied stress, the internal stress corresponding to a given strain rate, temperature and grain size was found to be independent of the strain level at which the measurement was made.

The parameters of the constitutive equation were estimated on the basis of effective stress and internal stress. Based on effective stress, the grain size exponent is found to be 2.8 ± 0.28, whereas the activation energy is 33.5 kJ/mole. Further, the activation energy (Q) and the strain rate sensitivity index (m) based on applied, internal and effective stresses are found to be related as per the following equations:

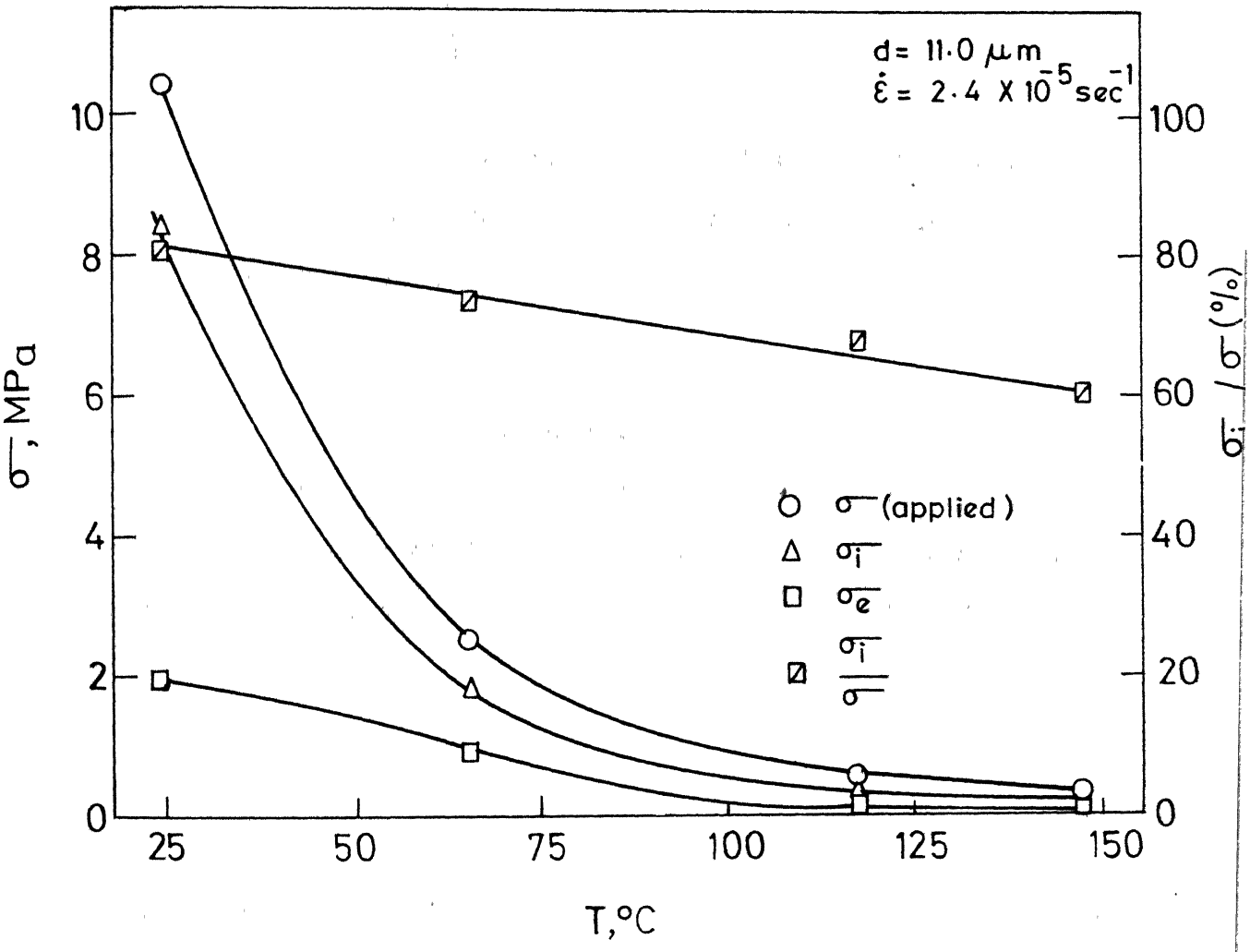

FIG. 35 INFLUENCE OF TEMPERATURE ON APPLIED, INTERNAL AND EFFECTIVE STRESSES IN REGION II

$$Q_j = Q_k + RT\, m_k \left(\frac{\partial \ln \sigma_k}{\partial \ln T}\right)_j \tag{21}$$

$$m_j = m_k \left(\frac{\partial \ln \sigma_k}{\partial \ln \sigma_j}\right)_T \tag{22}$$

where suffixes j and k refer to any two quantities out of three possible ones on the basis of applied, internal and effective stresses.

(b) Region III

As in the case of region II, the strain rate sensitivity index based on effective stress was seen to be higher than that of applied stress. It can be noted from Figure 33 that m_e in region III is of the order of 0.2 to 0.25. In general, the internal stress is a smaller fraction of the applied stress in comparison to that in region II (Table 10). The ratio σ_i/σ is observed to depend strongly on temperature and grain size. In the lower temperature range and for the larger grain size, the ratio of σ_i/σ is similar to that in region II. This ratio decreased rapidly with increasing temperature. This ratio is also found to decrease with increasing strain rate for a given temperature and grain size as in region II.

TABLE 10

Applied (σ), Internal (σ_i) and Effective (σ_e) Stresses in Region III

d (μm)	T (°C)	$\dot{\varepsilon}$ (sec^{-1})	σ (MPa)	σ_i (MPa)	σ_e (MPa)	σ_i/σ
11.0	66	6×10^{-3}	21.20	5.00	16.20	0.24
17.1	66	2×10^{-3}	21.60	10.70	10.90	0.50
23.4	118	2×10^{-3}	16.00	5.95	10.05	0.37

3.2.5 Microstructural Changes due to Deformation in Regions II and III

Microstructural changes due to deformation at various temperatures in regions II and III were followed in specimens of different grain sizes.

(a) Region II

Microstructural observations were made in specimens of different grain sizes as a function of strain in region II. In some cases, the observations were repeated along the longitudinal section of a single flat specimen at various strains. In general, it was observed that at elongations less than about 100%, there was no appreciable change in the grain size due to the deformation. The only noticeable change in the microstructure in these cases was that interphase boundaries became rounder due to deformation. At higher strains, there was some tendency towards grain coarsening especially in specimens of smaller grain sizes. Some of these observations are reported below.

Microstructural changes at different strain levels at 148°C were followed in the longitudinal section of flat tensile samples. These microstructural observations were made repeatedly on the longitudinal section of the same sample at various strains. At different strain levels with an initial strain rate of 3×10^{-4} sec^{-1}, the microstructures remained unchanged. The grain sizes in the

longitudinal section corresponding to 0, 50 and 200 percent elongations are found to be the same ($\sim$26 μm). The transverse grain size in the beginning and at the end of this test was also checked and noted to be constant and equal to that of the longitudinal section.

Detailed microstructural studies before and after a large amount of deformation were made using round specimens having grain sizes 13.1, 16.5 and 21.1 μm at 66°C and 148°C. In these tests, two initial strain rates of 1.2×10^{-4} sec^{-1} and 2.9×10^{-3} sec^{-1} were used. These observations are summarized in Table 11. No change in the shape of the grains

TABLE 11

Changes in Grain Size (Equiaxed) due to Constant Cross Head Speed Deformation

Initial Strain Rate (sec^{-1})	Test Temperature (°C)	Elongation (%)	Grain Size, d (μm)	
			Before Deformation	After Deformation
1.2×10^{-4}	66	200	16.5 ± 1.6	22.5 ± 1.3
		375	13.1 ± 1.2	17.1 ± 0.9
	118	600	11.0 ± 0.6	19.1 ± 1.3
	148	200	21.1 ± 1.6	22.3 ± 1.6
		700	13.1 ± 1.2	21.5 ± 1.4
2.9×10^{-3}	148	375	13.1 ± 1.2	17.8 ± 0.7
		700	16.5 ± 1.6	21.1 ± 1.1

was noticed although some grain growth occurred in all the cases. It can also be seen that specimens having initially smaller equiaxed grains are more susceptible to grain coarsening due to deformation. The extent of coarsening was observed to increase with strain. For the smallest grain size, this increase was by a factor of 2 after 600% elongation at 118°C, whereas the grain coarsening was much less in specimens having initially larger grain size. The degree of grain coarsening was found to be more at higher test temperatures and lower strain rates. Thus, initially equiaxed grains remain essentially equiaxed after large superplastic deformation with no more than a slight coarsening of grain size. However, typical characteristics of deformed structures in superplastic region viz, wavy phase boundaries and fine scale protuberances by mutual interpenetration of phases with some change in distribution of phases, were seen. Figures 36 and 37 illustrate the typical microstructures in the longitudinal section after constant cross head speed deformation in the superplastic region.

(b) Region III

In region III, some grain elongation was evident due to deformation. Typical observations of this nature are given here. A flat tensile sample having a grain size of 26 μm was deformed at 148°C with an initial strain rate

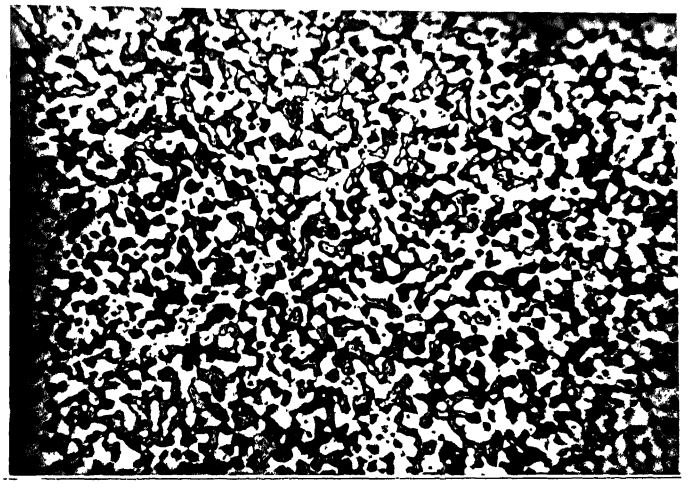

(a) Initial

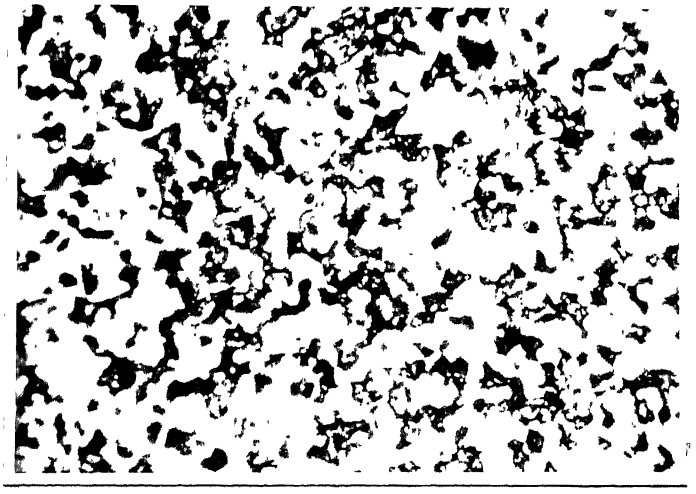

(b) Final

FIGURE 36. MICROSTRUCTURAL CHANGE DUE TO 375% NOMINAL STRAIN IN REGION II (INITIAL d = 13.1 μm, T = 148°C) (MAGNIFICATION: 300X).

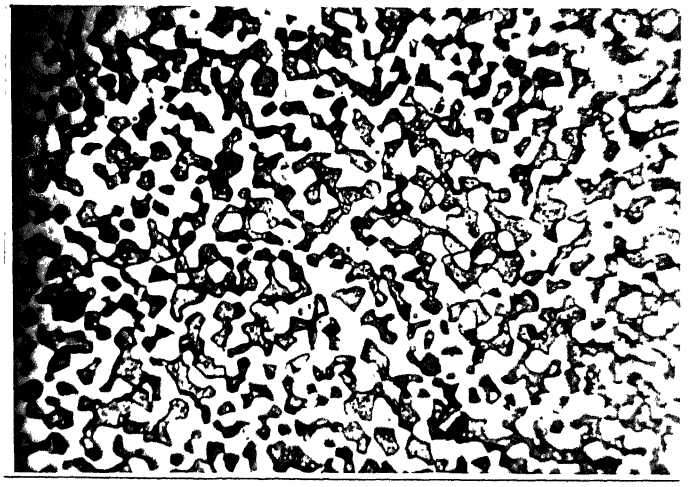

(a) Initial

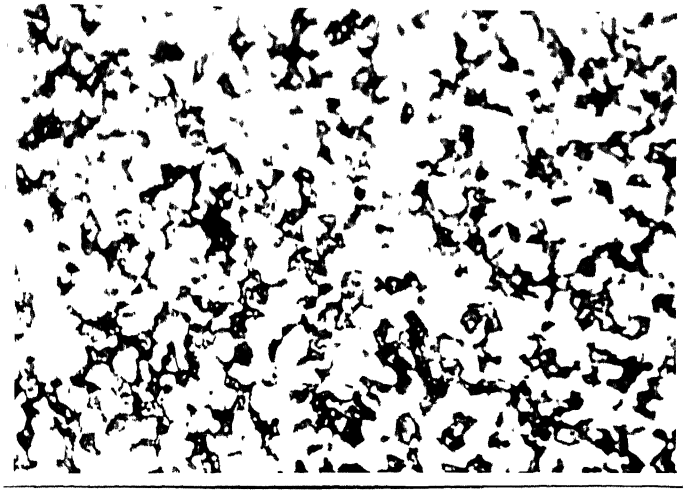

(b) Final

FIGURE 37. MICROSTRUCTURAL CHANGE DUE TO 700% NOMINAL STRAIN IN REGION II (INITIAL d = 16.5 μm, T = 148°C) (MAGNIFICATION: 300X).

of 4.5×10^{-3} sec^{-1} to about 70% elongation. The grains were seen to be elongated in the loading direction due to this deformation. At this stage of deformation, there was a neck formation in the tensile specimen. The grain elongation was observed to be more in the necked region in comparison to the regions outside the neck of the tensile specimen. No significant change in grain size was noticed in the transverse section.

Further, a round tensile sample having an initial equiaxed grain size of 21.1 μm (mean intercept length = 12.1 μm) was deformed with an initial strain rate of 2.9×10^{-3} sec^{-1} at 66°C. The microstructure in the transverse section is unaltered in shape and size, whereas in the longitudinal section of the necked region (local elongation = 400%) the grains are observed to become elongated with a grain aspect ratio of ~ 2, as shown in Figure 38. The intercept lengths measured from the microstructures of the necked portion of the tensile specimen are as follows:

$l_{//} = 20.4 \pm 0.9$ μm; $l_{\perp} = 10.9 \pm 0.9$ μm; $l_T = 10.5 \pm 0.9$ μm

3.3 MECHANICAL BEHAVIOUR OF SPECIMENS HAVING BANDED STRUCTURES AND ELONGATED GRAINS

The observations on mechanical behaviour of specimens with banded structures and elongated grains obtained by using the methods given in Section 2.3 are presented in this section.

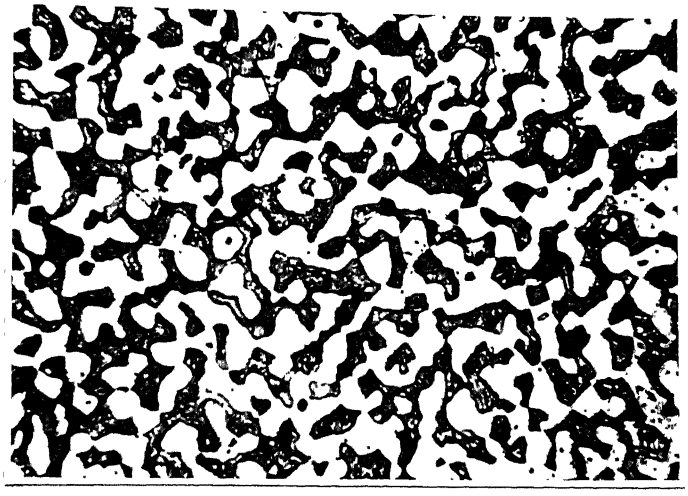

(a) Initial

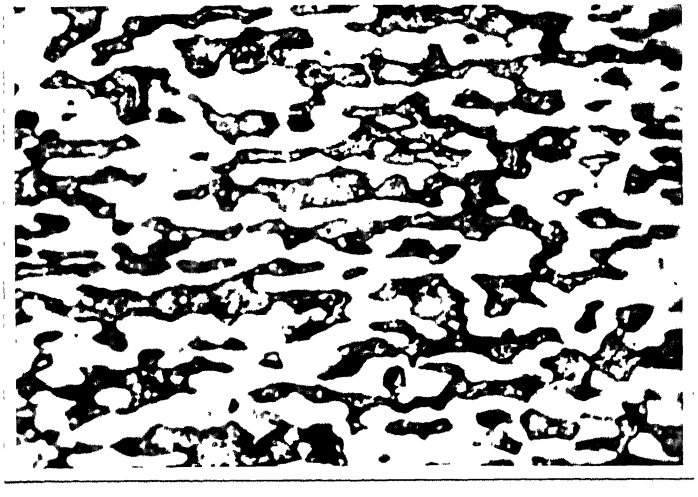

(b) Final

FIGURE 38. MICROSTRUCTURAL CHANGE DUE TO 400% NOMINAL STRAIN (AT THE NECK) IN REGION III (MAGNIFICATION: 300X).

3.3.1 Banded Structures

In the specimens having banded structures, there was clustering of Pb rich grains along the direction of working, whereas the distribution of phases was uniform in the transverse section. Typical longitudinal and transverse microstructures of these specimens are shown in Figure 39. The characterization of these banded structures was done in terms of the intercept lengths in the transverse section (b_T), as well as band length ($b_{\parallel}$) and band width ($b_{\perp}$) in the longitudinal section.

Specimens at orientations of 0°, 45° and 90° with respect to the extrusion axis were prepared for compression testing in order to check the anisotropy of strength in these banded structures. It can be noted from Figure 40, that the flow stress of these specimens did depend on orientation with a minimum for 45° orientation.

Tensile specimens with banded microstructures shown in Figure 39 were tested at various temperatures and the $\sigma - \dot{\varepsilon}$ data are shown in Figure 41. The strain rate sensitivity index obtained by the differential strain rate test as a function of strain rate is shown in Figure 42. From these data, activation energy values were estimated in region II and found to have two distinct values as in the case of specimens having equiaxed structures. The Q value in the lower temperature range is $\simeq$ 42 kJ/mole, while the higher temperature range value is $\simeq$ 91 kJ/mole.

(a)

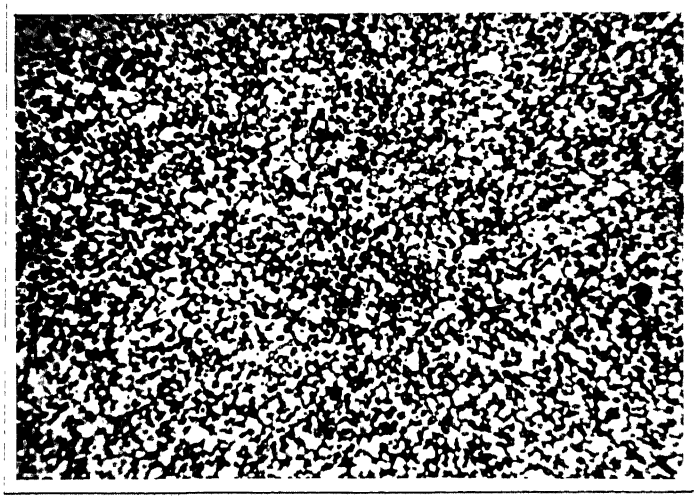

(b)

FIGURE 39. LONGITUDINAL (a) AND TRANSVERSE (b) MICROSTRUCTURES OF SPECIMENS HAVING BANDED STRUCTURES (MAGNIFICATION 300X).

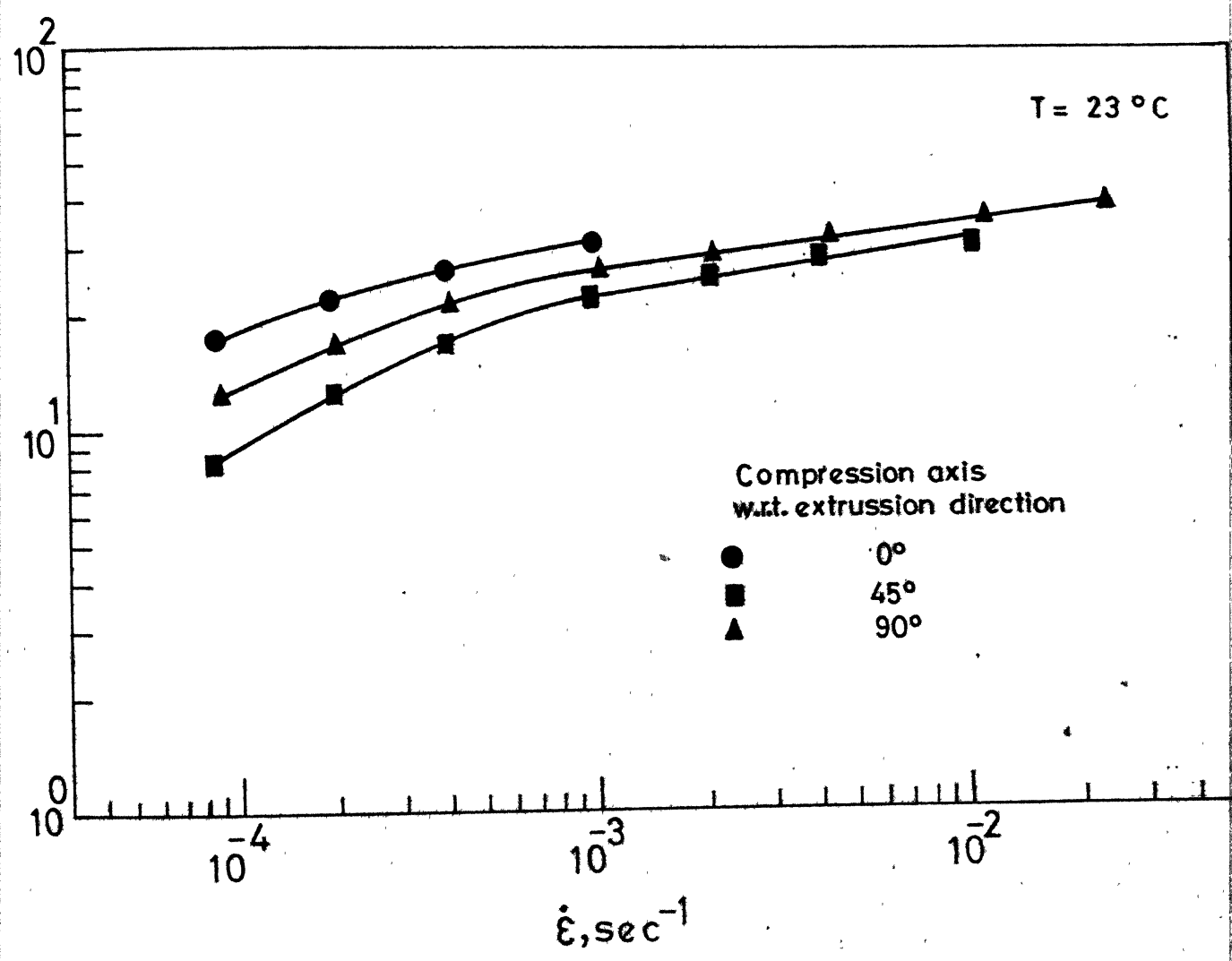

G. 40 ANISOTROPY IN σ-$\dot{\varepsilon}$ BEHAVIOUR OF A SPECIMEN W
BANDED STRUCTURE

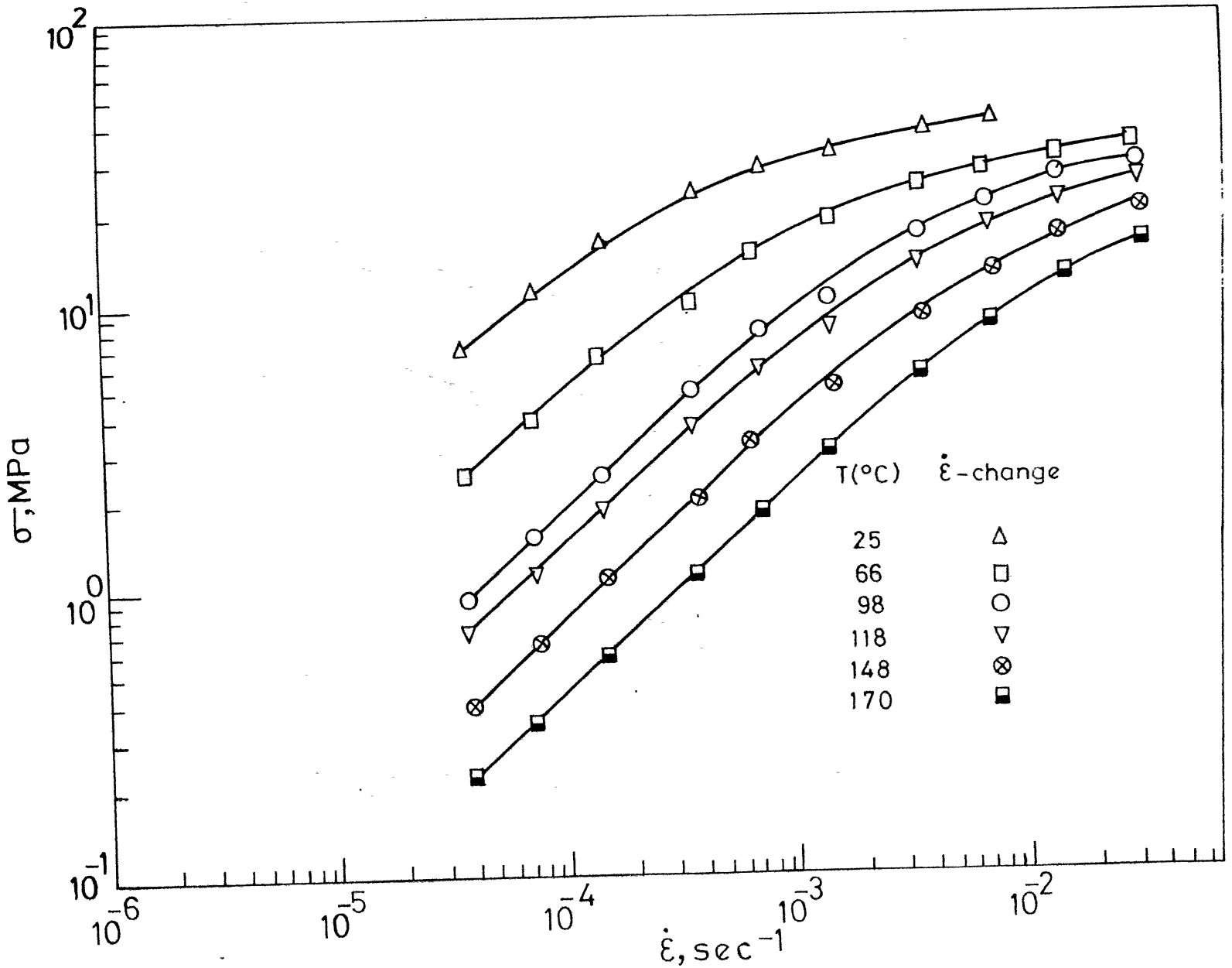

FIG. 41 $\sigma - \dot{\varepsilon}$ BEHAVIOUR OF SPECIMENS WITH BANDED STRUCTURES.
($d_\alpha = 22.5 \pm 2.8$ μm, $b_\alpha = 4.9 \pm 0.2$ μm, $b_T = 4.8 \pm 0.6$ μm)

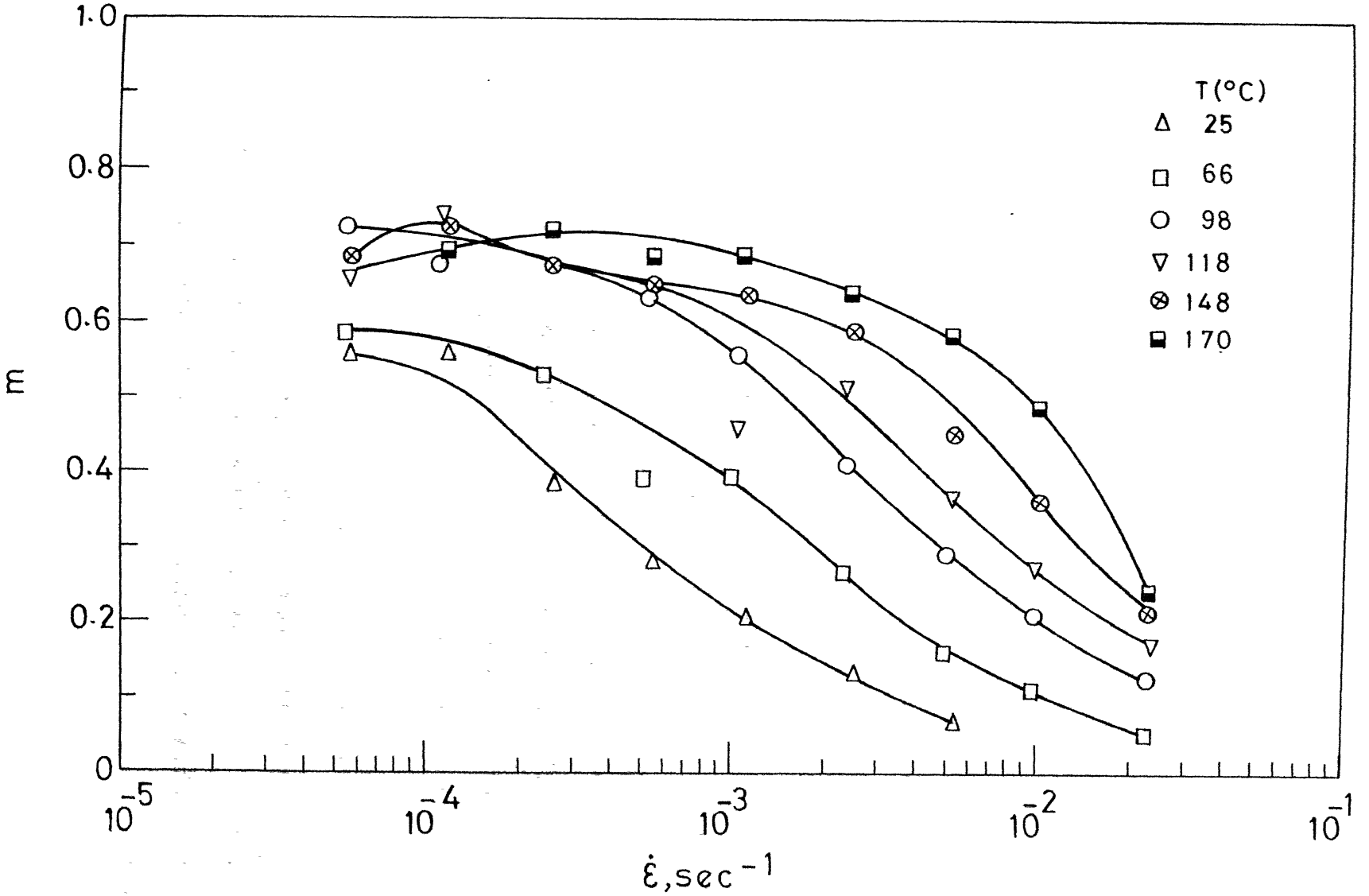

FIG. 42 m VS. $\dot{\varepsilon}$ PLOTS AT DIFFERENT TEMPERATURES FOR BANDED STRUCTURE
($b_{\parallel} = 23.5 \pm 2.8\ \mu m$, $b_{\perp} = 4.9 \pm 0.2\ \mu m$, $b_T = 4.8 \pm 0.6\ \mu m$)

The strain effects on the mechanical behaviour and microstructure were studied through strain rate cycling and constant cross head speed tests in samples having initially banded structures. Figure 43 shows the $\sigma - \dot{\varepsilon}$ data obtained by repeated strain rate cycling upto the sixth cycle in a test at 148°C. While the strain rate sensitivity index was not affected due to repeated strain rate cycling, there was some increase in flow stress at a given strain rate upto the third cycle beyond which no further change occurred. In another case, $\sigma - \dot{\varepsilon}$ data were collected in two strain rate cycles with an intermediate constant cross head speed deformation of 50% elongation at 148°C. Similar strain effects as in the previous case were noticed.

Also, by annealing the specimens having banded structures for a short time (3 hrs. at 148°C), it was found that the flow stress was higher than that of the unannealed specimen. On the other hand, the same annealing treatment given after the third cycle of the differential strain rate test did not influence the $\sigma - \dot{\varepsilon}$ behaviour in the subsequent cycles.

The stress-strain curves of specimens with banded structures obtained by constant cross head speed tests at 148°C at two different initial strain rates are shown in Figure 44. Also shown in this figure is the flow stress corrected for constant strain rate. It is seen that with

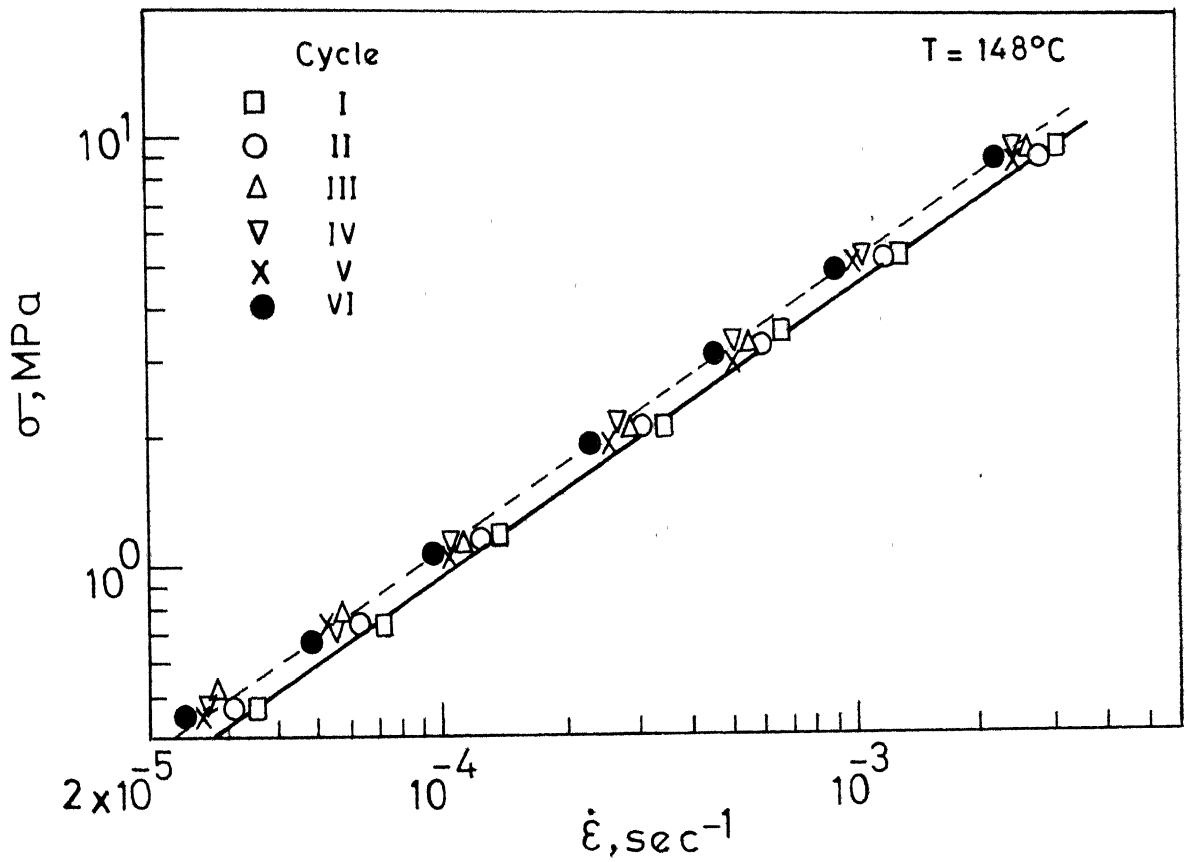

FIG. 4 3 EFFECT OF REPEATED STRAIN RATE CYCLING ON $\sigma - \dot{\varepsilon}$ BEHAVIOUR OF SPECIMEN WITH INITIALLY BAND STRUCTURE .($b_{\parallel} = 32.3\,\mu m$, $b_{\perp} = 6.0\,\mu m$, $b_T = 5.8$

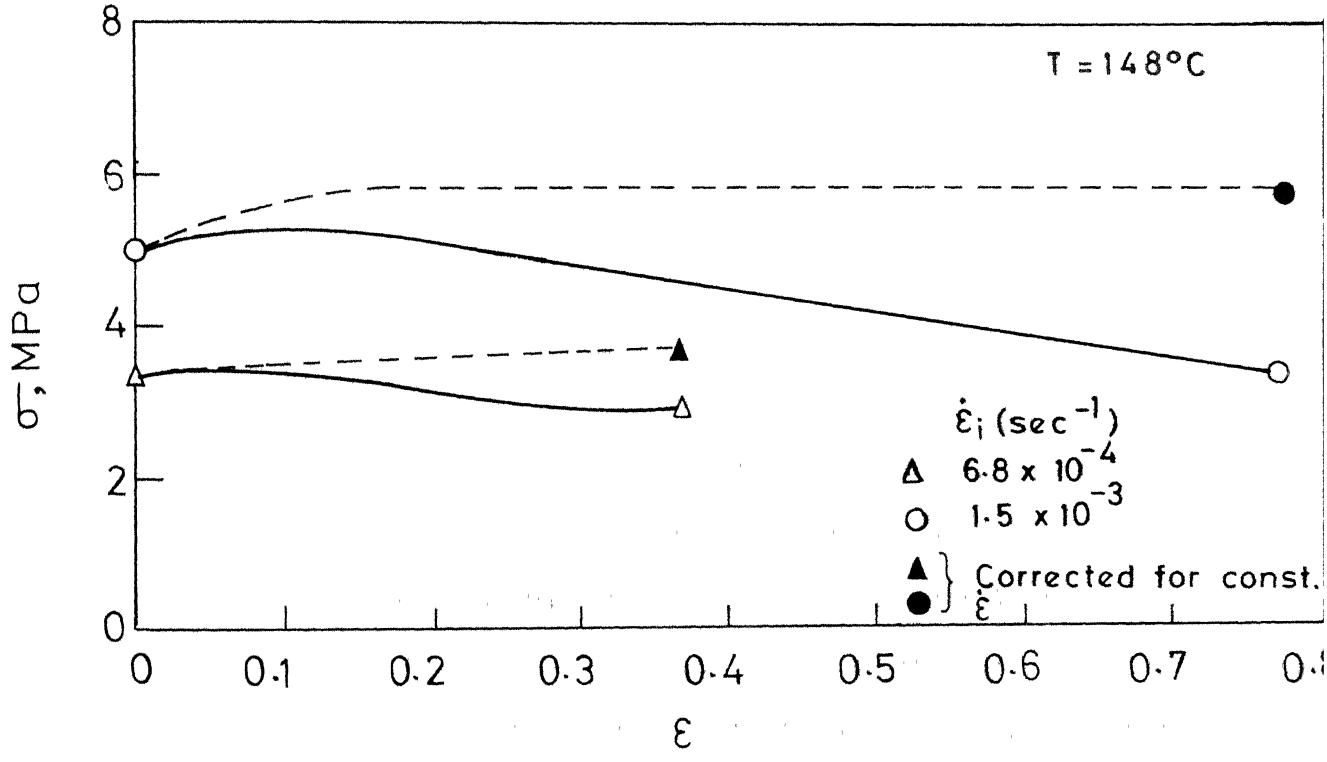

FIG. 44 $\sigma - \dot{\varepsilon}$ DATA OBTAINED FROM CONSTANT CROSS HEAD SPEED TESTS FOR SPECIMENS HAVING INITIALLY BA STRUCTURES ($b_{\parallel} = 32{\cdot}3\ \mu m$, $b_{\perp} = 6{\cdot}0\ \mu m$, $b_T = 5{\cdot}8\ \mu$

$\dot{\varepsilon} = 1.5 \times 10^{-3}$ sec^{-1} the stress level becomes independent of strain after some initial hardening. At a lower initial strain rate of 6.8×10^{-4} sec^{-1}, the initial hardening is less and the gradual increase in flow stress extends to a larger strain level. The microstructural parameters as a function of strain in these specimens are given in Table 12. The band length to width ratio decreased more rapidly with increasing strain than due to the static annealing alone. As in the case of linearly elongated grains, the extent of banding in these structures may be characterized by the degree of orientation [73] defined by

$$\text{Or},\% = \frac{100\left[(N_L)_{\perp} - (N_L)_{\parallel}\right]}{0.273(N_L)_{\parallel} + (N_L)_{\perp}} \qquad (23)$$

where N_L is number of bands per unit length and the subscript $\parallel$ refers to secants drawn parallel to the working direction in longitudinal section, $\perp$ refers to secants drawn perpendicular to the working direction in longitudinal section and $\perp$ refers to secants drawn in the transverse section having equiaxed grains. The degree of orientation thus calculated is observed to decrease with strain (Table 12). Microstructural changes representing the break up of the banded structures are shown in Figures 45 and 46. Significant grain coarsening due to deformation is evident from the microstructures of the transverse sections.

TABLE 12

Changes in Microstructural Parameters of Banded Structures due to Constant Cross Head Speed Deformation

Test Temperature = 148°C

Initial Strain Rate = 1.5×10^{-3} sec^{-1}

Elongation (%)	Band Intercept Lengths in Gauge Section (μm)			$\frac{b_{\parallel}}{b_{\perp}}$		Degree of Orientation or, (%)	
	Longitudinal		Transverse	Gauge	Shoulder	Gauge	Shoulder
	$b_{\parallel}$	$b_{\perp}$	b_T				
0	32.3±5.7	6.0±0.3	5.8±0.3	5.4	5.4	74.9	74.9
50	11.2±1.0	7.4±0.3	7.0±0.4	1.5	3.2	27.2	61.6
425	12.4±0.7	9.3±0.7	8.5±0.4	1.3	3.2	19.2	61.5

$b_{\parallel}$ = Band length measured parallel to tensile axis in longitudinal section

$b_{\perp}$ = Band length measured perpendicular to tensile axis in longitudinal section

b_T = Intercept length in transverse section.

(a)

(b)

(c)

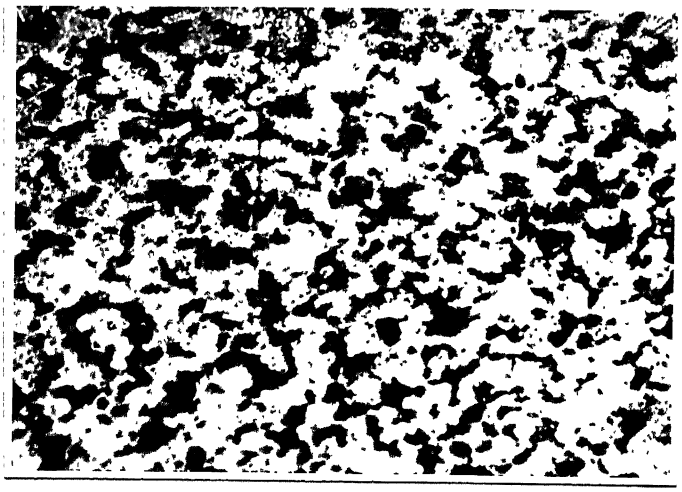

FIGURE 45. MICROSTRUCTURAL CHANGES IN LONGITUDINAL SECTION OF AN INITIALLY BANDED STRUCTURE (b_{ℓ} = 32.3 ± 5.7 μm, b_t = 6.0 ± 0.3 μm, b_T = 5.8 ± 0.3 μm) DUE TO DEFORMATION IN REGION II (MAGNIFICATION: 300X). (a) ε = 0%, (b) ε = 50% and (c) ε = 100%.

(a)

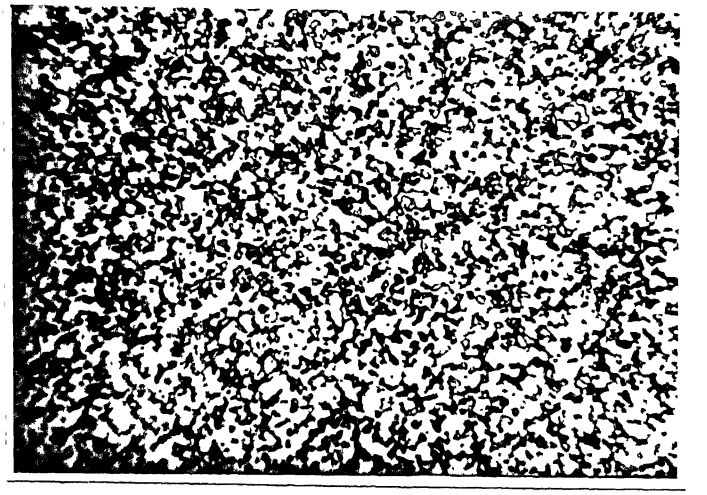

(b)

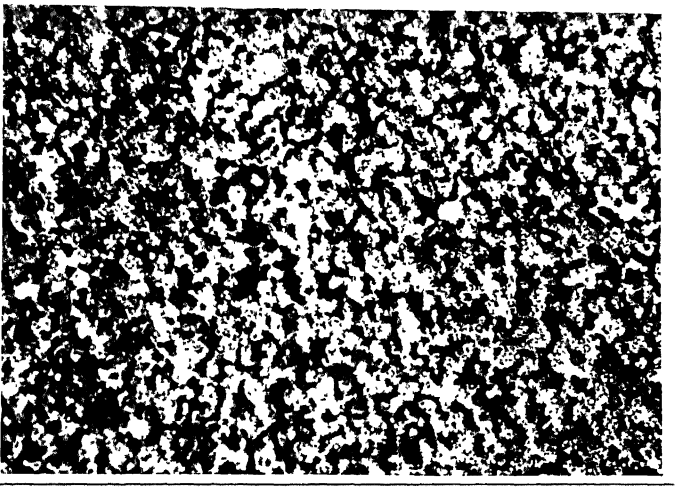

(c)

FIGURE 46. MICROSTRUCTURAL CHANGES IN TRANSVERSE SECTION OF A INITIALLY BANDED STRUCTURE ($b_{||} = 32.3 \pm 5.7$ μm, $b_{\perp} = 6.0 \pm 0.3$ μm, $b_T = 5.8 \pm 0.3$ μm) DUE TO DEFORMATION IN REGION II (MAGNIFICATION: 300X). (a) $\varepsilon = 0\%$, (b) $\varepsilon = 50\%$ and (c) $\varepsilon = 100\%$.

Internal stress measurements were also carried out at different temperatures. The values of applied, internal and effective stresses for a few cases are shown in Table 13.

TABLE 13

Applied (σ), Internal (σ_i) and Effective (σ_e) Stresses and Corresponding m Values for Banded Structures in Region II (Strain Rate = $\dot{\varepsilon}$ x 10^{-5} sec^{-1})

	Test Temperature (°C)			
	98	118	148	170
σ (MPa)	1.43	0.71	0.43	0.28
m	0.65	0.80	0.71	0.77
σ_i (MPa)	0.92	0.37	0.24	0.15
m_i	0.45	0.83	0.46	0.61
σ_e (MPa)	0.51	0.34	0.19	0.13
m_e	0.90	1.00	1.00	0.93

alongwith the corresponding m values in region II. Typical plots of σ_e vs. $\dot{\varepsilon}$ at 118°C, 148°C and 170°C are shown in Figure 47. The ratio σ_i/σ is seen to decrease with increasing strain rate at any given temperature. This ratio of σ_i/σ, when compared at a given strain rate, is observed to decrease with increasing temperature.

3.3.2 Elongated Grain Microstructures

The mechanical behaviour of specimens with two types of elongated grains (linear and planar-linear orientations) was studied.

(a) Microstructures Having Linear-Orientation of Grains

The tensile samples having linear-orientation of grains obtained by the process given in Section 2.3 2(b) were further deformed in tension to about 30% elongation before studying their mechanical behaviour. Microstructural observations of these specimens revealed distinct grain elongation in the longitudinal section and equiaxed shape in the transverse section (Figure 48). The microstructural characterization was done by measuring intercept lengths $l_{\parallel}$, $l_{\perp}$ and l_T. The grain aspect ratio, $l_{\parallel}/l_{\perp}$, was found to be 1.94. The degree of orientation as defined in equation (23) was found to be 33.43%. The $\sigma - \dot{\varepsilon}$ data of these tensile samples are shown in Figure 49. The m vs. log $\dot{\varepsilon}$ plots at various temperatures are shown in Figure 50. Two values of activation energy were noticed similar to those obtained in the two temperature ranges of equiaxed grains.

(b) Microstructures Having Planar-Linear Orientation of Grains

These microstructures have grain elongations in two directions viz. along the length and width of the rolled

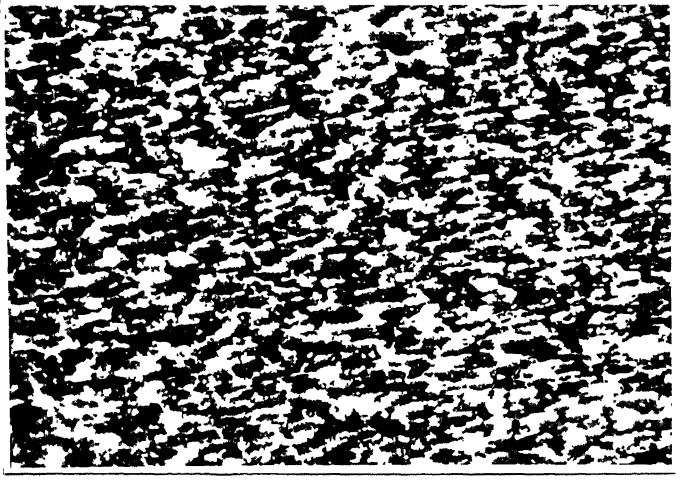

(a)

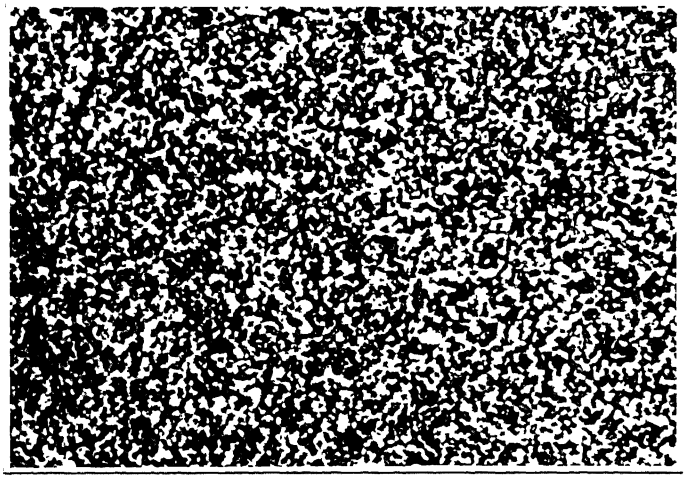

(b)

FIGURE 48. LONGITUDINAL (a) AND TRANSVERSE (b) MICROSTRUCTUI
OF A SPECIMEN HAVING ELONGATED GRAINS
(MAGNIFICATION: 300X).

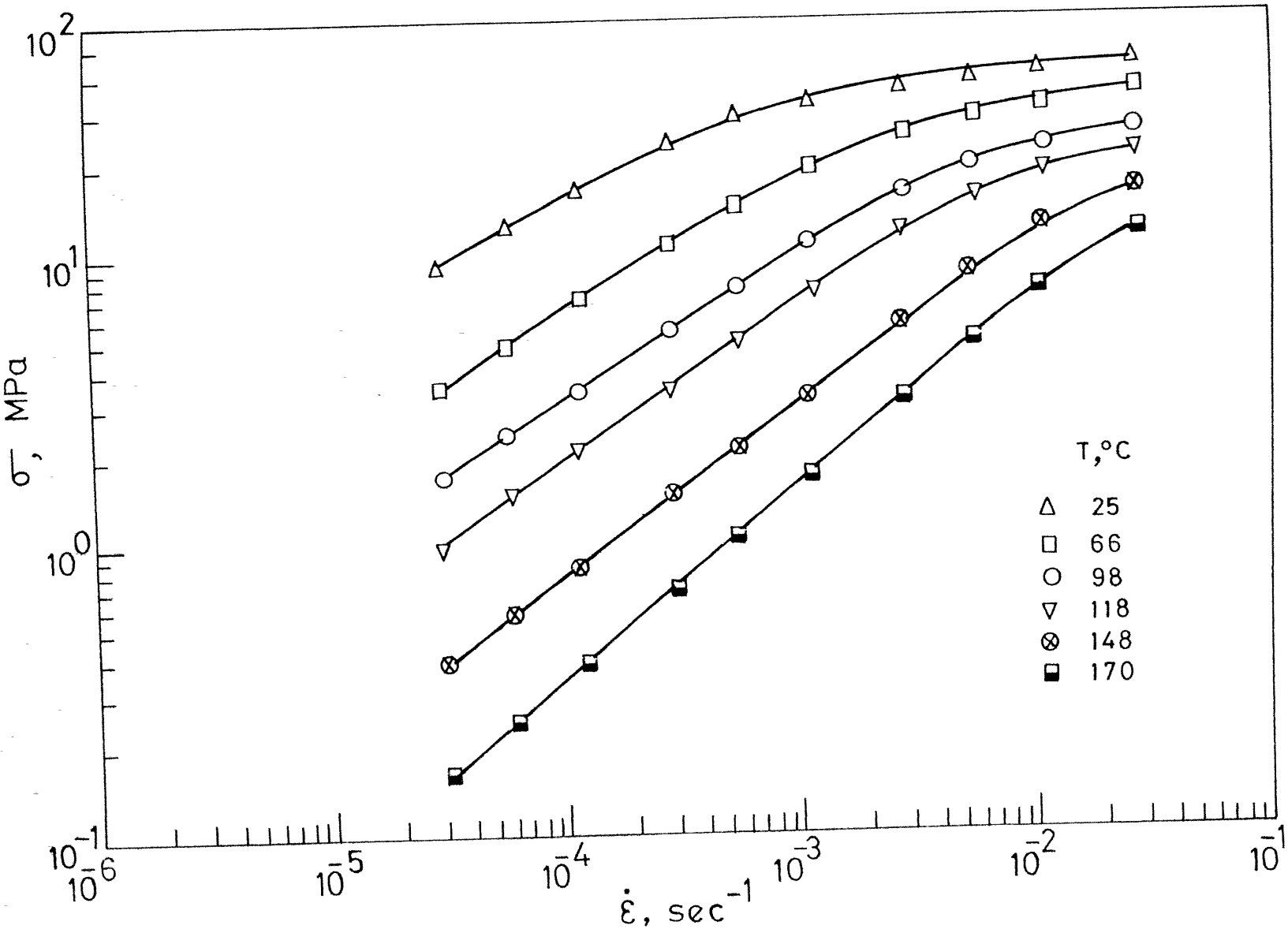

FIG. 49 $\sigma - \dot{\varepsilon}$ BEHAVIOUR OF SPECIMENS WITH ELONGATED GRAINS.
($l = 11.1 \pm 0.7$ μm , $l = 5.7 \pm 0.3$ μm , $l_T = 4.4 \pm 0.1$ μm)

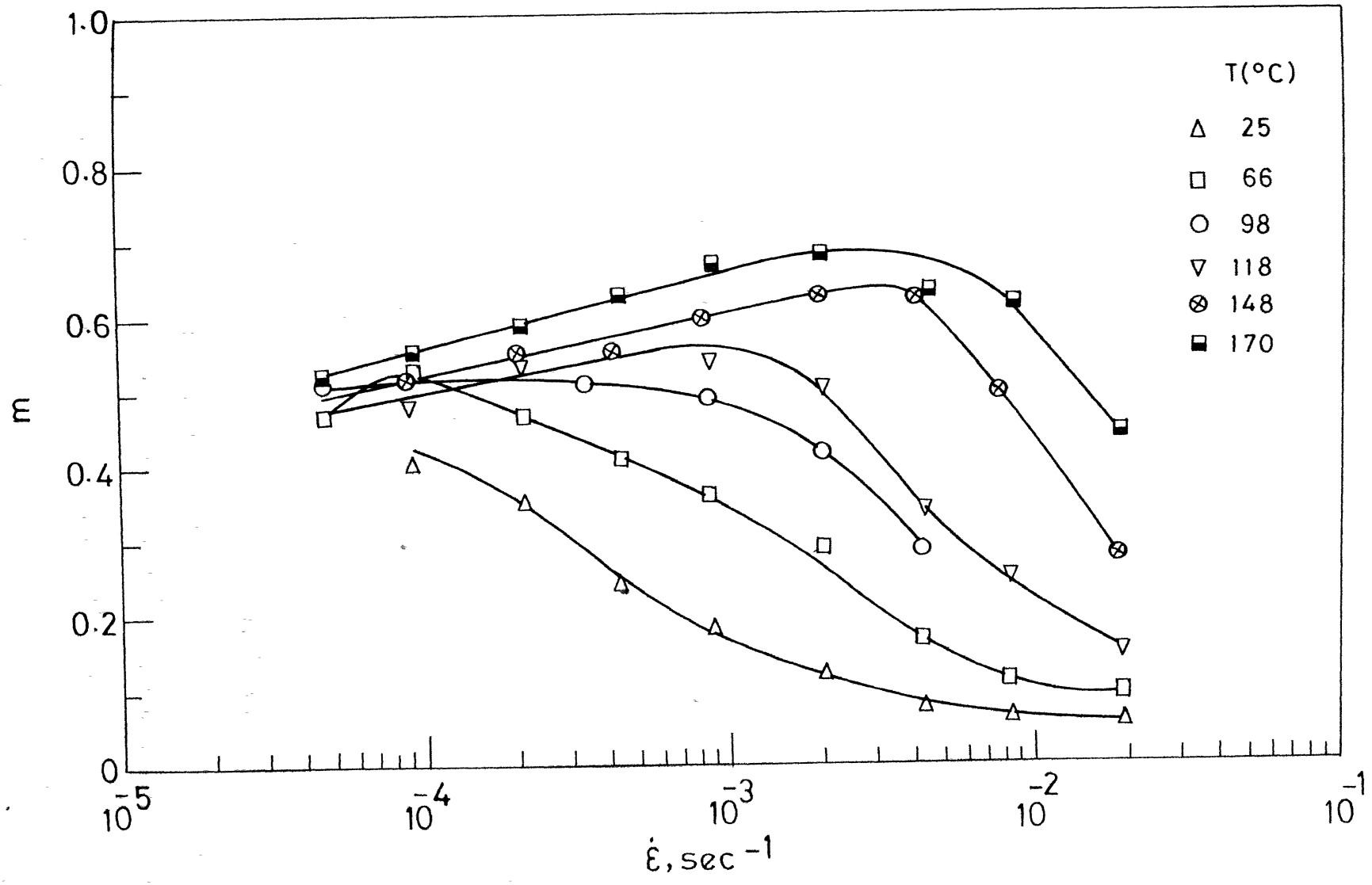

FIG. 50 m VS $\dot{\varepsilon}$ PLOTS AT DIFFERENT TEMPERATURES FOR ELONGATED GRAINS
($l_{\parallel} = 11.1 \pm 0.7\ \mu m$, $l_{\perp} = 5.7 \pm 0.3\ \mu m$, $l_T = 4.4 \pm 0.1\ \mu m$)

sheet. The intercept lengths in longitudinal section parallel to rolling direction, $l_{\parallel}$, and perpendicular to the rolling direction, $l_{\perp}$, were measured. In the transverse section, the grains are elongated along the width of the rolled sheet and therefore the measurements of intercept length in directions parallel to width, l_w, and parallel to thickness, l_t, of the rolled sheet were made. The value of l_w was observed to be equal to $l_{\perp}$.

Tensile samples were prepared such that their gauge lengths are along 0°, 45° and 90° to the rolling direction. These samples of different orientations were tested by the repeated strain rate cycling test at 25°C and 148°C. The flow stress values obtained from the second cycle were found to be lower than those of the first cycle in all cases. The extent of softening was observed to vary depending on the test temperature and orientation with respect to the rolling direction. The extent of softening was more at 148°C than that at 25°C; also it was maximum for 0° orientation and minimum for 45° orientation. The $\sigma - \dot{\varepsilon}$ data of these specimens at 148°C are shown in Figure 51. For the sake of clarity, only the first cycle data are shown in this figure. The m vs. $\dot{\varepsilon}$ data for first and second cycles are given in Figure 52 in the case of 0° and 90° orientations. The m values in the second cycle were found to be slightly higher than the first cycle

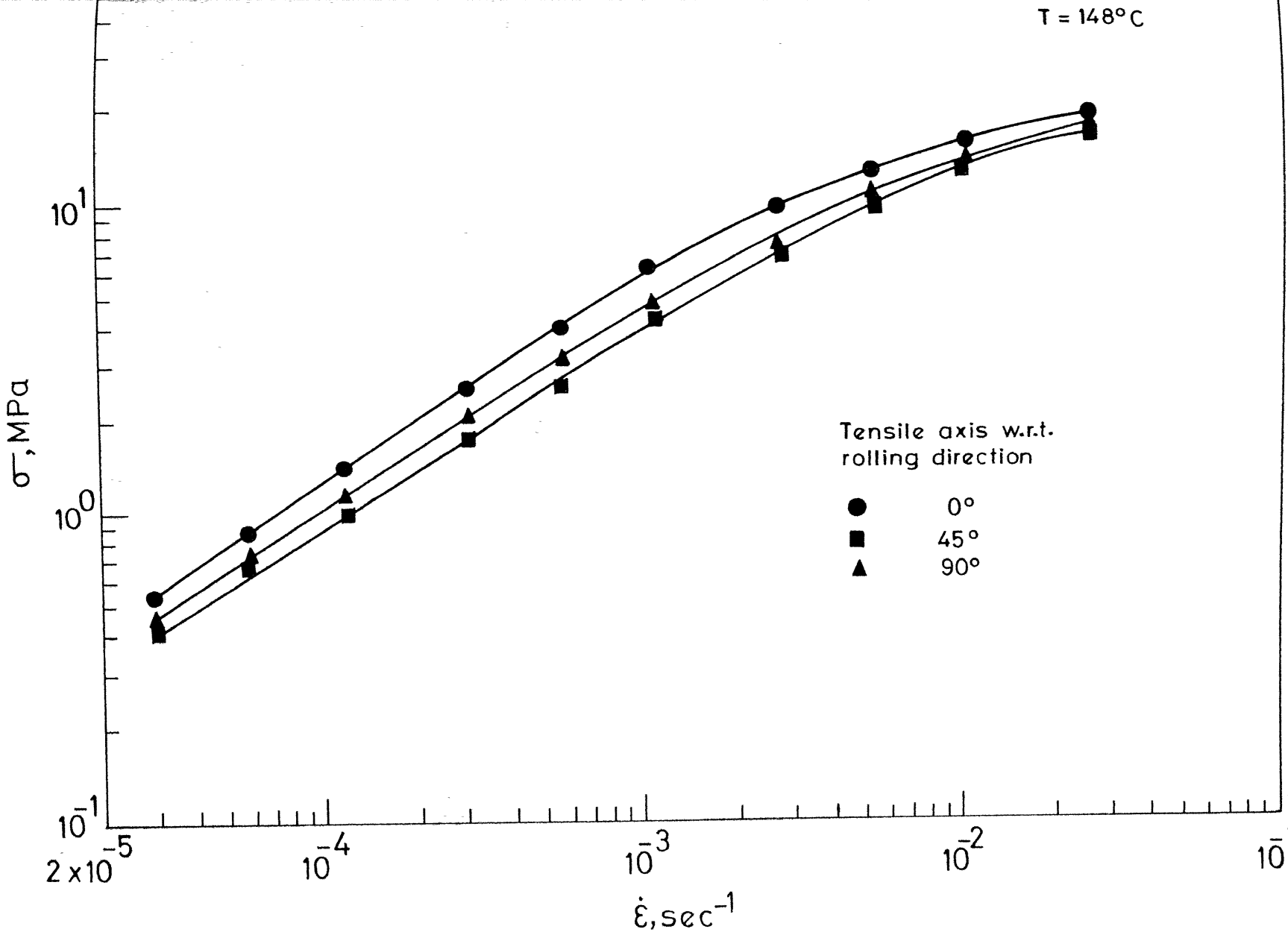

FIG. 51 ANISOTROPY IN $\bar{\sigma} - \dot{\bar{\varepsilon}}$ BEHAVIOUR OF SPECIMENS WITH GRAINS ELO
ATED IN TWO DIRECTIONS.

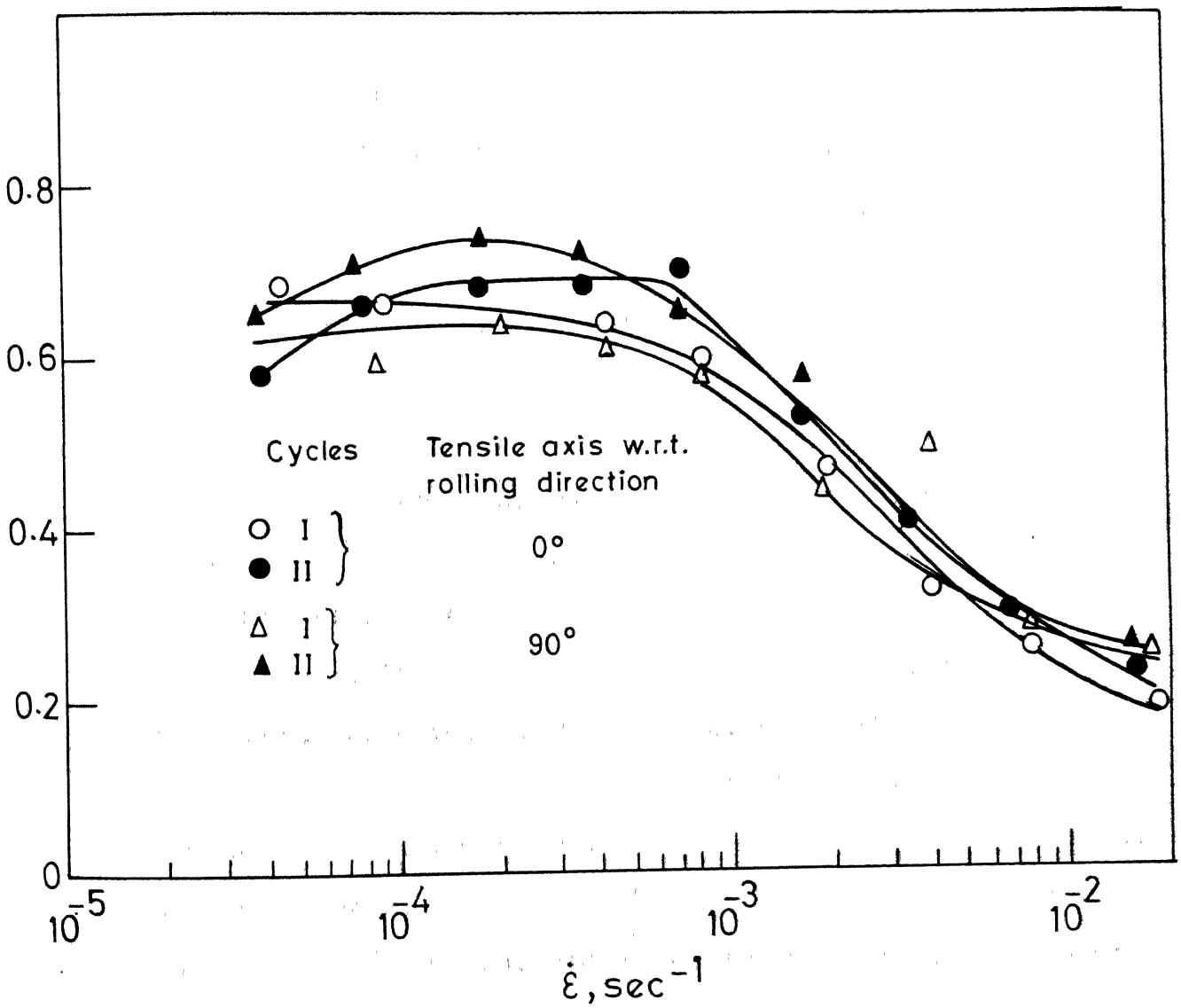

FIG. 52 EFFECT OF REPEATED STRAIN RATE CYCLING ON m VS $\dot{\varepsilon}$ DATA OF SPECIMENS WITH PLANAR-LINEAR ORIENTATION OF GRAINS

value in all cases. The activation energy value in region II calculated from the first cycle data of specimens of different orientations found to be independent of orientation and this value is similar to that of specimens having equiaxed microstructures in the lower temperature range.

Constant cross head speed tests were also performed at room temperature for all the three orientations. The stress-strain curves thus obtained are shown in Figure 53 from which it can be seen that the specimen of 45° orientation has minimum flow stress, while for 0° orientation it was maximum. Initially the flow stresses of specimens having 0°, 90° and 45° orientations are in the ratio of 1.2 : 1.1 : 1, whereas after 135% elongation they were similar. But softening continued at the same rate with further strain in all the three cases. Figure 54 shows the initial microstructures and those after deformation along the rolling direction. It can be seen that the microstructures tend to become equiaxed with deformation. The changes in microstructural parameters due to deformation in all orientations are shown in Table 14. In these tests the strain ratio $R = \frac{\varepsilon_w}{\varepsilon_t}$, where ε_w and ε_t are the true strains along the width and thickness of the specimens respectively, was monitored as a function of strain. The R values were independent of strain in the investigated range with the values of 0.86, 1.0 and 0.77 for 0°, 45° and 90° orientations respectively.

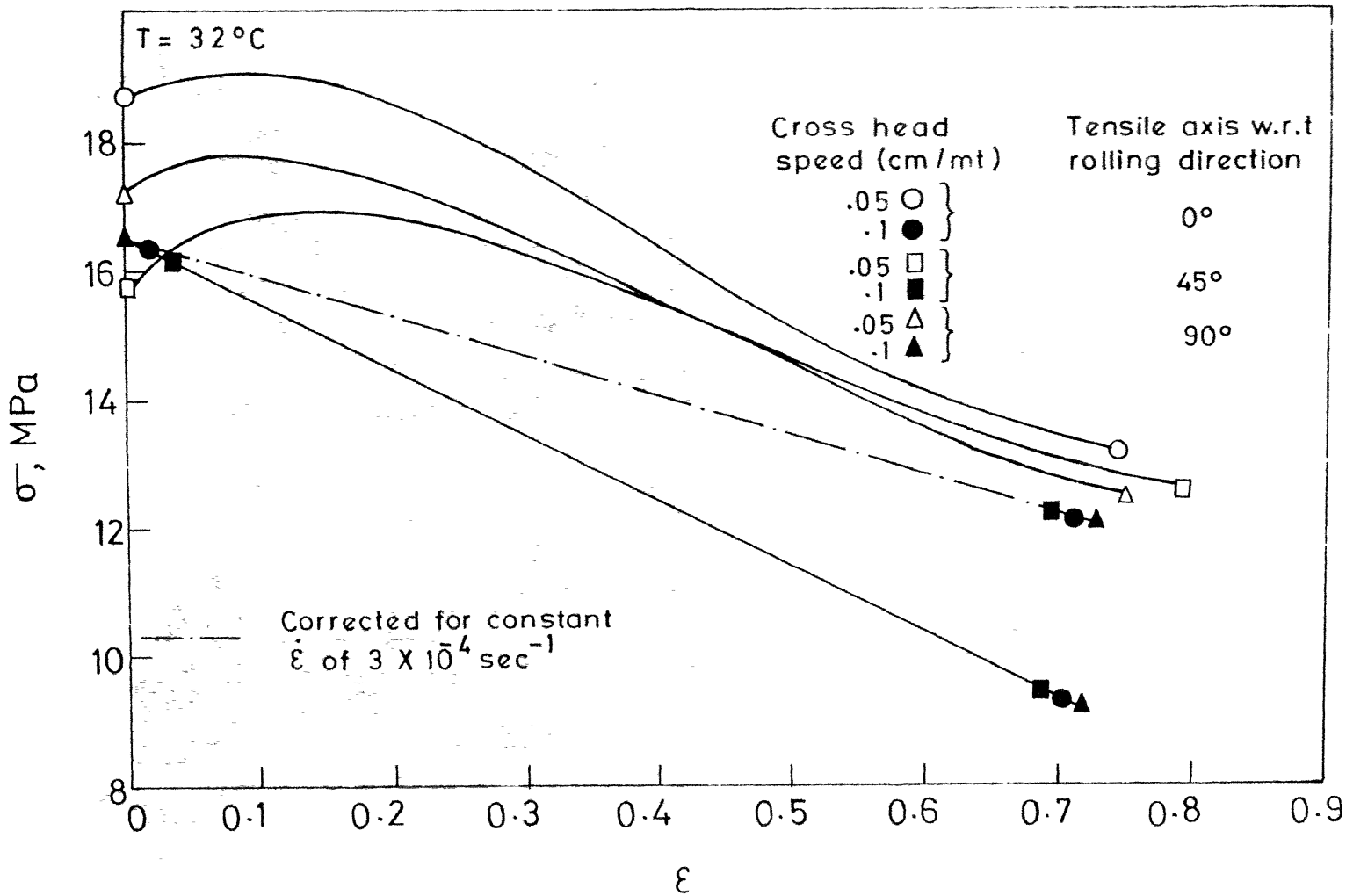

FIG. 53 ANISOTROPIC $\sigma - \varepsilon$ BEHAVIOUR OF SPECIMENS WITH GRAINS ELONGATED IN TWO DIRECTIONS.

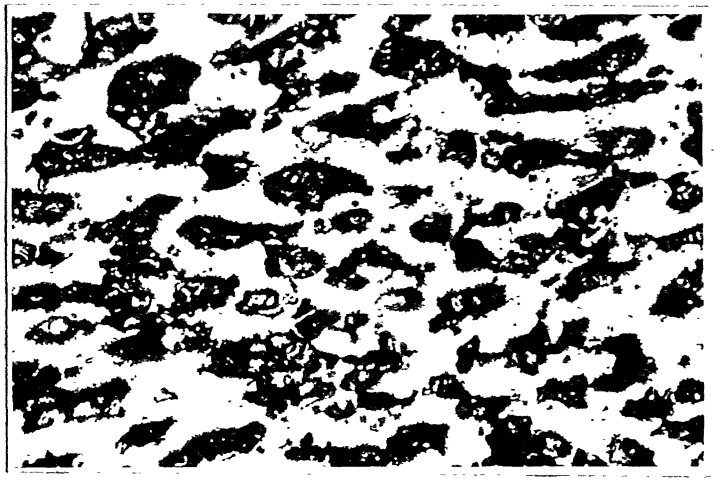

(a) Longitudinal

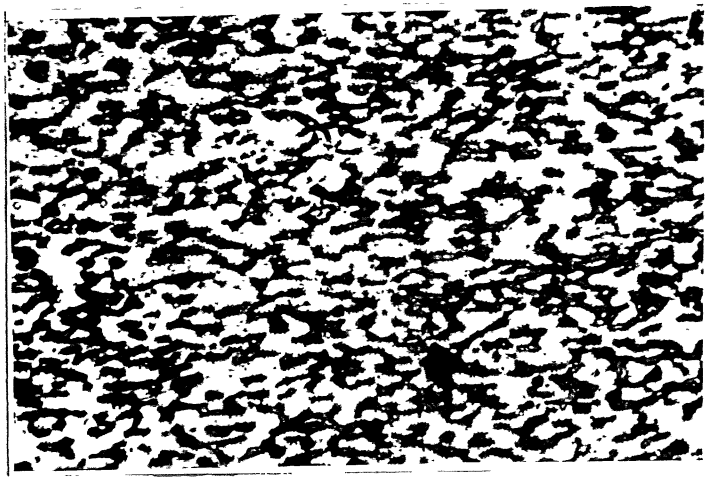

(b) Transverse

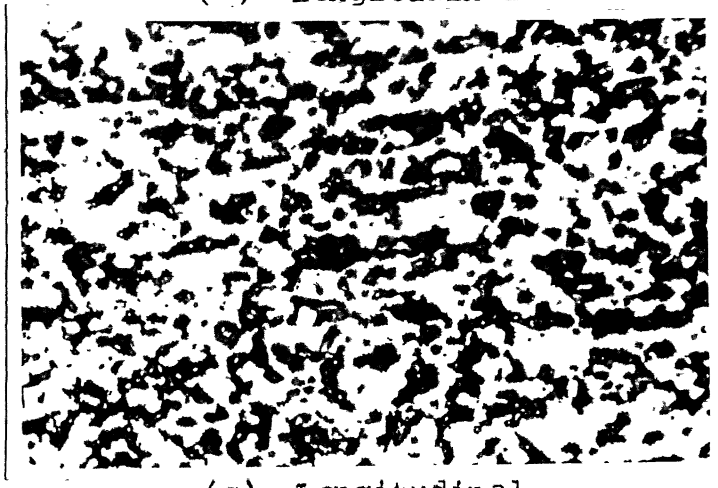

(c) Longitudinal

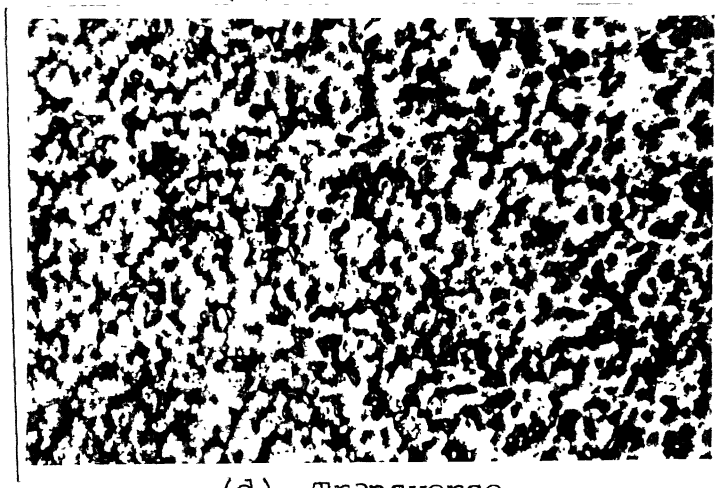

(d) Transverse

FIGURE 54. MICROSTRUCTURAL CHANGES OF A SPECIMEN HAVING INITIALLY ELONGATED GRAINS IN TWO DIRECTIONS DUE TO DEFORMATION IN REGION II. BEFORE DEFORMATION: (a) AND (b), AFTER DEFORMATION: (c) AND (d) ($\sim$ 135% ELONGATION) (MAGNIFICATION: 300X).

TABLE 14

Changes in Microstructural Parameters of Specimens Having Elongated Grains in Two Directions due to Constant Cross Head Speed Deformation

Test Temperature = 32°C Initial Strain Rate = 3.0×10^{-4}

Specimen Details	Intercept Lengths (μm)		
	$l_{//}$	$l_{\perp}$	l_{f}
As rolled sample	23.1 ± 2.3	11.4 ± 0.7	6.1 ± 0.3
Tensile axis parallel to rolling direction elongation ~ 135%	12.5 ± 1.1	10.0 ± 0.6	7.6 ± 0.6
Tensile axis 45° to rolling direction elongation ~ 135%	8.9 ± 0.7	4.5 ± 0.2	9.7 ± 0.4
Tensile axis 90° to rolling direction elongation ~ 135%	10.8 ± 0.6	11.3 ± 0.5	7.9 ± 0.4

$l_{//}$ refers to secants drawn parallel to the orientation plane on the longitudinal analysis plane

$l_{\perp}$ refers to secants drawn perpendicular to the orientation plane on the transverse analysis plane

l_{f} refers to secants drawn parallel to the orientation plane on the transverse analysis plane.

CHAPTER IV

DISCUSSION

4.1 ROLE OF DEFORMATION PROCESSING OF THE CAST ALLOY IN ALTERING THE MICROSTRUCTURE AND PROPERTIES

In the as cast state, the microstructure of the Pb-Sn eutectic consists of many colonies of alternate Pb-rich and Sn-rich lamellae with a preferred orientation in individual colonies. It is well known that the cast alloy exhibits high strength and low strain rate sensitivity of strength [83]. The lamellar structure with misorientation of the colonies with respect to each other and also with respect to the tensile axis is responsible for this behaviour. Deformation of as cast structure under conventional super-plastic conditions is known to transform the microstructure into the characteristic small grains of equiaxed shape. For example, in the Al-Cu eutectic alloy, the stress level drops by about a factor of 20 whereas the strain rate sensitivity of flow stress rises from a lower limit close to 0.2 to the value 0.6 on deforming the cast alloy at a temperature above half the homologous melting point [65]. On hot working of Pb-Sn eutectic alloy, similar micro-structural change takes place and the break up of lamellar structure into equiaxed grains consisting of Pb-Rich and Sn-rich phases is generally responsible for the observed

drop in high temperature strength and increase in strain rate sensitivity of flow stress. However, for smaller reduction of the cast material, the structure changes heterogeneously depending on the orientation of the lamellae in individual colonies with respect to the working direction. The degree of heterogeneity also varies with geometrical constraints imposed by neighbouring grains. It has been reported [84] that the lamellae parallel to tensile axis are more stable and exhibit higher strength than the lamellae inclined to tensile axis and thus the latter tend to transform into equiaxed grains more readily. The present observations indicate that the degree of heterogeneity in microstructure decreases with increasing reduction in area.

To achieve a fully homogeneous equiaxed microstructure, deformation processing of the cast alloy to the extent of about 80% RA at room temperature is found to be necessary. On the other hand, for lesser amounts of working long annealing treatment would also lead to coarse equiaxed microstructures. Further working of the alloy at room temperature by extrusion or rolling results in a smaller grain size with some grain elongation. In order to obtain fine equiaxed grains the most effective way is observed to be through heavy reduction involving frequent changes in the direction of mechanical working of the cast alloy.

The present observations also indicate that the increase in flow stress at any strain rate in region II due to greater degree of mechanical working of the cast alloy beyond about 80% RA is primarily due to the corresponding increase in grain aspect ratio. It is seen that the grain aspect ratio increased to 3.2 in the case of a specimen subjected to 99.2% RA by extrusion and swaging. Thus, the grain shape is an important factor that affects the high temperature strength and in such cases, it is not sufficient to consider the grain size in the transverse section of specimens alone, for structure-property correlations.

4.2 ON THE NEED FOR PRESTRAINING OF THE AS WORKED ALLOY TO OBSERVE STEADY STATE FLOW

The important point emerging from the mechanical behaviour of the alloy in the as worked state or after short annealing treatment following the mechanical working is that the strain is an important variable in the high temperature deformation of these states because of the accompanying rapid mechanical and/or microstructural instability. The present observations indicate that the microstructures of Pb-Sn eutectic alloy specimens processed by the normal metal working operations such as extrusion, rolling, forging and swaging of the cast alloy are not equiaxed but elongated in the direction of working with a grain aspect ratio of

~1.5. This directionality in the alignment and shape of the grains reflects in their mechanical behaviour. These specimens exhibit strength anisotropy depending on the direction of loading relative to that of prior mechanical working. Further, they show non-steady state deformation in the subsequent tension or compression test. There has been a rapid change in flow stress with increasing strain up to some strain. The concurrent microstructural change seems to be the reduction in grain aspect ratio by virtue of the deformation. From Table 2 it can be seen that reduction in grain aspect ratio is through the reduction in $l_{\parallel}$ and increase in intercepts along the other two perpendicular directions. Thus the breaking up of elongated grains and grain coarsening concurrently occur during deformation. The reduction in grain aspect ratio seems to be responsible for softening in this material. On the other hand, the grain coarsening leads to an increase in flow stress. Depending on the initial microstructure, the reduction in grain aspect ratio or grain coarsening can dominate. It appears that specimens with smaller grains are more susceptible to grain coarsening as compared to those having larger grains for a given grain aspect ratio especially in the higher test temperature range. In contrast, reduction in grain aspect ratio without much coarsening leading to a drop in flow stress is observed more commonly at lower test

temperatures. In some cases, these two effects cancel each other leading to a constant flow stress that is independent of strain, but with a distinct change in microstructure.

The flow stress is thus observed to be dependent on strain, unlike the normal high temperature steady state deformation where the flow stress is not a function of strain. If the deformation is only of the order of a few percent at each cross head speed of the Instron machine in differential strain rate tests meant for determining the strain rate sensitivity index and flow stress at various strain rates, the strain effect on the data thus obtained may not be noticeable at all. Such data are representative of transient or pseudo-steady state behaviour rather than the steady state deformation that is characteristic of high temperature creep. A manifestation of this pseudo-steady state behaviour is the wide difference in the stress-strain rate data obtained from the first and subsequent cycles of deformation in a differential strain rate test. The non-steady state or transient nature of deformation in the as worked state of several fine grained materials has also been reported by Suery and Baudelet [65].

The as worked material did exhibit high strain rate sensitivity of flow stress (region II) followed by lower strain rate sensitivity region at higher stresses (region III). Because of the pseudo-steady state or transient nature of their deformation, the flow behaviour

of these specimens is more complex involving strain dependency of flow stress and microstructural evolution. Accordingly the usual constitutive equation typical of superplastic materials in region II, where flow stress is a function of $\dot{\varepsilon}$, T and d, is inadequate in the as worked state. These aspects of the deformation involving evolution of microstructure towards an equiaxed one have been pointed out by Suery and Baudelet [65].

In the present study, equiaxed microstructures were produced in the as worked state by special processing techniques and also by a long annealing treatment of the worked alloy. It is noteworthy from the results on the mechanical behaviour of such equiaxed specimens that their deformation behaviour is also of non-steady state type. Although mechanical isotropy is found to be characteristic of these equiaxed microstructures, the strain effect could not be eliminated even with such microstructures prepared by either of annealing treatment of as worked alloy or of changes in direction of working of the cast alloy. Softening or hardening of these specimens with increasing strain is noticed depending on the temperature of deformation and strain rate. Thus the steady state flow behaviour is not simply achieved by having an equiaxed microstructure alone. Another important aspect of the flow behaviour of the equiaxed microstructures in the as worked condition is that

the flow stress of such specimens increases by a short time annealing treatment without any noticeable change in the grain size due to this annealing treatment. This is also true for specimens with elongated grains which had no indication of microstructural change.

This increase in flow stress due to short annealing of specimens without any accompanying change in grain size is possibly due to changes in the structure of grain or interphase boundaries as a result of the annealing treatment. The changes in the density of grain boundary ledges and micro-segregation of the solutes at the grain boundaries are likely to be the structural features of the boundaries that may be affected by the annealing treatment. In the as worked state irrespective of the shape of grains the regions near the grain boundaries can possess higher dislocation density. These dislocations may play an important role in the high temperature deformation. On annealing, these dislocations may be absorbed in the boundary, leading to an increase in height or density of grain boundary ledges. With progress of deformation, these grain boundary regions may become smooth leading to a constant flow stress level that is characteristic of steady state.

Another factor that may affect the flow stress due to the annealing treatment is as follows. The solubility of Sn in Pb decreases from 10.5 wt.% Sn at 150°C

to about 2 wt.% Sn at room temperature. On cooling to room temperature after annealing at a high temperature, the supersaturated solid solution is obtained. Turnbull and Treaftis [85] have observed that an extremely rapid cellular precipitation, largely along grain boundaries, can drain at least 60% of the excess tin from the supersaturated phase within a few minutes at room temperature. This may consequently increase the strength of the alloy over that of the as worked state.

Determination of m involves ratio of loads (or stresses) at two cross head speeds (or strain rates). The stress values at constant temperature depend not only on strain rate but also on strain in the as worked alloy. This dependency on strain through microstructural instability is also a function of strain rate and therefore m can somewhat be a complex function of these variables. The value of m thus calculated may show higher or lower value than that for steady state depending on which of the effects (softening or hardening) is dominant and to what extent these are dominating at the two strain rates under consideration. For example, it is reported [86] in Ti-6 Al-4 V alloy as a result of hardening by concurrent grain growth, the strain-rate sensitivity decreases with strain. Similar argument also explains the difference in activation energy value. The activation energy determination at constant

stress involves ratio of strain rates at two temperatures. If the microstructural and mechanical instabilities persist at these temperatures the corresponding strain rates are likely to be higher or lower depending on softening or hardening respectively to different extents depending on test temperatures. Thus the activation energy value will be different from that obtained from steady state deformation. The activation energy thus calculated will also depend on the temperatures involved in estimating it. In a Cu-P alloy, the activation energy value has been reported [87] to increase by 80% due to the microstructural and mechanical instabilities. Similarly, the grain size dependency of stress or strain rate will also be affected by the microstructural instabilities depending on the test variables involved.

From the present results on the parameters of the constitutive equations of specimens having equiaxed grains with and without standard prior tensile prestrain, it can be seen that m, p and Q values differ to the extent of about 20%. Thus, because of the non-steady state deformation of even the equiaxed microstructures, differences in the values of various parameters to this extent can occur. On the other hand, if specimens having non-equiaxed grains in the as worked state are used for obtaining the parameters of the constitutive relations without giving any

prestrain, the differences in values thus obtained are likely to be even more significant from the viewpoint of assessing the various operative mechanisms.

It can also be noted that, in contrast to the suggestion of Rai and Grant [69], and Suery and Baudelet [65], no indication for a change in slope of the stress-strain rate plots representative of region I behaviour is noticed in the present observations inspite of the micro-structural instabilities observed in the as worked alloy. Thus, it appears that microstructural instability cannot, in general, be responsible for region I of the stress-strain rate plots.

The results of this investigation relating to checking the uniqueness of stress-strain rate relation during superplastic flow, indicate that if the microstructure is stable and equiaxed, the flow stress is independent of the cross head speed of the tensile testing machine or the gauge length of the specimen. Irrespective of the cross head speed and thus the path through which a particular strain rate is achieved, the stress is observed to be uniquely dependent on strain rate. The effect of large strain as well as the path through which a given strain rate is achieved on stress-strain rate relation in the superplastic region has been widely explored in this study. The results of these tests confirm the uniqueness of

stress-strain rate relation as long as the microstructure is stable and equiaxed. The conditions of microstructural stability and equiaxed initial microstructures are better attained by giving some standard prior deformation to the hot worked alloy specimens. If specimens in the as worked state are directly used to obtain stress-strain rate relation, the uniqueness is violated to the extent of microstructural variations due to strain and in these situations the strain is to be considered as a variable in the constitutive equation. But for the strain effects through microstructural instability, the cross head speed effects of the kind observed by Padmanabhan et al [70] were not evident even with specimens in the as worked state directly. It is also evident from the present results that the gauge length to diameter ratio of tensile specimens has no influence on the $\sigma - \dot{\varepsilon}$ relation.

The pseudo-steady state behaviour of the as worked microstructure leads to stress being a multivalued function of strain rate bringing about the necessity of including strain as a variable in the constitutive equation. In order to obtain a true steady state behaviour it is essential to prestrain the deformation processed material in an appropriate manner. The unique stress-strain rate relation is a characteristic of high temperature steady state deformation. The non-uniqueness of $\sigma - \dot{\varepsilon}$ relation

reported in the literature [70-72] may be minimized to a great extent by prestraining these specimens before obtaining the $\sigma - \dot{\varepsilon}$ data.

4.3 ON THE MECHANISMS OF DEFORMATION IN REGIONS II AND III

The present results are based on the steady state deformation of the Pb-Sn eutectic alloy with mechanical and microstructural stability. In view of the relatively coarser grain size used in this investigation and the precautions taken in stabilizing the microstructure by prior tensile deformation and suitable annealing, the grain size has been observed to be stable upto elongations over 100% in region II with a slight coarsening at larger elongations. Thus, the present data of region II are truly representative of steady state deformation rather than the pseudo-state that is characteristic of many of the previously reported results on this alloy. Because of the constancy of grain size during deformation in region II, it is not necessary to consider either the evolution of microstructure or the strain in obtaining the constitutive equations for flow. In the investigated ranges of temperature, grain size and strain rate, only regions II and III are observed. Although there is some indication towards the occurrence of region I in some cases, this region could not be studied in detail because of the inapplicability of stress relaxation method

at high temperatures in covering strain rate range below about 10^{-5} sec^{-1}. The present observations in regions II and III reveal some new features in addition to supporting the characteristics brought out by previous studies. It may be seen that the rate sensitive superplastic flow is observed even in specimens having a grain size of about 32 μm (mean intercept length of 18.5 μm) and thus the superplastic flow is not restricted to grain sizes below 10 μm as commonly reported. In other words, the grain size effect is dominant in steady state deformation even at these relatively coarser grain sizes. It is worthwhile to compare the present results with those of the previous investigations before assessing various deformation mechanisms that are operative in regions II and III. These comparisons are made below in the two regions separately for convenience.

4.3.1 Comparison of the Present Results With the Existing Data in Region II

The $\sigma - \dot{\varepsilon}$ data for the wider range of grain size and temperature show that the region II extends over two orders of magnitude of stress and strain rate with a constant strain rate sensitivity index over this range. Hence, it cannot be simply treated as a transition region between the other two regions. The comparison of different parameters of the constitutive equation between the present and previous investigations can be seen from Table 15.

TABLE 15

Comparison of Experimental Parameters of Constitutive Equation in Region II for the Pb-Sn Eutectic with Earlier Investigations

Investigator	T	m	p	l (μm)	Q (kJ/mole)	Ref.
Avery and Backofen	0.5 T_m	0.59	2	2.5-2.8	-	83
Martin and Backofen	RT	0.55	2-4	1.0-4.1 (mean free path)	-	88
Zehr and Backofen	26-170°C	0.5-0.7	2-3	1.7-7.5	-	66
Cline and Alden	0-80°C	0.5	-	2-10	48±10	89
Avery and Stuart	-50 to +50°C	0.5	4	1.5-3.65	47-75	90
Aldrich and Avery	0-50°C	0.6	1.7-5.25	1.38-6.10	32 & 50	91
Baudelet and Suery	-44 to +30°C	0.45	-	1	48.2±2.1	92
Geckinli and Barrett	-5 to +71°C	0.4	3	3-11.7	45±5	61
Mohamed and Langdon	63 to 149°C	0.6	2.3	3.3-8.3	57.3±0.5	54
Present Investigation	25 to 170°C	0.6±0.1	3.34±0.23	5.6-18.4	44.7±1.1 (<135°C) 81.1±3.9 (>135°C)	

The strain rate sensitivity index is observed to be independent of strain rate and only slightly dependent on temperature and grain size. This observation is similar to that of Mohamed and Langdon [54]. Most of the other investigations reveal that m is more dependent on some or all of these variables.

While the grain size exponent value of the present investigation is in the general range of the reported values, it differs from most of the reported values. For example, the p value reported by Mohamed and Langdon [54] is 2.3, whereas the result of the present study is 3.34. Many of the previous studies report a range of p value from 2 to 4. In some cases, there is enough scatter in the reported data that p may be anywhere in the range 2 to 4 for the same set of data. Because of the wider grain size range explored in this work and the precautions taken in stabilizing the grain sizes, the value of the present study is more representative of region II deformation. The grain size exponent is observed to be independent of test temperature over a wide range.

The reported activation energy values for Pb-Sn eutectic in region II vary from 33 to 57 kJ/mole with the exception of one investigation where a value upto 75 kJ/mole is reported depending on stress and temperature. All these except that of Mohamed and Langdon are apparent

activation energies. The present investigation shows that there are two values of Q in region II rather than the single value reported so far for the Pb-Sn eutectic. Similar observations have been reported in the case of other superplastic materials. For example, in the case of Ni alloys [93], the activation energy in the higher temperature range is reported to be twice that of lower temperature range. Similarly Chaudhuri [94] observed two different activation energies in the superplastic deformation of Zn-Al eutectoid alloy. The activation energy, Q = 44.7 kJ/mole, in the lower temperature range below $\sim 0.89\ T_m$ is similar to what has been observed by others and the activation energy for grain boundary diffusion in pure Sn.The reported value of Q_{gb} for pure Pb varies over a wide range, the upper value being similar to that of the observed Q. At higher temperature, above $0.89\ T_m$, the observed activation energy value of 81.1 kJ/mole, is found to be significantly higher than the lower temperature value, but it is somewhat smaller than the activation energy for lattice diffusion in pure Sn or Pb and also for impurity diffusion of tin in lead. The various activation energy values that are available and of interest to the present study are listed in Table 16 in order to facilitate comparisons with the present experimental data.

TABLE 16

Activation Energy Values for Diffusion, Creep and Grain Boundary Sliding in Sn, Pb and Pb-Sn Alloys

	Activation Energy (kJ/mole)		
	Sn	Pb	Pb-Sn
Q_l	106.2±3.8*	107.5±1.0*	100.6* (0-2 at.% Sn)
Q_{gb}	40.0±2.9*	1.72±3.5 to 38.2±12.1* (120-222°C) 65.8 (214-260°C)*	-
Q_{gbs}	79.6 [95]	54.5 to 108.9 [95]	-
Q_c	46.0($T/T_m < 0.8$) 109.2($T/T_m > 0.8$) [96]	116.9	100.6 to 117.3 [97] (4.4 to 19.4 at.% Sn)

* From reference [82].

It is interesting to note that the activation energy for steady state creep of pure tin is 46.2 kJ/mole in the temperature range of 0.6-0.8 T_m (30°C-131°C) where T_m is the melting point of Sn in K and it increases to that of self diffusion in tin at temperatures above 0.8 T_m, whereas the activation energy for creep of pure lead is closer to lattice diffusion activation energy at temperatures above 0.6 T_m (87°C) where T_m is the melting point of lead in K. In the case of tin, the activation energy for self diffusion becomes equal to that of lattice diffusion only

at temperatures above 0.8 T_m. In the present investigation, the activation energy for deformation in region II is equal to that of grain boundary diffusion upto about 135°C, which is also about 0.8 T_m of pure tin. Above this temperature, the activation energy for deformation is found to be lower than the self diffusion activation energy for tin. It may also be noted that the activation energy for deformation in the high temperature region is very similar to the grain boundary sliding activation energy in pure tin. The higher temperature activation energy may also be a consequence of diffusion through the interphase boundaries, as it has been generally observed to be larger than grain boundary diffusion activation energy [98].

Direct comparison of A with the earlier investigations is not possible due to lack of appropriate data for this purpose. However, the present value of A seems to be significantly different from the value that can be calculated from the previous data.

4.3.2 Comparison of the Present Data With Theoretical Predictions in Region II

To assess the operative mechanisms in the superplastic region, the parameters of the constitutive equations n, p, Q and A determined from the experimental $\bar{\sigma} - \dot{\bar{\varepsilon}}$ data are compared with those predicted by theoretical considerations. This comparison based on present experimental

results and the values listed in Table 1 for different models are discussed below.

Among all the n values of the proposed mechanisms, the value of n = 2 remaining constant over a wide range of strain rate in region II is closer to the present data. The models of Ball and Hutchison and Mukherjee predict this kind of behaviour. The model proposed by Gittus also predicts a similar value of n but it remains constant only at a stress level well above the threshold stress. All the other models excepting the N-H and Coble diffusional flow mechanisms predict a continuous change in n value with a limiting value of 1, which is inconsistent with the present $\sigma - \dot{\varepsilon}$ behaviour. The N-H and Coble mechanisms have the drawback of predicting a value of n = 1 in explaining the present data.

The grain size exponent prediction of 3 has been made only for the Coble mechanism and has been incorporated in the Ashby and Verrall model. In the latter case, the value of p = 3 is predicted under conditions where the grain boundary sliding is accommodated by Coble diffusional flow. The present value of p is closer to these predictions. All the other models predict a value of p = 2, which is not supported by the present results.

In the case of activation energy for deformation, all mechanisms except the N-H diffusional flow predict a

value which is equal to the grain boundary diffusion activation energy. On the other hand, N-H mechanism and Ashby and Verrall mechanism in the situation in which N-H diffusional flow is the accommodation process, would lead to lattice diffusion activation energy. Thus, in the case of diffusional flow, the diffusion path can change over from grain boundaries to lattice on increasing the temperature leading to an increase in activation energy. Ashby and Verrall considered both the diffusional paths for accommodation of GBS and arrived at the effective diffusion coefficient combining both grain boundary and lattice diffusion coefficients. Accordingly, the effective diffusion coefficient can be dominated by the grain boundary diffusion at lower temperatures and lattice diffusion at higher temperatures closer to the melting point of the eutectic alloy. In order to determine whether the observed change in activation energy is due to the dominance of lattice diffusion at higher temperatures, the various diffusivities for Pb, Sn and Pb-Sn eutectic alloy for two typical temperatures and grain sizes are listed in Table 17. It can be seen that even at 0.97 homologus temperature of the eutectic alloy (170°C), the effective diffusivities are dominated by the grain boundary diffusivities and thus it appears that the observed increase in activation energy for deformation at higher temperatures cannot be attributed

TABLE 17

Various Diffusion Coefficients of Sn, Pb and Pb-Sn Eutectic Alloy at Two Temperatures

	T = 100°C			T = 170°C		
	Pure Pb	Pure Sn	Pb-Sn Eutectic	Pure Pb	Pure Sn	Pb-Sn Eutectic
T/Tm	0.62	0.74	0.82	0.74	0.88	0.97
D_l (cm^2/sec)	1.0×10^{-14}	4.0×10^{-14}	2.2×10^{-14}	1.7×10^{-13}	6.7×10^{-13}	3.7×10^{-13}
D_{gb} (cm^2/sec)	4.7×10^{-6}	7.9×10^{-8}	1.1×10^{-7}	3.1×10^{-5}	6.0×10^{-7}	7.9×10^{-7}
D_{eff} (cm^2/sec)(l = 5.6 μm)	2.8×10^{-9}	4.7×10^{-11}	6.4×10^{-11}	1.9×10^{-8}	3.4×10^{-10}	4.7×10^{-10}
D_{eff} (cm^2/sec)(l = 16.3 μm)	9.5×10^{-10}	1.6×10^{-11}	2.2×10^{-11}	6.4×10^{-9}	1.2×10^{-10}	1.6×10^{-10}

$D_{eff} = D_l\left(1 + \frac{3.3\,\delta}{l}\,\frac{D_{gb}}{D_l}\right)$ where δ is the thickness of the grain boundary region

$D_{eutectic} = \frac{D_{Pb}D_{Sn}}{N_{Pb}D_{Sn} + N_{Sn}D_{Pb}}$ where D_{Pb} and D_{Sn} are diffusivities of pure Pb and pure Sn and N_{Pb} and N_{Sn} are atomic fractions of Pb and Sn in the eutectic alloy.

Relevant data obtained from [82].

to the lattice diffusion. The dominance of the grain boundary diffusion even at 170°C is because of the finer grain size of this alloy and relatively lower homologus temperature for Pb or Sn. Further, the observed activation energy in the high temperature range is significantly lower than the self diffusion activation energy for pure Pb or Sn. Thus the observed increase in activation energy suggests a change in mechanism other than the change in accommodation process from grain boundary to lattice diffusional flow for grain boundary sliding as per the model of Ashby and Verrall. If it were a change in accommodation process of diffusional flow from Coble to N-H mechanism for GBS, there would be a corresponding change in the grain size exponent along with the change in activation energy. But no such change in grain size exponent is observed.

Further, the value of A is in disagreement with the predicted value of any of the mechanisms. In fact, it is surprisingly closer to that of the usual dislocation climb controlled creep. Thus it is evident, from a comparison of individual parameters of the constitutive equations predicted by different models with the experimental ones of the present work, that none of the mechanisms shows one to one correspondence with the experimental results. However, in the lower temperature range ($\sim$135°C) models by Ball and Hutchison, Mukherjee, and Gittus are in better

agreement with the present results, as far as the various parameters of the constitutive relations are concerned.

Alternatively, direct comparison of $\sigma - \dot{\varepsilon}$ behaviour predicted by different mechanisms with the observed behaviour can be made to further assess the applicability of different mechanisms to the present results. For this purpose two typical grain sizes are considered at test temperatures in the lower as well as upper range. In the calculation of $\sigma - \dot{\varepsilon}$ data by different mechanisms, the intercept lengths and shear modulus were used, wherever necessary as per the theoretical constitutive relations. In the case of a few typical mechanisms, the predicted data are shown against the observed data in Figure 55. For the Ashby and Verrall model, the threshold stress has been neglected because of its small value. The grain boundary diffusion activation energy has been used in place of interphase diffusion activation energy in calculating the $\sigma - \dot{\varepsilon}$ data from the model of Gittus. Since the N-H diffusional flow gives rise to stresses that are several orders of magnitude higher than the observed ones in the strain rate range of interest, the predicted data from the N-H mechanism are not included in the above plot. Similarly, the Coble mechanism also yields much higher stresses than the observed ones. In the case of Ashby and Verrall model, the strain rate is about an order of magnitude faster than the experimental value

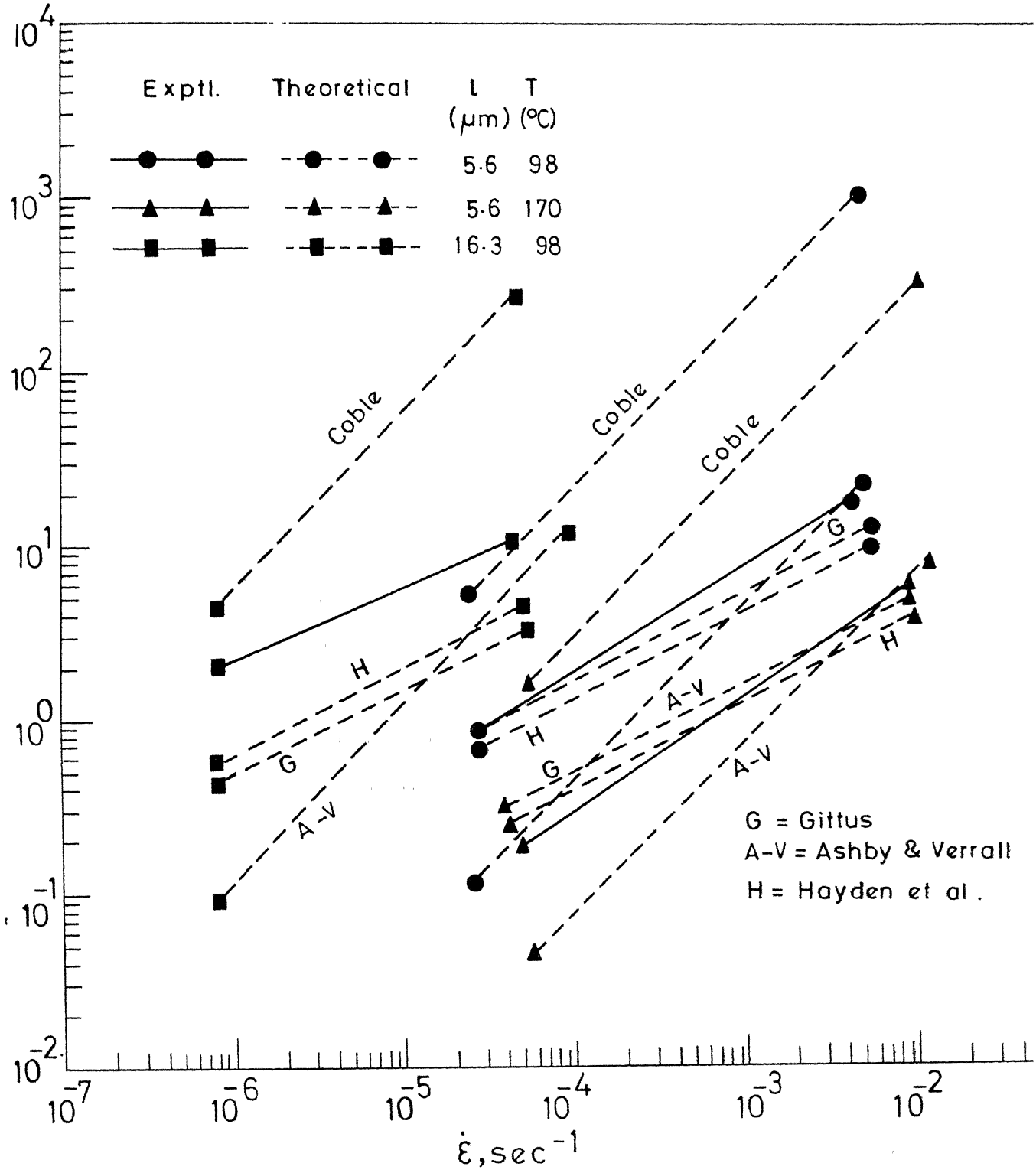

G.55 COMPARISON OF THE EXPERIMENTAL $\sigma - \dot{\varepsilon}$ DATA WIT
THEORETICAL PREDICTIONS OF VARIOUS MODELS IN REGIO

in the lower range of strain rate. This discrepancy is observed to reduce with increasing strain rate and temperature and decreasing grain size. The agreement seems to be better at the highest strain rates of the region II under the investigated conditions. It is interesting to note that predictions made by Gittus model are in better agreement with the observed $\sigma - \dot{\varepsilon}$ data in the smaller grain size range. In the case of larger grain size all the models seem to predict faster strain rates than the observed ones. The models proposed by Ball and Hutchison, Mukherjee and Gifkins resemble with the model of Gittus except for a slight difference in A and therefore lead to a similar result. Because of this similarity, the data calculated by these models are not shown in Figure 55 and their agreement with the experimental data can be examined by means of the model of Gittus.

Another model that is of interest in this connection is due to Hayden et al [93]. In this model, the diffusional flow, grain boundary sliding accompanied by dislocation creep and direct dislocation creep are considered as independent mechanisms contributing to high temperature steady state deformation. In the case of fine grained materials, the grain boundary sliding accompanied by dislocation creep would be the dominant mechanism with the constitutive relation given by

$$\dot{\varepsilon} = \frac{24\, K_1 \pi\, (1-\nu)\, D_p\, b^3\, \sigma(\sigma - \sigma_o)}{d^3\, GkT} \quad \text{at } T < T_c \qquad (24)$$

$$\dot{\varepsilon} = \frac{0.6\, K_1 \pi\, (1-\nu)\, D_v\, b^2\, \sigma(\sigma - \sigma_o)}{d^2\, GkT} \quad \text{at } T > T_c \qquad (25)$$

where K_1 is an empirical constant, ν the Poisson's ratio, D_p the dislocation pipe diffusivity, D_v the lattice diffusivity, σ_o the threshold stress either that necessary to nucleate a dislocation from a grain boundary source or the lattice friction stress and T_c the temperature at which the rate controlling process changes from pipe to volume diffusion.

This mechanism is basically similar to those of Ball and Hutchison, Mukherjee, and Gittus which involve grain boundary sliding accommodated by dislocation creep. It predicts that $n = 2$, $p = 3$ and $Q = Q_p$ when $\sigma \gg \sigma_o$ and $T < T_c$, whereas $n = 2$, $p = 2$ and $Q = Q_v$ at $T > T_c$. In the lower temperature range, this mechanism predicts a value of $p = 3$ unlike the other similar models which predict a value of $p = 2$. The overall $\sigma - \dot{\varepsilon}$ data can also be compared on the basis of this model of Hayden et al as shown in Figure 55 and the agreement is similar to that of Gittus model.

It is also possible to determine the temperature T_c at which the transition from pipe diffusion to volume

diffusion takes place using the diffusion data of pure Pb or Sn and it turns out to be well above the eutectic temperature of the Pb-Sn system. Thus it is unlikely that the higher activation energy in the higher temperature range of the present observations can satisfactorily be attributed to the change in the accommodation mode of dislocation creep from pipe diffusion to volume diffusion.

Thus, none of the existing models agrees with the present set of data in region II over the whole range of grain size, temperature and strain rate that has been studied in the present investigation. So far, all the existing models of superplasticity have been based on the widely reported values of $p = 2$ and $Q = Q_{gb}$ in region II. Since the present data differ from these values, the existing models are inadequate in explaining the present observations. The present results further suggest that there is a distinct change in the operative mechanism in region II above $\sim$ 135°C. Hence, there is a need to evolve alternate models that may be more satisfactory in accounting for the present results.

4.3.3 Behaviour in Region III

The $\sigma - \dot{\varepsilon}$ behaviour in region III shows that the full development of this region is dependent on the grain size and temperature in the investigated strain rate range.

For the smallest grain size region III is present only to a slight extent at room temperature whereas it is not prominent in the investigated strain rate range at higher temperatures. For the largest grain size, on the other hand, even at 170°C the region III is prominent. This region extends to more than two orders of magnitude of strain rates at lower temperatures in larger grained specimens. This observation agrees with other investigations on this and other alloys. So far in the literature, there has been no detailed study of region III in the Pb-Sn eutectic alloy. The strain rate sensitivity index, m = 0.09 (or n = 11.1) which is constant in region III, irrespective of grain size, temperature and strain rate, agrees with earlier reports on this alloy [83] and corresponds to conventional plasticity [26]. Sometimes higher values of m have been reported which may be representative of transition region between regions II and III rather than the fully developed region III. There is no reported value of the grain size exponent for region III in the Pb-Sn eutectic in order to compare with the present value of 1.0. The earlier data [99] on Zn-22% Al tended to indicate an independence of grain size, p = 0, in this region. Recent work by Shei and Langdon [100] on a quasi single phase copper alloy confirms the grain size dependency for high temperature deformation of fine grained material in region III and the value of p reported to be

$\sim$ 1.2 is claimed to be more reliable. The result of the present investigation supports the existence of grain size dependence in log σ - log $\dot{\varepsilon}$ data in region III. Although several investigations have been carried out on high temperature deformation in the Pb-Sn eutectic, the attention towards evaluating absolute magnitude of activation energy in region III for this alloy appears to be scarce. The present value of activation energy in this region, 100 kJ/mole, is similar to that reported for creep in Pb-Sn alloys [97] and so also to the lattice diffusion for pure Pb or Sn. This value is further similar to that for creep of pure Pb above 0.6 T_m (110 kJ/mole). Although the present value of activation energy is comparable with that for creep in pure Sn it appears that the agreement is valid above 0.8 homologus temperature of Sn only but not in the lower temperature range involved in this work, since below this temperature the grain boundary diffusion is reported to control the creep behaviour in pure Sn. The existence of one value of activation energy in region III, unlike region II, for the whole range of temperature suggests, that the Pb-rich phase may play a more important role in region III inspite of the large volume fraction of Sn in the eutectic alloy.

The overall features of region III including the observed grain elongation are in general agreement with the

dislocation creep model. However, there are important differences between the present observations and the predictions of the dislocation climb controlled recovery creep. While the activation energy for deformation is equal to the lattice diffusion activation energy as per the recovery creep theory, the high stress exponent and the grain size exponent p = 1 differ significantly from the prediction of the theory. Typical parameters of dislocation climb controlled steady state creep are p = 0 and n = 4-5. Especially the observed mild grain size dependency in region III is in sharp contrast with the prediction of the theory that the behaviour is independent of grain size. Gifkins recovery creep model [55] which is based on grain boundary sliding accommodated by dislocation movement in triple point folds predicts a grain size exponent of 1 and the present result is in agreement with this theory. Further the dimensionless constant A predicted by the Gifkins model with the grain size taken as the subgrain size due to the small grain size and F_y as 1 cm, is also in good agreement with the present observations. Only the observed stress exponent is about twice the predicted value. This discrepancy in the stress exponent can be reduced by considering the effective stress rather than the applied stress. Thus the Gifkins model for region III is in reasonable agreement with the present observations.

4.4 INTERNAL STRESS DATA AND THE MECHANISMS OF DEFORMATION IN REGIONS II AND III

4.4.1 On the Measurement of Internal Stresses by the Stress Dip Test

In the case of high temperature deformation the internal stress can rapidly change with time during the course of its measurement because of recovery effects. The internal stress is to be viewed as a value representative of the dynamic situation of deformation. Hence, the measurement of the internal stress should be carried out in as small an interval of time as possible from the steady state deformation condition for which the internal stress is being measured. If not, there can be serious errors in its measurement. It is for this reason that continuous relaxation tests or intermittent unloading during the relaxation test to attain a zero load relaxation rate would not yield reliable internal stress values. The stress dip test is a better method for this purpose because of no more than a time of one second is involved in unloading from the steady state stress to achieve zero relaxation rate condition. Recently, Toma et al [101] have proposed an extrapolation method of measuring the internal stress in high temperature deformation to further minimize the small errors of the stress dip test. In the present investigation only the stress dip test was adopted and hence it is

possible that the present data of internal stresses might represent slightly lower values than those obtained by the extrapolation method.

Another aspect that is to be considered in internal stress measurement is the anelastic effect in the high temperature deformation. Since the anelastic effect is dominant in the high temperature stress relaxation behaviour of the Pb-Sn eutectic alloy, it is of interest to know whether the internal stress measurement by the stress dip test is influenced by the anelastic effect. The extent to which the anelastic effect is important in the determination of internal stress can be assessed by means of the rheological model (Figure 25) due to Schneibel and Hazzledine [80]. The internal stress measurement by the stress dip test involves sudden unloading to a stress level at which the load relaxation rate becomes zero. In the absence of any anelastic effect, the stress level at which the load relaxation rate is zero would be a measure of the internal stress. When the applied stress is just equal to or below the internal stress, the nonlinear dash pot representing the superplastic behaviour would not undergo any deformation in the relaxation test. This is indicated by the constancy of the stress in the relaxation test by the stress dip method. When the anelastic element is present along with the elastic and superplastic elements, on sudden unloading

in the stress dip test there could be contraction of the anelastic element and in some cases the rate of contraction of the anelastic element may just be equal to the rate of extension of the nonlinear dash pot leading to an overall effect of zero relaxation rate. In this situation, the stress corresponding to the zero relaxation rate in the dip test would erroneously be identified as internal stress and the extension rate of the superplastic element is not really zero. In order to assess this kind of effect due to anelasticity, the following method is being suggested here. If the anelastic element is loaded to a stress σ_o for a sufficiently long time to attain the corresponding equilibrium strain and then suddenly unloaded to a stress σ, the instantaneous contraction rate of the anelastic element is given by $\frac{\sigma_o - \sigma}{\eta}$. If this matches with the instantaneous extension rate of the superplastic element $(\frac{\sigma}{K})^{1/m}$, then the stress relaxation rate would be zero even though the stress σ does not correspond to the internal stress. In other words, the initial relaxation rate following sudden unloading can be written as

$$\dot{\sigma} = -E_w \left[(\frac{\sigma}{K})^{1/m} - (\frac{\sigma_o - \sigma}{\eta})\right] \qquad (26,$$

which will be zero if $(\frac{\sigma}{K})^{1/m} = \frac{\sigma_o - \sigma}{\eta}$ although σ is not the internal stress. In order to check the influence of anelasticity in the measurement of internal stresses by

the stress dip test, it is thus necessary to have experimental data of anelastic relaxation times for different grain sizes of the Pb-Sn eutectic alloy at various temperatures. Such data being available only for room temperature, it was possible to consider this effect in the lower temperature range of the present investigation and the anelastic effect seems to be unimportant under these conditions. In the higher temperature range, its role could not be assessed properly due to lack of appropriate anelastic data. Further comments on comparisons and interpretations of the internal stress measurements are based on the assumption that there is no significant influence of anelastic effect in the measurement of internal stresses even at higher temperatures.

4.4.2 Comparison of the Present Data with Earlier Investigations and Comments on Mechanisms

Not much work has been reported on internal stresses in superplastic materials. Some studies incorporating only a few aspects of internal stress are available in region II. The present work, therefore, was aimed at obtaining constitutive equations on the basis of effective stress.

In the case of the Pb-Sn eutectic there have been no more than two investigations which report internal stress data. Therefore the present results are compared with overall existing reports on this aspect of superplastic

materials in general. As seen in Chapter III the internal stress increases with increasing strain rate in region II and is a decreasing proportion of the applied stress corresponding to these strain rates of σ_i on strain rate in this alloy. Similar observation is reported in Al-Cu alloys [103] and in a superplastic Mg alloy [104]. The ratio σ_i/σ is normally reported to be more than 50% over a wide strain rate range in region II except in Al-bronze [105] where the internal stress is found to be $\sim$ 4.5-9.7%. The present observations also indicate that the internal stress is a high fraction of the applied stress. The observation that the internal stress is independent of strain at all strain rates, is different from that observed by Geckinli and Barrett [106] in Pb-Sn eutectic. In their investigation the internal stress is reported to depend on strain in the same manner as the applied stress and the ratio σ_i/σ was independent of strain. Such a strain dependency indicates the existence of microstructural and mechanical instabilities. In the as worked state, the present observations also indicate such a strain dependency of internal stresses. After standard prior deformation, no such strain effects are noticed.

The observed decrease in the ratio σ_i/σ with increasing temperature for any particular grain size is similar to that reported in the superplastic Al-Cu eutectic

alloy [103]. The value of the strain rate sensitivity index, $m_{\bar{\sigma}}$, based on the effective stress, which is close to unity is also similar to the observation reported in the Al-Cu eutectic alloy. On the other hand, m_i is noted to be high indicating that the internal stress is also strain rate sensitive but to a lesser extent than that of the effective stress. This result is in variance with the reported observation in Al-Cu alloy that the internal stress is relatively strain rate insensitive. Thus on the basis of the present results, the internal and effective stresses cannot directly be identified with the strain rate insensitive and strain rate sensitive parts of the applied stress respectively.

The present internal stress measurements can also be compared with those of Furushiro and Hori [102] based on the extrapolation technique to minimize the dynamic recovery effects. Because of the similarity in these results, it appears that the error in the internal stress measurement by the direct stress dip test is not too significant in the data of region II. Moreover, the observed one to one correspondence between the strain rate before and at the start of the relaxation test in the present investigation would also indicate that the internal stress is somewhat lower than the applied stress. Hence the underestimation of the internal stress by the direct stress dip test

rather than the extrapolation technique does not appear to be too serious at least in region II.

In region III, there is only one reported internal stress measurement in the Pb-Sn eutectic alloy at room temperature. Furushiro and Hori [102] report that at room temperature the ratio σ_i/σ is close to unity, whereas the present value at room temperature is $\simeq 0.9$. But it is significant to note that this ratio decreases rapidly with increasing temperature as shown by the present results.

Since the internal stress measurements were only possible in the temperature range lower than $\sim 148°C$, comments on mechanisms can be made only for the lower temperature range of the present investigation. On comparing the parameters of the constitutive equation based on the effective stress in region II with those of different mechanisms, it is evident that they are in better agreement with those due to the model of Ashby and Verrall. Further, the overall effective stress versus strain rate data for various grain sizes can be compared with those due to the model of Ashby and Verrall by using the effective stress in place of the applied stress in the theoretical relation. Such a comparison is shown in Figure 56 which shows good agreement between the theoretical and observed data for a wide range of grain size and temperature. It may be noted that in the theoretical prediction based on the effective

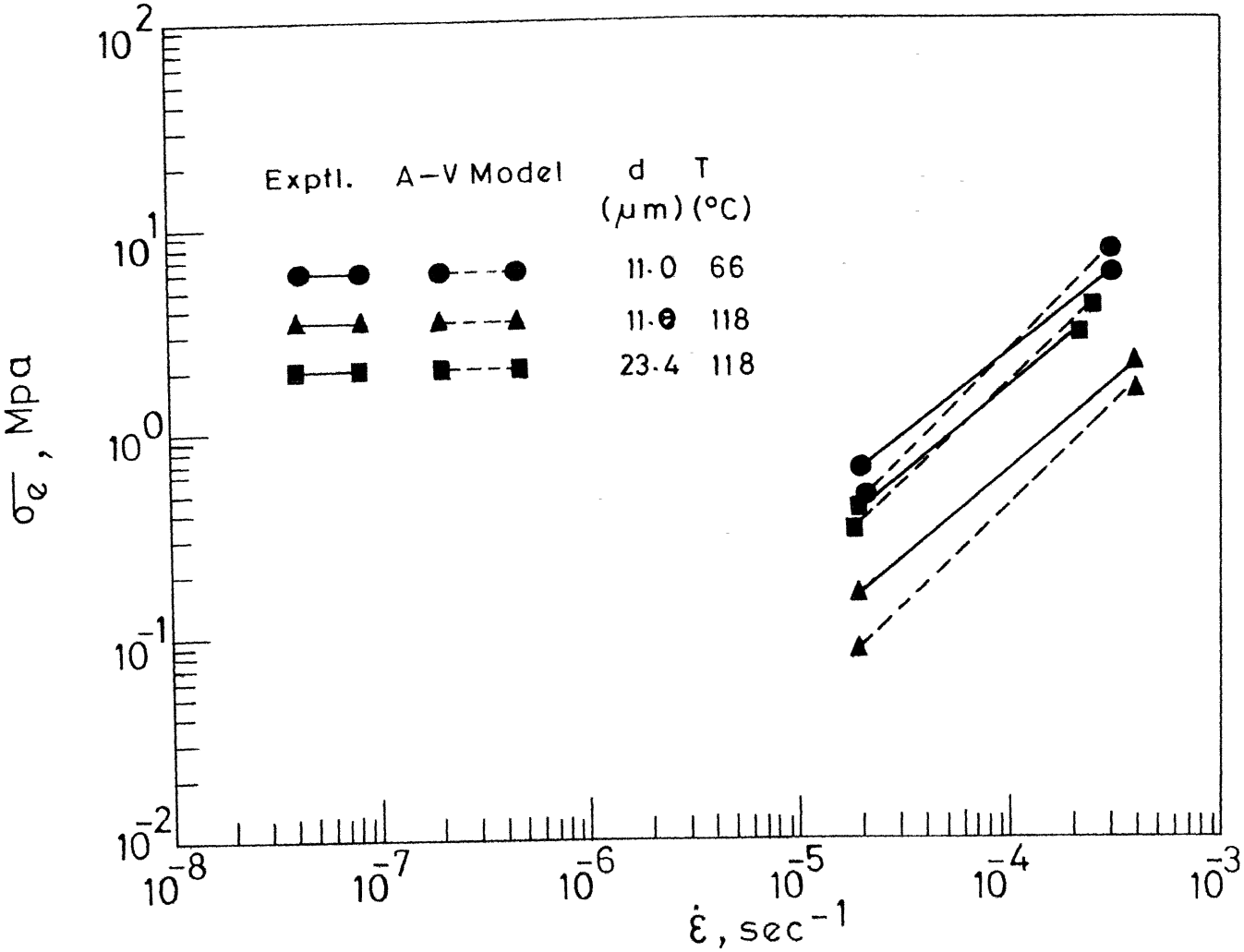

FIG. 56 COMPARISON OF THE EXPERIMENTAL $\sigma - \dot{\varepsilon}$ DATA WITH THE ASHBY-VERRALL MODEL ON THE BASIS OF EFFECTIVE STRESS IN REGION II

stress, the threshold stress σ_o is essentially replaced by the appropriate internal stress which is not a constant unlike the threshold stress but depends on strain rate, temperature and grain size. Similar comparisons with other models based on the effective stress were found to yield more discrepancies between the predictions and the experimental data. The agreement between the experiment and the Ashby and Verrall model based on the effective stress suggests further that the flow mechanism in region II is grain boundary sliding accommodated by the Coble diffusional flow. This might also imply that the effective stress rather than the applied stress is the parameter that is to be considered for stress directed diffusional accommodation.

In order to assess the mechanism of deformation in region III, it is of interest to consider the internal stresses in the usual dislocation creep of the pure metals and alloys. In the recovery creep region of pure Al [101], it has been shown that the internal stress is measured to be nearly equal to the applied stress by the extrapolation technique. Further it has been shown that the ratio σ_i/σ is smaller than unity if the internal stress is measured by the usual stress dip test and this difference is because of the dynamic recovery which is rapid enough to give rise to lower internal stress in this case. In region III of the Pb-Sn eutectic alloy, the internal stress is found to

be a smaller fraction of the applied stress except at 25°C. This observation differs from those of recovery creep region in pure metals. It is not known whether the discrepancy is because of the usual stress dip test adopted in this case or any other factor and it can only be resolved by further internal stress measurements in region III of the Pb-Sn eutectic alloy by the extrapolation method. On the other hand, the internal stress becoming a smaller fraction of the applied stress at higher creep rates has been reported in the case of Al-Mg alloys [107], by means of the extrapolatior method. This behaviour of Al-Mg alloys where the creep is controlled by the viscous glide of dislocations is similar to the present observations in region III. Thus the issue whether the recovery creep models are applicable to region III can only be clarified by further measurements of internal stress in superplastic materials. The observed decrease in n from a value of 11 to 4 or 5 on the basis of the effective stress in region III is in agreement with the recovery creep models. However, the usual recovery creep model is not directly applicable to region III, as discussed earlier. The Gifkins model [55] which incorporates the grain size effect appears to be more suitable for the flow behaviour in region III.

4.5 NON-EQUIAXED MICROSTRUCTURES

Because of difficulty of etching grain boundaries in two-phase structures, the distinction between two sources [27] of grain elongation, viz. (1) each grain may have grain aspect ratio greater than unity, or (2) the grains having equiaxed shape may be preferentially connected to other grains of the same phase, is not clearly made in the literature. In the present work the first category has been referred as elongated grains while the second one is called banded structure.

The existence of banded structures similar to the present one is common among many superplastic alloys [87, 108] in the hot worked state. The origin of this structure seems to be the dynamic recrystallization of the initially elongated grains of each phase during hot working. The elongated grains have also been reported in the hot worked state in some alloys [68, 93]. Thus depending on the processing route adopted, either of the above structures are observed in the hot worked state.

The important feature which distinguishes the non-equiaxed microstructures from equiaxed microstructures is the microstructural instability in the former during high temperature deformation. Superplastic deformation tends to eliminate these instabilities and the microstructures become equiaxed. The transformation of elongated/banded

structures into equiaxed structures can be due to cumulative effect of dynamic recrystallization followed by grain boundary sliding and diffusional flow. It was seen in annealing of elongated/banded structures that long Pb-rich grains split into smaller ones along with penetration of Sn-rich phase grains in between them. While the process of splitting of elongated grains is very slow by the annealing treatment alone, it gets accelerated by high temperature deformation. Also the observed decrease in volume of grains during superplastic deformation suggests the break up of initially elongated grains by recrystallization, grain boundary sliding and diffusion. Banded structures seem to undergo such microstructural changes more readily whereas under identical conditions elongated grains require higher strength and larger strains to reach a common state of final microstructures. It is reported [109] that elongated structures possess subgrains and high dislocation density which may eventually change to high angle grain boundaries during superplastic deformation. After this stage the elongated structure may resemble the banded structures. Subsequently, in both the structures grain boundary sliding and its associated rotation can lead to the removal of directionality exhibiting increase in interphase boundaries and decrease in grain boundaries in the microstructures. This evolution of more interphase boundaries by superplastic

deformation may be favoured for stable condition through lower interfacial energy of the interphase boundaries in comparison to the grain boundaries of individual phases. This microstructural change has been exploited to get fine scale equiaxed grains through superplastic deformation by some investigators [110, 111]. These microstructural changes resulting from deformation of banded structures or elongated grains are similar to the previous observations of this nature [68, 87, 110, 112]. These microstructural changes are responsible for softening or hardening and elimination of strength anisotropy. The mechanical anisotropy of specimens having elongated grains seems to be due to the greater difficulty of grain boundary sliding when the tensile axis is parallel to the grain elongation in comparison to the case where the tensile axis is at 45° to the direction of grain elongation. The break up of this elongated structure is observed to be more rapid when the tensile axis is at 45° to the direction of grain elongation. Similar mechanical anisotropy having higher and lower strengths in 0° and 25° orientations respectively have been reported in the case of lamellar Pb-Sn eutectic alloy [84]. The reason for the anisotropic mechanical behaviour in the case of banded structures may be as follows. When the tensile axis is parallel or perpendicular to the bands, sliding is likely to be mostly either through Pb-Pb or Sn-Sn

grain boundaries. On the other hand, when the tensile axis is at 45° to the bands, the grain boundary sliding can also take place along interphase boundaries due to their favourable orientation for the same. Because of the differences in sliding resistance of various boundaries in two phase alloys, variations in flow stress may thus be expected depending on the direction of loading relative to the bands. Eventually, the isotropy in mechanical behaviour seems to be achieved in all cases.

The overall mechanical behaviour of these specimens is very much similar to those of as worked specimens discussed in Section 4.1. However, the difference in some features of superplastic deformation is brought more distinctly in the case of present elongated and banded structures. This is, in particular, the nature of variation of m with strain rate and strain. In the study of as worked materials m is found to be relatively constant, whereas in the present case of elongated and banded structures the variation in m as a function of strain rate and strain through repeated strain rate cycling is more significant. The activation energy does not seem to be much affected by the differences in microstructures. The overall mechanical behaviour of different initial microstructures has been compared by considering $\sigma - \dot{\varepsilon}$ data corresponding to identical test conditions. It is seen that despite much

microstructural instability in such structures, there has been no evidence for the pseudo-region I arising from this microstructural instability. On the other hand, the grain size estimation from cube root of the volume of grains or average of intercept lengths in three mutually perpendicular directions in equiaxed, elongated and banded structures seems to be useful in qualitatively relating the grain size to flow stress in all microstructures. However, quantitative correlation must involve grain shape especially, grain aspect ratio and other microstructural details as pointed out by earlier investigations [71, 72]. Not many theoretical attempts were made in the literature to evolve suitable constitutive relations for such structures. Hayden et al [93] have modified their model to suit fibrous structures. But the predictions of this model do not favourably compare with the present experimental results.

CHAPTER V

CONCLUSIONS

(1) In the as worked state the Pb-Sn eutectic normally exhibits elongated grains leading to anisotropy in flow stress in proportion to its grain aspect ratio. In this state, irrespective of the initial grain shape including the equiaxed grains in some cases, mechanical and/or microstructural instability occurs resulting in a non-unique $\sigma - \dot{\varepsilon}$ relationship. Because of their transient or pseudo-steady state nature of deformation, the as worked material is not suitable from the viewpoint of assessing the operative mechanisms of superplastic flow which are based on steady state flow behaviour.

(2) Non-equiaxed grains tend to become equiaxed and achieve mechanical isotropy by superplastic deformation. The reduction in grain aspect ratio is more rapid at lower temperatures. This microstructural change results in softening. In the higher temperature range grain coarsening is more predominant and can lead to hardening during superplastic deformation.

(3) Prior tensile deformation to the extent of about 30% elongation with or without annealing of the as worked alloy eliminates microstructural and mechanical

instabilities during subsequent deformation leading to a steady state deformation with unique $\sigma - \dot{\varepsilon}$ relation which is independent of the cross head speed and path through which a given strain rate is achieved.

(4) Regions II and III have been observed in the steady state deformation of the Pb-Sn eutectic alloy having grain sizes in the range 9.7 μm to 32.0 μm over the investigated temperature and strain rate range. Both these regions are observed to extend over two orders of magnitude of strain rate. In region II, the grain size is observed to be almost constant up to about 100% elongation and at higher strains there is some coarsening of grain size.

(5) In region II, two distinct activation energy values are observed depending on test temperature. Below 0.89 T_m this value is 44.7 $\pm$ 1.1 kJ/mole, whereas above this temperature, it is 81.1 $\pm$ 3.9 kJ/mole. The strain rate sensitivity index m is 0.6 $\pm$ 0.1 and it is relatively insensitive to temperature and grain size. The grain size exponent p is found to be equal to 3.34 $\pm$ 0.23 which is independent of test temperature. The values of these parameters are affected by using effective stress to yield m $\simeq$ 0.82, Q $\simeq$ 33.5 kJ/mole (below 0.89 T_m), and p $\simeq$ 2.8.

(6) The experimental results, on the basis of applied stress, are not in agreement with the analytical predictions of any of the models of superplasticity that have been proposed so far for region II. However, the comparison on the basis of effective stress suggests agreement with the Ashby and Verrall model in region II.

(7) In region III, mild grain size dependency with grain size exponent $p = 1.00 \pm 0.72$ is observed. The observed activation energy is 100 ± 8.8 kJ/mole and the strain rate sensitivity index is 0.09 ± 0.01. The strain rate sensitivity index based on the effective stress is in the range of 0.2 to 0.25.

In this region, the experimental observations are in better agreement with the Gifkins' recovery creep model rather than the usual recovery creep models.

(8) In the deformation of specimens with banded structures or elongated grains, flow stress anisotropy and non-unique $\sigma - \dot{\varepsilon}$ relation are observed. These non-equiaxed structures evolve towards equiaxed grains during superplastic deformation leading to elimination of strength anisotropy.

(9) Stress relaxation test, as a means to collect $\sigma - \dot{\varepsilon}$ data in superplastic materials, finds limited utility due to the influence of anelasticity. Its feasibility depends sensitively on the grain size and test temperature.

REFERENCES

1. Conrad, H., "Experimental Evaluation of Creep and Stress Rupture", in Mechanical Behaviour of Materials at Elevated Temperatures, edited by J.E. Dorn (McGraw-Hill, New York), 1961, p. 149.

2. McLean, D., "Deformation at High Temperatures", Met. Rev., 7 (1962), 481.

3. Sherby, O.D. and Burke, P.M., "Mechanical Behaviour of Crystalline Solids at Elevated Temperature", in Progress in Materials Science, Vol. 13 (Pergamon Press), 1967, p. 325.

4. Bird, J.E., Mukherjee, A.K. and Dorn, J.E., "Correlations Between High- emperature Creep Behaviour and Structure", in Quantitative Relation Between Properties and Microstructure, edited by D.G. Brandon and A. Rosen (Israel Univ. Press, Jerusalem), 1969, p. 255.

5. Gifkins, R.C., "Hot and Strong", J. Aust. Inst. Metals, 19 (1974), 149.

6. Takeuchi, S. and Argon, A.S., "Review Steady-State Creep of Single Phase Crystalline Matter at High Temperature", J. Mater. Sci., 11 (1976), 1542.

7. Weertman, J., "Theory of Steady-State Creep Based on Dislocation Climb", J. Appl. Phys., 26 (1955), 1213.

8. Weertman, J., "Steady-State Creep Through Dislocation Climb", J. Appl. Phys., 28 (1957), 362.

9. Weertman, J., "Steady-State of Crystals", J. Appl. Phys., 28 (1957), 1185.

10. Weertman, J., "Dislocation Climb Theory of Steady-State Creep", Trans. ASM, 61 (1968), 681.

11. Mukherjee, A.K., Bird, J.E. and Dorn, J.E., "Experimental Correlations for High Temperature Creep", Trans. ASM, 62 (1969), 155.

12. Barrett, C.R. and Sherby, O.D., "Influence of Stacking-Fault Energy on High-Temperature Creep of Pure Metals", Trans. Met. Soc. AIME, 233 (1965), 1116.

13. Garofalo, F., "An Empirical Relation Defining the Stress Dependence of Minimum Creep Rate in Metals", Trans. Met. Soc. AIME, 227 (1963), 351.

14. Nix, W.D. and Barrett, C.R., "Interpretation of Steady State Creep in Terms of the Relation Between Dislocation Glide and Recovery", Trans. ASM, 61 (1968), 695.

15. Ahlquist, C.N. and Nix, W.D., "The Measurement of Internal Stresses During Creep of Al and Al-Mg Alloys", Acta Met., 19 (1971), 373.

16. Jonas, J.J., "The Back Stress in High Temperature Deformation", Acta Met., 17 (1969), 397.

17. Saxl, I. and Kroupa, F., "Relations Between the Experimental Parameters Describing the Steady-State and Transient Creep", Phys. Stat. Sol. (a), 11 (1972), 167.

18. Davies, P.W., Nelmes, G., Williams, K.R., and Wilshire, B., "Stress-Change Experiments During High-Temperature Creep of Copper,, Iron, and Zinc", Metal Sci. J., 7 (1973), 87.

19. Williams, K.R. and Wilshire, B., "On the Stress- and Temperature-Dependence of Creep of Nimonic 80A", Metal Sci. J., 7 (1973), 176.

20. Parker, J.D. and Wilshire, B., "The Effects of a Dispersion of Cobalt Particles on High-Temperature Creep of Copper", Metal Sci. J., 9 (1975), 248.

21. Mukherjee, A.K., "High-Temperature Creep", in Treatise on Materials Science and Technology, Vol. 6 (Academic Press, New York), 1975, p. 164.

22. Barrett, C.R., Lytton, J.L. and Sherby, O.D., "Effect of Grain Size and Annealing Treatment on Steady-State Creep of Copper", Trans. Met. Soc. AIME, 239 (1967), 170.

23. Underwood, E.E., "A Review of Superplasticity and Related Phenomena", J. Metals, 14 (1962), 914.

24. Backofen, W.A., Azzarto, F.J., Murty, G.S. and Zehr, S.W., "Superplasticity", in Ductility (American Society of Metals, Cleveland), 1968, p. 279.

25. Johnson, R.H., "Superplasticity", Met. Rev., 4 (1970), 115.

26. Davies, G.J., Edington, J.W., Cutler, C.P. and Padmanabhan, K.A., "Superplasticity: A Review", J. Mater. Sci., 5 (1970), 1091.

27. Alden, T.H., "Review Topics in Superplasticity", in Treatise on Materials Science and Technology, Vol. 6 (Academic Press, New York), 1975, p. 225.

28. Baudelet, B., "Superplasticite", Proceedings of the 4th International Conference on the Strength of Metals and Alloys, 1 (1976), 2.

29. Hazzledine, P.M. and Newbury, D.E., "Role of Grain Boundaries in Superplasticity", in Grain Boundary Structure and Properties, edited by G.A. Chadwick and D.A. Smith (Academic Press, London), 1976, p. 235.

30. Edington, J.W., Melton, K.N. and Cutler, C.P., "Superplasticity", in Progress in Materials Science, Vol. 21 (Pergamon Press, Oxford), 1976, p. 63.

31. Langdon, T.G. and Taplin, D.M.R., "Rupture of Strain-Rate Sensitive Alloys" : S.M. Archieves, 2 (1977), 329.

32. Gifkins, R.C. and Langdon, T.G., "Comments on Theories of Structural Superplasticity", Mater. Sci. Eng., 36 (1978), 27.

33. Hayden, H.W. and Brophy, J.H., "The Interrelation of Grain Size and Superplastic Deformation in Ni-Cr-Fe Alloys", Trans. ASM, 61 (1968), 542.

34. Chaudhari, P., "A Dislocation Cascade Mechanism in Superplasticity", Met. Trans., 5 (1974), 1692.

35. Nabarro, F.R.N., "Deformation of Crystals by the Motion of Sing.e ~ons", Report on a Conference on the Strength of Solids (The Physical Society, London), 1948, p. 75.

36. Herring, C., "Diffusional Viscosity of Polycrystalline Solid", J. Appl. Phys., 21 (1950), 437.

37. Coble, R.L., "A Model for Boundary Diffusion Controlled Creep in Polycrystalline Materials", J. Appl. Phys., 34 (1963), 1679.

38. Lifshitz, I.M., "On the Theory of Diffusion-Viscous Flow of Polycrystalline Bodies", Soviet Phys., 17 (1963), 909.

39. Gibbs, G.B., "The Role of Grain-Boundary Sliding in High-Temperature Creep", Mater. Sci. Eng., 2 (1967), 262.

40. Gifkins, R.C. and Langdon, T.G., "Grain Boundary Displacements due to Diffusional Creep", Scripta Met., 4 (1970), 563.

41. Cannon, W.R., "The Contribution of Grain Boundary Sliding to Axial Strain During Diffusion Creep", Phil. Mag., 25 (1972), 1489.

42. Gibbs, G.B., "The Sliding Contribution to the Total Strain of a Polycrystalline Aggregate", Metal Sci., 11 (1977), 65.

43. Ball, A. and Hutchison, M.M., "Superplasticity in the Aluminium-Zinc Eutectoid", Metal Sci. J., 3 (1969), 1.

44. Mukherjee, A.K., "The Rate Controlling Mechanism in Superplasticity", Mater. Sci. Eng., 8 (1971), 83.

45. Ashby, M.F. and Verrall, R.A., "Diffusion-Accommodated Flow and Superplasticity", Acta Met., 21 (1973), 149.

46. Gifkins, R.C., "Grain Boundary Sliding and Its Accommodation During Creep and Superplasticity", Met. Trans. A, 7A (1976), 1225.

47. Gittus, J.H., "Theory of Superplastic Flow in Two-Phase Materials : Role of Interphase-Boundary Dislocations, Ledges, and Diffusion", Trans. ASME, 99 (1977), 244.

48. Gittus, J.H., "High-Temperature Deformation of Two-Phase Structures", Phil. Trans. R. Soc. Lond., A 288 (1978), 121.

49. Padmanabhan, K.A., "A Theory of Structural Superplasticity", Mater. Sci. Eng., 29 (1977), 1.

50. Kê, T.S., "A Grain Boundary Model and the Mechanism of Viscous Intercrystalline Slip", J. Appl. Phys., 20 (1949), 274.

51. Holt, D.L. and Backofen, W.A., "Superplasticity in the Al-Cu Eutectic Alloy", Trans. ASM, 59 (1966), 755.

52. Karim, A., "On the Nature of Superplastic Deformation in the Mg-Al Eutectic", Scripta Met., 3 (1969), 887.

53. Gifkins, R.C., "Superplasticity, Creep and Grain Boundary Sliding", Scripta Met., 7 (1973), 27.

54. Mohamed, F.A. and Langdon, T.G., "Creep Behaviour in the Superplastic Pb-62% Sn Eutectic", Phil. Mag., 32 (1975), 697.

55. Gifkins, R.C., "The Grain Size Dependence of Creep Rate in Recovery Creep", J. Aust. Inst. Metals, 18 (1973), 137.

56. Floreen, S., "Superplasticity in Pure Nickel", Scripta Met., 1 (1967), 19.

57. Gifkins, R.C., "Superplasticity During Creep", J. Inst. Metals, 95 (1967), 373.

58. Matsuki, K., Minami, K., Tokizawa, M. and Murakami, Y., "Superplastic Behaviour in Nominally Single-Phase and Two-Phase Al-Cu Alloys", Metal Sci., 13 (1979), 619.

59. Brown, L.M., "Deformation of 2-Phase Alloys", Mater. Sci. Eng., 25 (1976), 181.

60. Dunlop,G.L. and Taplin,D.M.R., "Texture and Anisotropic Flow of a Superplastic Aluminium Bronze", J. Aust. Inst. Metals, 16 (1971), 195.

61. Geckinli, A.E. and Barrett, C.R., "Superplastic Deformation of the Pb-Sn Eutectic", J. Mater. Sci., 11 (1976), 510.

62. Vastava, R.B. and Langdon, T.G., "An Investigation of Intercrystalline and Interphase Boundary Sliding in the Superplastic Pb-62% Sn Eutectic", Acta Met., 27 (1979), 251.

63. Backofen, W.A., Turner, I.R. and Avery, D.H., "Superplasticity in an Al-Zn Alloy", Trans. ASM, 57 (1964), 980.

64. Arieli, A. and Rosen, A., "Measurements of the Strain Rate Sensitivity Coefficient in Superplastic Ti-6 Al- 4 V Alloy", Scripta Met., 10 (1976), 471.

65. Suery, M. and Baudelet, B., "Rheological and Metallurgical Discussion of Superplastic Behaviour", Rev. Phys. Appl., 13 (1978), 53.

66. Zehr, S.W. and Backofen, W.A., "Superplasticity in Lead-Tin Alloys", Trans. ASM, 61 (1968), 300.

67. Naziri, H. and Pearce, R., "Superplasticity in a Zn-0.4% Al Alloy", Acta Met., 22 (1974), 1321.

68. Suery, M. and Baudelet, B., "Flow Stress and Microstructure in Superplastic 60/40 Brass", J. Mater. Sci., 8 (1973), 363.

69. Rai, G. and Grant, N.J., "On the Measurements of Superplasticity in an Al-Cu Alloy", Met. Trans. A, 6A (1975), 385.

70. Padmanabhan, K.A., Moles, M.D.C. and Davies, G.J., "Non-Unique Stress-Strain-Rate Relations During Superplastic Flow", J. Mater. Sci., 12 (1977), 632.

71. Chandan, H.C. and Murty, G.S., "Role of Prior Mechanical and Thermal Treatments in Superplasticity of Tin-Lead Eutectic", Ind. J. Tech., 11 (1973), 742.

72. Paton, N.E. and Hamilton, C.H., "Microstructural Influences on Superplasticity in Ti-6 Al-4 V", Met. Trans. A, 10A (1979), 241.

73. Underwood, E.E., "Surface Area and Length in Volume", in Quantitative Microscopy, edited by R.T. DeHoff and F.N. Rhines (McGraw-Hill Book Company, U.S.A.), 1968, p. 77.

74. Guiu, F. and Pratt, P.L., "Stress Relaxation and the Plastic Deformation of Solids", Phys. Stat. Sol., 6 (1964), 111.

75. Subramanyam, B., "Elastic Moduli of Some Eutectic Alloy Systems", Trans. Japan Inst. Metals, 13 (1972), 89.

76. Smithells, C.J., "Elastic Properties and Damping Capacity", Metals Reference Book, Vol. III, 4th Edition (Plenum Press, New York), 1967, p. 708.

77. Köster, W., "Die Temperaturabhängigkeit des Elastizitasmoduls reiner Metalle", Z. Metallk., 39 (1948), 1.

78. Lloyd, D.J. and Embury, J.D., "The Role of Internal Stress in the High-Temperature Deformation of Copper", Metal Sci. J., 4 (1970), 6.

79. Hilliard, J.E., "Estimating Grain Size by the Intercept Method", Metal Prog., 85 (1964), 99.

80. Schneibel, J.H. and Hazzledine, P.M., "The Influence of Anelasticity on the Stress Relaxation Behaviour of Superplastic Pb-Sn Eutectic", Scripta Met., 11 (1977), 953.

81. Gleiter, H. and Chalmers, B., "High-Angle Grain Boundaries", in Progress in Materials Science, Vol. 16 (Pergamon Press, Oxford), 1972, p. 228.

82. Smithells, C.J., "Diffusion in Metals", Metals Reference Book, Vol. II, 4th Edition (Plenum Press, New York), 1967, p. 637.

83. Avery, D.H. and Backofen, W.A., "A Structural Basis for Superplasticity", Trans. ASM, 58 (1965), 551.

84. Cagnon, M., Suery, M., Eberhardt, A. and Baudelet, B., "High Temperature Deformation of the Pb-Sn Eutectic", Acta Met., 25 (1977), 71.

85. Turnbull, D. and Treaftis, H.H.,"Kinetics of Precipitation of Tin from Lead-Tin Solid Solution", Acta Met., 3 (1955), 43.

86. Ghosh, A.K. and Hamilton, C.H., "Mechanical Behaviour and Hardening Characteristics of a Superplastic Ti-6 Al-4 V Alloy", Met. Trans. A, 10A (1979), 699.

87. Herriot, G., Baudelet, B. and Jonas, J.J., "Superplastic Behaviour of Two-Phase Cu-P Alloys", Acta Met., 24 (1976), 687.

88. Martin, P.J. and Backofen, W.A., "Superplasticity in Electroplated Composites of Lead and Tin", Trans. ASM, 60 (1967), 352.

89. Cline, H.E. and Alden, T.H., "Superplasticity in Lead-Tin Alloys", Trans. AIME, 239 (1967), 710.

90. Avery, D.H. and Stuart, J.M., "The Role of Surfaces in Superplasticity", Surfaces and Interfaces II : Physical and Mechanical Properties, edited by J.J. Burke, N.L. Reed and V. Weiss (Syracuse: Syracuse Univ. Press), 1968, p. 371.

91. Aldrich, J.W. and Avery, D.H., "Alternating Strain Behaviour of a Superplastic Metal", in Ultrafine-Grain Metals, edited by J.J. Burke and V. Weiss (Syracuse: Syracuse Univ. Press), 1970, p. 397.

92. Baudelet, B. and Suery, M., "Constant Stress Creep and Constant True Strain-Rate Tensile Tests of the Superplastic Alloy Pb-Sn", J. Mater. Sci., 7 (1972), 512.

93. Hayden, H.W., Floreen, S. and Goodell, P.D., "The Deformation Mechanisms of Superplasticity", Met. Trans., 3 (1972), 833.

94. Chaudhari, P., "Deformation Behaviour of Superplastic Zn-Al Alloy", Acta Met., 15 (1967), 1777.

95. Gleiter, H. and Chalmers, B., "High-Angle Grain Boundaries", in Progress in Materials Science, Vol. 16 (Pergamon Press, Oxford), 1972, p. 185.

96. Poirier, J.P., "Is Power Law Creep Diffusion-Controlled?", Acta Met., 26 (1978), 629.

97. Weertman, J., "Creep of Indium, Lead, and Some of Their Alloys with Various Metals", Trans. AIME, 218 (1960), 207.

98. Bondy, A., Regnier, P. and Levy, V., "Diffusion Dans Les Interfaces", Scripta Met., 5 (1971), 345.

99. Mohamed, F.A. and Langdon, T.G., "Creep at Low Stress Levels in the Superplastic Zn-22% Al Eutectoid", Acta Met., 23 (1975), 117.

100. Shei, S.-A. and Langdon, T.G., "The Mechanical Properties of a Superplastic Quasi-Single Phase Copper Alloy", Acta Met., 26 (1978), 639.

101. Toma, K., Yoshinaga, H. and Morozumi, S., "Internal Stresses during High-Temperature Deformation of Pure Aluminium and an Al-Mg Alloy", Trans. Japan Inst. Metals, 17 (1976), 102.

102. Furushiro, N. and Hori, S., "Direct Determination of the Strain Rate Sensitivity of Flow Stresses Based on Grain Boundary Sliding in a Sn-Pb Eutectic during Superplastic and Non-superplastic Deformation", Scripta Met., 13 (1978), 653.

103. Furushiro, N. and Hori, S., "The Origin of High Strain Rate Sensitivity of Flow Stresses in Superplastic Al-Cu Alloys", Scripta Met., 12 (1978), 35.

104. Murty, G.S., "Internal Stress in a Superplastic Mg Alloy", Scripta Met., 6 (1972), 663.

105. Dunlop, G.L. and Taplin, D.M.R., "The Tensile Properties of a Superplastic Aluminium Bronze", J. Mater. Sci., 7 (1972), 84.

106. Geckinli, A.E. and Barrett, C.R., Internal Stresses and Superplastic Flow in the Pb-Sn Eutectic", Scripta Met., 8 (1974), 115.

107. Oikawa, H., Sugawara, K. and Karashima, S., "Creep Behavior of Al-2.2 at.% Mg Alloy at 573 K", Trans. Japan Inst. Metals, 19 (1978), 611.

108. Stowell, M.J., Robertson, J.L. and Watts, B.M., "Structural Changes during Superplastic Deformation of the Al-Cu Eutectic Alloy", Metal Sci. J., 3 (1969), 41.

109. Bricknell, R.H. and Edington, J.W., "Deformation Characteristics of an Al-6 Cu-0.4 Zr Superplastic Alloy", Met. Trans. A, 10A (1979), 1257.

110. Grimes, R., Stowell, M.J. and Watts, B.M., "Superplastic Aluminium-Based Alloys", Metals Technol., 3 (1976), 154.

111. Watts, B.M., Stowell, M.J., Baikie, B.L. and Owen, D.G.E., "Superplasticity in Al-Cu-Zr Alloys, Part I: Material Preparation and Properties", Metal Sci., 10 (1976), 189.

112. Watts, B.M. and Stowell, M.J., "The Variation in Flow Stress and Microstructure during Superplastic Deformation of the Al-Cu Eutectic", J. Mater. Sci., 6 (1971), 228.